Thermochemical Cycles for High-Temperature Solar Hydrogen Production

Tatsuya Kodama* and Nobuyuki Gokon

Department of Chemistry and Chemical Engineering, Faculty of Engineering, and Graduate School of Science and Technology, Niigata University, 8050 Ikarashi 2-nocho, Nishi-ku, Niigata 950-2181, Japan

Received March 8, 2007

Contents

1. Introduction

The greatly insolated "sunbelt" regions of the world include the southwestern United States, southern Europe, all of Australia, and broad regions of the developing world.[1] The maximum direct insolation frequently reaches 1 kW m^{-2} in these regions. The reflection and concentration of direct insolation can be achieved by sun-tracking mirrors called collectors or heliostats. Some modern solar-concentrating systems have maximum concentration factors in the 1500−5000 range and can provide high-temperature solar thermal heat (up to a few hundred kilowatts, and even tens of megawatts in the sunbelt regions).[1−27] The concentrated solar radiation is focused upon a solar receiver, where maximum temperatures can exceed 1500 °C, depending upon the configuration of the solar concentrating system. The receiver efficiency depends on a concentration factor. The concentrated solar high-temperature heat has the potential to produce hydrogen from water thermochemically.

The conversion of solar radiation into a chemical fuel such as hydrogen is an engineering challenge. Chemical fuels offer the advantages of being transportable as well as storable for extended periods of time. This point is important because energy demand is rarely synchronous with or geographically matched to incident solar radiation. This paper reviews the thermochemical conversion of solar radiation to hydrogen via a high-temperature water-splitting cycle. A conceptual diagram of the overall water-splitting process is as follows:

solar radiation → collectors or heliostats →
heat on receiver (→ working fluid) or in reactor →
reactants (H_2O, metal oxide, etc.) →
regeneration of the reactants, except for H_2O →
product fuels extraction (H_2, O_2)

As is well-known, the high-temperature nuclear heat is another primary energy source for thermochemical water-splitting cycles. Many of the thermochemical cycles reviewed herein were developed to be coupled with an advanced high-temperature gas-cooled (HTGR) nuclear reactor. As is discussed further below, the maximum cycle temperature matches the optimum temperature for an advanced high-temperature nuclear reactor at <1200 K. Thermochemical cycles involving higher temperatures are available only when coupled with a solar thermal energy source, as described below. A good review of nuclear hydrogen production was written by Yalçcin.[28]

The first step of this process is the reflection and concentration of direct insolation using collectors/heliostats. Large-scale solar concentrating systems have been developed for about three decades.[1−27] Primarily four types of solar concentrating systems have been developed—parabolic trough, power tower, dish, and double-concentration systems—which are continually increasing in their capability to convert high-temperature heat from concentrated solar radiation into electricity, process heat, and chemical fuels. These four systems are shown schematically in Figure 1. Parabolic trough systems (Figure 1a) use linear parabolic concentrators to focus sunlight along the focal lines of the collectors. Solar energy is absorbed by a fluid in pipes located along the focal line. The concentration factor is only in the range of 30−100, generating temperatures in the fluid on the order of 200−400 °C (for thermo oils). This system is currently used for some commercial solar thermal power generation plants, for example, the 350 MW_e Solar Electric Generating System (SEGS) at Kramer Junction in California.[9−11] However, the maximum temperature of the solar heat is insufficient to

* Corresponding author (telephone/fax +81-25-262-7335; e-mail: tkodama@eng.niigagta-u.ac.jp).

10.1021/cr050188a CCC: $65.00
Published on Web 10/10/2007

Tatsuya Kodama received his Ph.D. degree in chemistry from the Tokyo Institute of Technology, Japan, under the direction of Professor Yutaka Tamaura. He then spent a year as a postdoctoral fellow at the same Institute. At the Institute, he conducted research involving CO_2 decomposition with iron oxides. In 1995 he moved to the Department of Chemistry and Chemical Engineering, Faculty of Engineering, at Niigata University, Japan, as an Assistant Professor. Following a period as Associate Professor from 1997 to 2003, he has been Professor in the same department at Niigata University since 2003. His main research field is now "solar chemistry" for converting high-temperature solar heat to chemical fuels, involving the solar thermochemical water-splitting cycle, solar re-forming of natural gas, and solar gasification of coal for solar hydrogen production. He has contributed to more than 100 scientific publications and is an expert on solar chemistry. He is an Associate Editor for the field of solar chemistry and bioconversion with the *Journal of Solar Energy Engineering*.

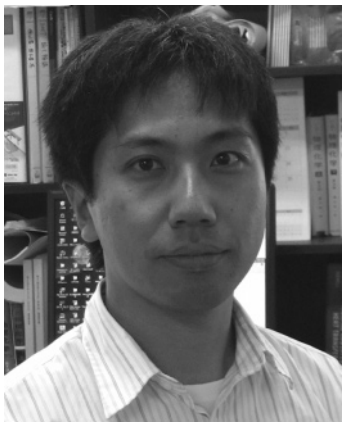

Nobuyuki Gokon received his doctorate degree in 2000 from Tokyo Institute of Technology in materials science and chemistry of solids. He then worked as a postdoctoral fellow with Professor Y. Tamaura in the research center for Carbon Recycling and Energy at the Tokyo Institute of Technology in 2000–2003, where he studied the synthesis/thermodynamic evaluation of mixed iron oxide materials (ferrites) and their application to two-step water splitting cycles with ferrites for hydrogen production from water. In 2003 he became an Assistant Professor at the Tokyo Institute of Technology, where he worked on the development of organic/inorganic magnetic nanosized beads involving ferrite nanoparticles. Since 2005 he has worked as an Assistant Professor of solar chemistry at Niigata University. His current research interests focus on the developments of solar working ferrite materials and new solar water-splitting reactors for solar hydrogen production.

supply the process heat necessary for existing or developing thermochemical water-splitting cycles, as mentioned below. In a central power tower system (Figure 1b), a field of two-axis tracking mirrors reflects direct insolation onto a receiver/reactor mounted at the top of a centrally located tower. The power tower systems usually achieve concentration ratios of 300−1500, and the maximum operating temperature of the receiver/reactor can reach up to 1500 °C. The capacities

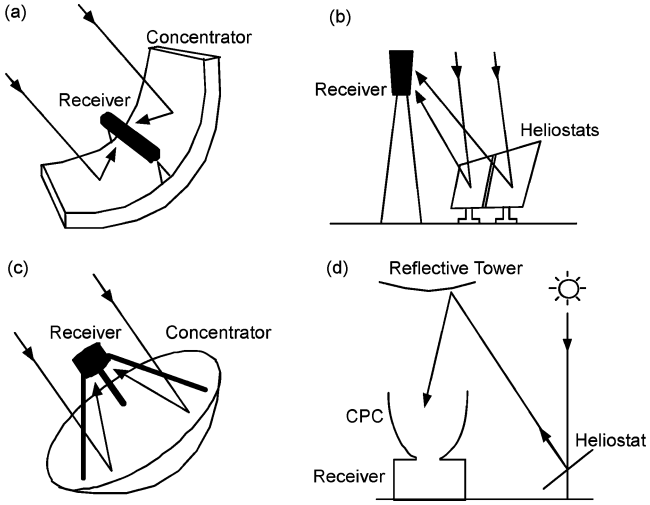

Figure 1. Main concepts of large-scale solar concentrating systems: (a) parabolic trough; (b) central power tower; (c) parabolic dish; (d) double concentration. (Reprinted with permission from ref 1. Copyright 2003 Elsevier Ltd.)

are quite large—generally tens of megawatts. For solar thermal power generation, this technology has been developed in pilot test plants such as the Solar Two plant in Barstow, CA[12,13], and the 11 MW_e "PS10" plant currently under construction in southern Spain.[15−17] Dish systems (Figure 1c) use a parabolic dish concentrator to focus the direct insolation on a receiver/reactor. A parabolic dish reflector is a point-focus collector that tracks the sun along two axes, concentrating the insolation onto a receiver located at the focal point of the dish. The concentration ratios usually range from 1000 to 5000, and temperatures in excess of 1500 °C can be achieved. The largest existing dish system (∼400 m^2 concentrator) has been developed by the Australia National University.[19] A fourth type of solar concentrating system, the double-concentration, or reflective tower system with beam-down optics (Figure 1d), has been newly developed.[20−27] It consists of a heliostat field, the "reflective tower," and a ground receiver equipped with a secondary concentrator. The optical path of the reflective tower comprises the heliostat field illuminating a hyperboloidal reflector. The reflector is placed on a tower below the target point of the field. The upper focal point of the hyperboloid coincides with the target point of the field. The reflector directs the beams downward. On the ground, secondary concentrators of the compound parabolic concentrator (CPC) type are arranged to further enhance the concentration of the solar energy. Note that CPCs can be used in any of the other concentrating systems to increase the concentration factor, if needed. The concentration factor for double-concentration systems is in the range of 5000−10000, and the receiver/reactor on the ground can achieve temperatures in excess of 1300 °C. A 300 kW system was built at the Weizmann Institute of Science in Israel.[24,26]

Thus, the high (1000−1500 °C) temperature heat needed to split water via a multistep thermochemical cycle can be obtained from tower, dish, and double-concentration systems in the sunbelt. Production of fuels from the solar-generated high-temperature heat is a subject of current interest.[29−33]

Compared to electrochemical water splitting coupled with solar thermal power generation, direct thermochemical water splitting has a potential efficiency advantage—efficiency losses due to heat transformation to electricity do not occur. If energy efficiency or chemical storage efficiency is defined

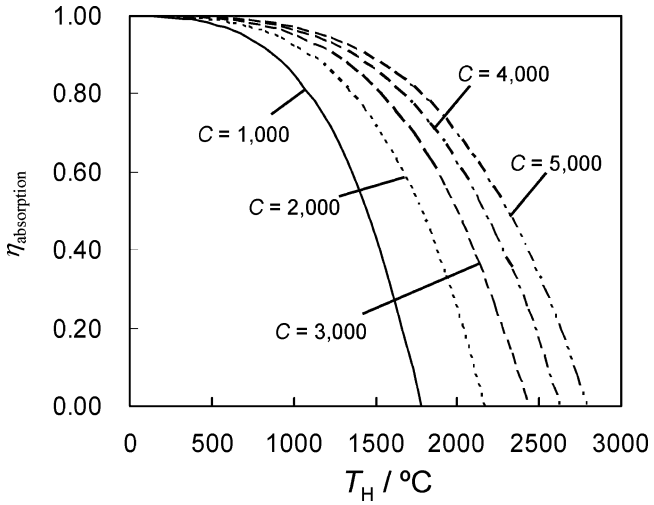

Figure 2. Temperature variation of efficiency of the receiver absorption ($\eta_{absorption}$) for solar concentration ratios of $C = 1000-5000$ according to eq 1 with $\alpha_s = \epsilon = 1$ (as a blackbody receiver) and $I = 1$ kW m^{-2}.

by the percentage of incident solar energy transformed into chemical fuels as chemical enthalpy change, the ideal thermodynamic limit is close to 100%—the second law of thermodynamics does not limit conversion of heat to chemical enthalpy change via an endothermic reaction. At high temperatures, however, the power absorbed by a solar receiver is diminished, mostly by radiative losses from the receiver. The absorption efficiency of the receiver is defined as the net rate at which energy is being absorbed, divided by the solar power from the concentrator. If there are no conduction and convection losses, the absorption efficiency is given by[34,35]

$$\eta_{absorption} = \frac{\alpha_s IC - \epsilon\sigma T^4}{IC} \quad (1)$$

where I is the intensity of solar radiation, T is the operating temperature of the receiver, C is the concentration ratio of the solar concentrating system, α_s and ϵ are the effective absorptance for solar radiation and the emittance of the receiver, respectively, and σ is the Stefan−Boltzmann constant. The absorbed power can be utilized as high-temperature process heat to drive endothermic chemical reactions. Parametric plots of eq 1 with $\alpha_s = \epsilon = 1$ (as a blackbody receiver) and $I = 1$ kW m^{-2} are shown for concentration ratios of 1000−5000 in Figure 2.

On the other hand, if the chemical storage efficiency or system efficiency is defined by the power stored as the chemical free energy of the products (Gibbs free energy of the reaction products), divided by the solar power from the concentrator, it is limited by the Carnot efficiency, as[34,35]

$$\eta_{system} = \eta_{absorption}\left(\frac{T - T_L}{T}\right) \quad (2)$$

where T_L is the temperature of the cold thermal reservoir. For a concentration ratio of 5000, the peak of the system efficiency plot as a function of temperature T can be found at 1200 °C, where the system efficiency reaches 76% as shown in Figure 3.

The simplest pathway for thermochemical hydrogen production from water is a direct or single-step water splitting. However, as shown in Figure 4, the Gibbs free

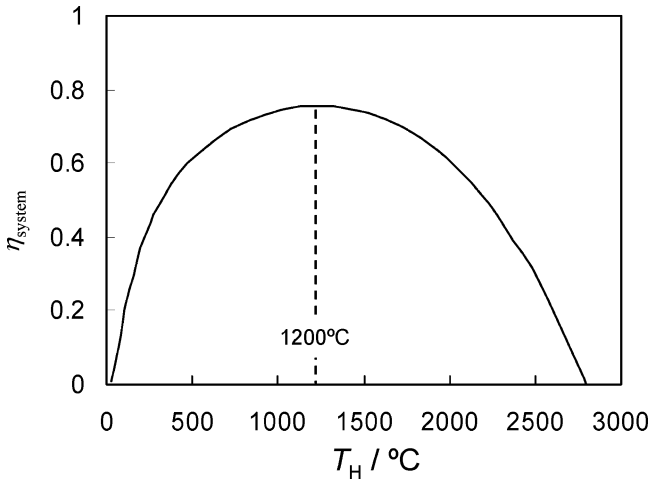

Figure 3. Temperature variation of efficiency of the overall system (η_{system}) for a solar concentration ratio of $C = 5000$ according to eqs 1 and 2 with $\alpha_s = \epsilon = 1$ (as a blackbody receiver), $I = 1$ kW m^{-2} and $T_L = 298$ K.

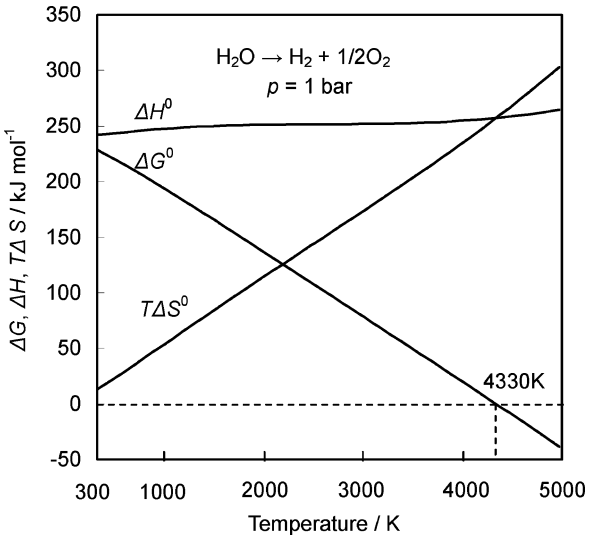

Figure 4. Temperature variations of ΔH^0, $T\Delta S^0$, and ΔG^0 for a direct thermal water splitting ($H_2O \rightarrow H_2 + {}^1/_2O_2$) at 1 bar. (Reprinted with permission from ref 1. Copyright 2003 Elsevier Ltd.)

energy change for direct thermochemical water splitting of $H_2O \rightarrow H_2 + {}^1/_2O_2$ equals zero at about 4300 K under a pressure of 1 bar. Nevertheless, there have been investigations into the feasibility of single-step thermochemical water splitting.[34−43] Nakamura[36] reported that the thermodynamic requirements for a direct thermal water splitter are difficult to realize from a structural viewpoint and that existing separation methods are not applicable to the gas separation process at such extremely high operating temperatures (>2500 K). Kogan[41] identified the problems encountered during the development of a single-step, solar-thermochemical water-splitting process as follows:

- Very high solar reactor temperatures must be achieved by secondary concentration of solar energy.
- Material problems are encountered in the manufacturing of the solar reactor.
- Special porous ceramic membranes must be developed to separate reaction products, which resist clogging by sintering at very high temperatures.
- Recombination of products and intermediates (e.g., OH) occurs.

These challenges to a single-step thermochemical water-splitting process are too difficult to overcome given the current state of the ceramic, solar, and other technologies involved. To lower the extremely high operating temperatures required and to eliminate the need for high-temperature gas separation, various "multistep" thermochemical water-splitting cycles have been proposed and demonstrated. Under the U.S. Department of Energy (DOE) Hydrogen Program,[44] promising thermochemical cycles were screened in 2005.[45] Two sources were most helpful in their literature research—one was the summary report by Carty et al.[46] and the other was a report by McQuillan et al.[47] The Carty report includes the results of in-house experimental work as well as literature surveys of the chemical viability of the process. Of the 200 cycles examined, 11 cycles were identified as promising. The McQuillan report considered 202 cycles, but more were awaiting evaluation. In phase I screening, thermochemical cycles were scored according to 16 criteria affecting cost, development risk, environmental risk, and sensitivity to power fluctuations. The 50 cycles selected in phase I were analyzed in phase II for energy efficiency. The efficiency calculations resulted in a consolidated ranking of the top 14 cycles. These 14 cycles were grouped into five classes by chemical similarities: metal sulfates, volatile metal oxides, nonvolatile metal oxides, the sulfur−iodine cycle, and other interesting cycles. Almost all of these are two- or three-step cycles, and many are reviewed herein.

This paper reviews chemical and technological developments in multistep thermochemical water-splitting cycles for the conversion of high-temperature solar energy to hydrogen. It also presents some of our recent experimental results for the improvement of solar thermochemical water-splitting technologies.

2. Two-Step Water-Splitting Cycle by a Metal Oxide Redox Pair (Metal Oxide Process)

2.1. Introduction

Two-step reaction cycles are naturally the simplest multistep thermochemical water-splitting methods and may be classified into one of the following three types of reactions:[36]

oxide type

$$XO \rightarrow X + {}^1/_2O_2 \quad (3)$$

$$X + H_2O \rightarrow XO + H_2 \quad (4)$$

hydride type

$$XH_2 \rightarrow X + H_2 \quad (5)$$

$$X + H_2O \rightarrow XH_2 + {}^1/_2O_2 \quad (6)$$

hydroxide type

$$2XOH \rightarrow 2X + H_2O + {}^1/_2O_2 \quad (7)$$

$$2X + 2H_2O \rightarrow 2XOH + H_2 \quad (8)$$

Funk and Reinstrom[29] investigated the potential for the first two cycle types at temperatures up to 1100 °C, but feasible two-step cycles were not found. This is in agreement with the thermodynamic analysis made by Abraham and Schreiner,[48] which indicates that the minimum number of reaction steps for thermochemical cycles operating between 298 and 1000 K is three, as inferred from the required entropy change. However, by raising the temperature limit, the thermochemical constraints for chemical compounds to form via two-step cycles are less stringent.

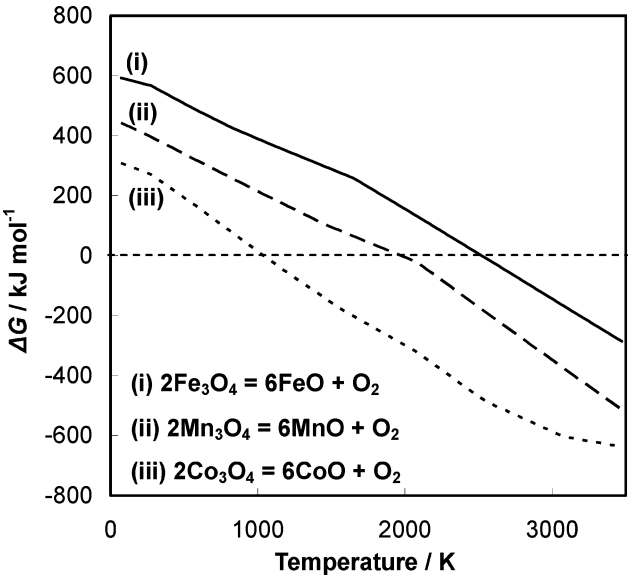

Figure 5. Variations of ΔG^0 for the thermal decomposition of (i) Fe_3O_4, (ii) Mn_3O_4, and (iii) Co_3O_4 (metal oxide → reduced metal oxide + O_2) as a function of temperature at 1 bar.

Two-step thermochemical water splitting by a metal oxide redox pair represents the first type of cycle (oxide type) and is called the "metal oxide process". Nakamura[36] first proposed a two-step water-splitting cycle by a redox pair of Fe_3O_4/FeO and conducted a thermodynamic analysis. The two-step cycle proceeds as follows:

$$Fe_3O_4 \rightarrow 3FeO + {}^1/_2O_2 \quad (9)$$

$$H_2O + 3FeO \rightarrow Fe_3O_4 + H_2 \quad (10)$$

The first high-temperature thermal reduction of Fe_3O_4 is highly endothermic ($\Delta H°_{298K}$ = 319.5 kJ/mol), and the second low-temperature hydrolysis by FeO is slightly exothermic ($\Delta H°_{298K}$ = −33.6 kJ/mol). The two-step process eliminates the need for high-temperature H_2/O_2 separation.

We estimated the variation of $\Delta G°$ with temperature for the thermal reduction of Fe_3O_4 (Figure 5) and that for the hydrolysis reaction by FeO (Figure 6). The MALT2[49] software program was used to compute thermodynamic analyses. Figure 5 indicates that the first solar high-temperature step of the thermal reduction of magnetite (Fe_3O_4) to wustite (FeO) proceeds at temperatures above 2500 K under 1 bar. On the other hand, the second step of the hydrolysis reaction thermodynamically proceeds at temperatures below 1000 K as shown in Figure 6. Two-step water-splitting cycles by an iron-based oxide (or ferrite) redox pair were developed as early as 1977 on the basis of this thermodynamic principle and are frequently called "iron oxide processes" or "ferrite processes".

To investigate promising metal oxide redox pairs such as Fe_3O_4/FeO, such a thermodynamic analysis was conducted for a number of others, such as Mn_3O_4/MnO, Co_3O_4/CoO, Nb_2O_5/NbO_2, ZnO/Zn, In_2O_3/In, SnO_2/Sn, etc.[50−54] Figure 5 also shows the variations in $\Delta G°$ for Mn_3O_4/MnO and Co_3O_4/CoO. As can be seen, the $\Delta G°$ values for the thermal

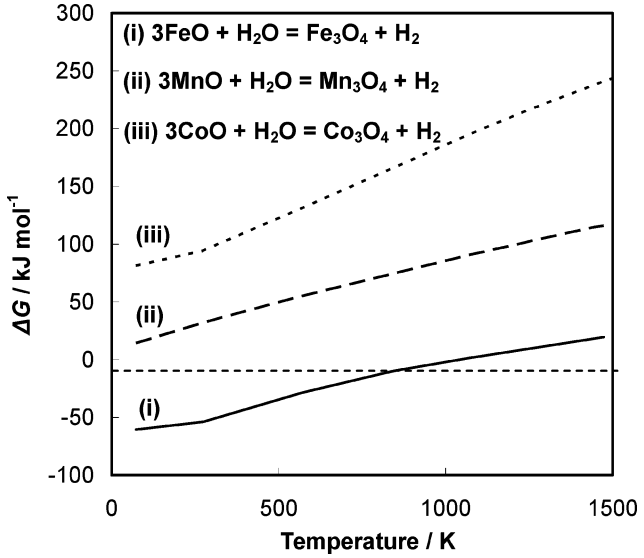

Figure 6. Variations of ΔG^0 for water decomposition with (i) FeO, (ii) MnO, and (iii) CoO (reduced metal oxide + H_2O → metal oxide + H_2) with temperature at 1 bar.

reduction of Mn_3O_4 to MnO and of Co_3O_4 to CoO equal zero at temperatures lower than the corresponding "Fe_3O_4 to FeO". However, the MnO and CoO are not able to produce hydrogen thermodynamically from water in significant amounts over a wide temperature range (100−1500 K), as shown in Figure 6. Lundberg[50] conducted more detailed thermodynamic analyses for the redox pairs Mn_3O_4/MnO, Co_3O_4/CoO, Nb_2O_5/NbO_2, and Fe_3O_4/FeO. The redox pairs Mn_3O_4/MnO and Co_3O_4/CoO can be thermally reduced in air at 1810 and 1175 K, respectively. However, the H_2 yields were only 0.002% and 4×10^{-7}% at 900 K for Mn_3O_4/MnO and Co_3O_4/CoO, respectively.

For the Nb_2O_5/NbO_2, CdO/Cd, In_2O_3/In, WO_3/W, and SnO_2/Sn redox pairs, the $\Delta G°$ variations with temperature for the thermal reduction and hydrolysis reaction are shown in Figures 7 and 8. The $\Delta G°$ value for the thermal reduction of CdO to Cd equals zero also at a lower temperature than that corresponding to "Fe_3O_4 to FeO," whereas Cd is not able to thermodynamically decompose water above ambient temperature. In comparison to Fe_3O_4/FeO, the Nb_2O_5/NbO_2, WO_3/W, and SnO_2/Sn redox pairs require higher thermal reduction temperatures, at which the $\Delta G°$ values for the thermal reduction equal zero. The thermodynamic analysis by Lundberg[50] showed that the H_2 yield at 900 K reaches 99.7% for Nb_2O_5/NbO_2, but the reduction temperature of 3600 K in air is extremely high and is much higher than their melting points.

The thermal reduction of In_2O_3 to metallic indium proceeds at temperatures above 2780 K (Figure 7b), and the metallic indium can thermodynamically decompose H_2O below about 1000 K (Figure 8b). However, in practice, In_2O_3(s) is reduced to In_2O(g) before being reduced to metallic indium. Thus, In_2O vapor has to be quenched to separate it from the product gas containing oxygen molecules to avoid recombination with oxygen, and then the reaction, $3In_2O(g) \rightarrow In_2O_3 + 4In$, occurs during quenching. Then, metallic indium can be reacted with steam to generate hydrogen in a practical water-splitting cycle. This process is similar to the ZnO process below in which Zn vapor has to be quenched from the oxygen-containing product gas of the thermal reduction step. The In_2O_3 process will be more difficult than the ZnO process because it requires a much higher thermal reduction temperature (about 3000 K) than that of ZnO process (about 2300 K). In contrast to such volatile metal oxide systems, nonvolatile metal oxide systems allow the continuous removal of the evolved oxygen molecules from the "stationary" solid redox metal oxides during the thermal reduction, eliminating the problem of recombination during quenching.

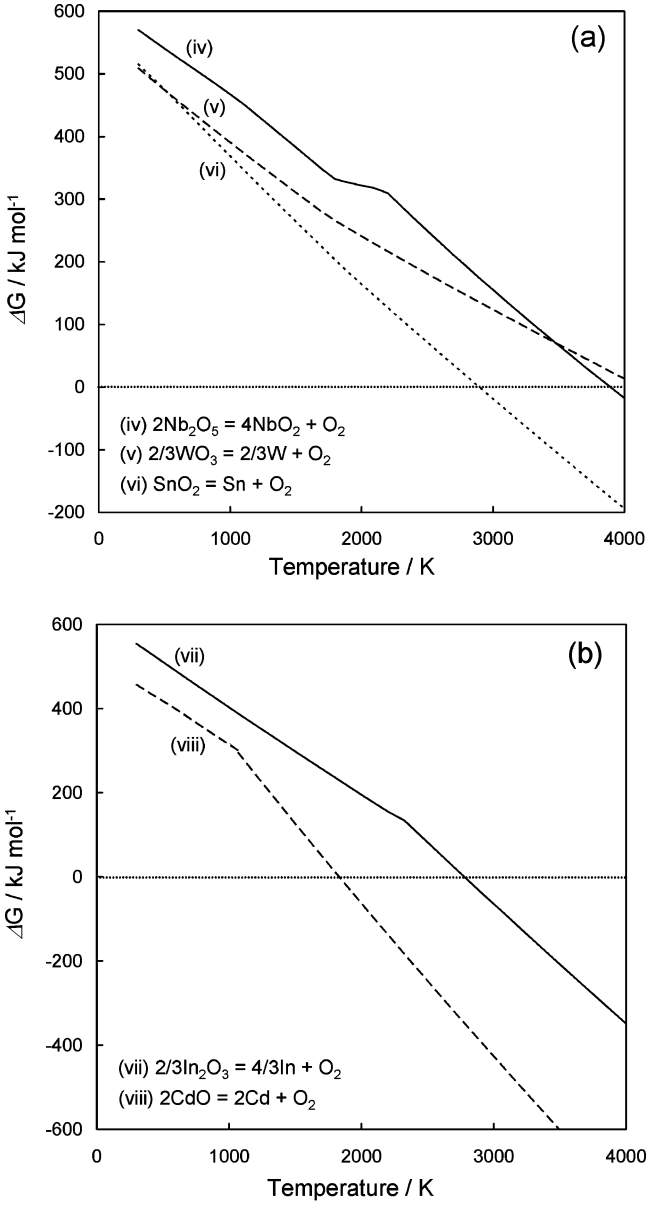

Figure 7. Variations of ΔG^0 for the thermal decomposition of (a) (iv) Nb_2O_5, (v) WO_3, and (vi) SnO_2, and (b) (vii) In_2O_3 and (viii) CdO (metal oxide → reduced metal oxide + O_2) as a function of temperature at 1 bar.

In addition to Fe_3O_4/FeO, ZnO/Zn can be a potential candidate for a functional redox pair in two-step thermochemical water splitting.[55−59] The two-step water-splitting cycle by a ZnO/Zn redox pair (the "ZnO process") has been developed as described below.

$$ZnO \rightarrow Zn(g) + {}^1/_2O_2 \quad (11)$$

$$Zn + H_2O \rightarrow ZnO + H_2 \quad (12)$$

The thermal decomposition of ZnO proceeds endothermically ($\Delta H°_{298} = 478$ kJ), and the temperature for which the $\Delta G°$

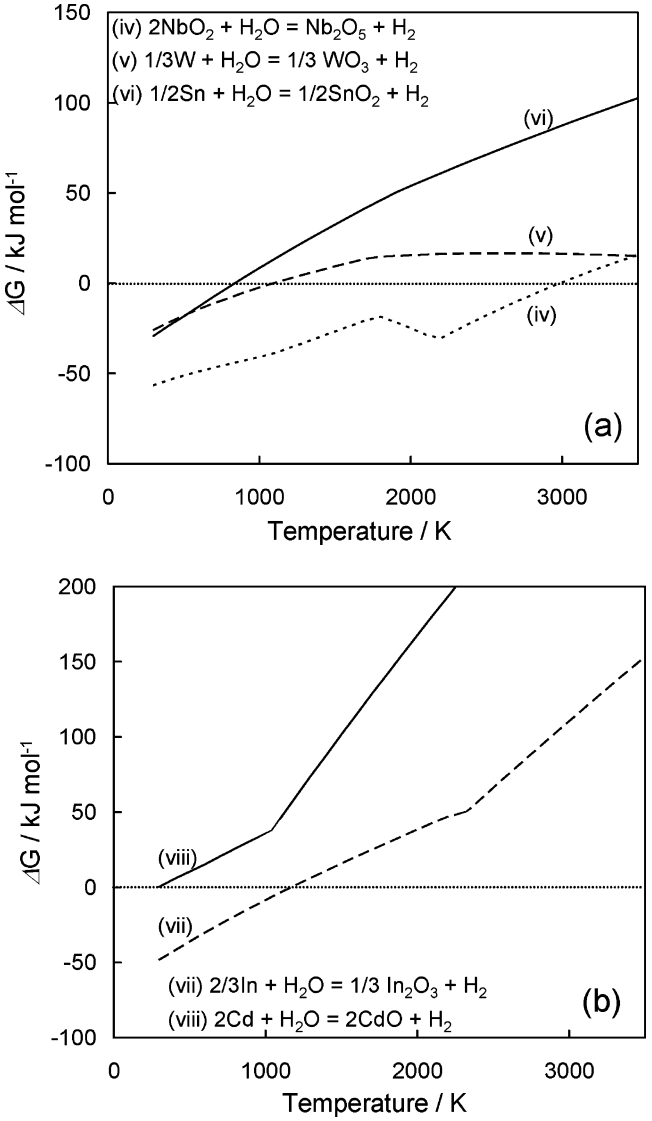

Figure 8. Variations of ΔG^0 for water decomposition with (a) (iv) NbO_2, (v) W, and (vi) Sn, and (b) (vii) In and (viii) Cd (reduced metal oxide + H_2O → metal oxide + H_2) with temperature at 1 bar.

equals zero is 2235 K.[56] The hydrolysis by metallic zinc thermodynamically proceeds at temperatures below 1400 K under1 bar.[59]

Recently, Abanades et al.[52] have screened another set of potentially attractive thermochemical water-splitting cycles. A database containing 280 thermochemical water-splitting cycles was developed at PROMES-CNRS (Processes, Materials, and Solar Energy Laboratory, France). The database includes many other "two-step" metal oxide processes such as MoO_2/Mo, SiO_2/SiO, and HgO/Hg as well as multistep processes (more than three steps). The following criteria were applied to the database to reduce the number of cycles to a more manageable number: maximum temperature of the cycle; number of reactions and separation steps in the cycle; number of elements in the cycle and nature of the cycle (purely thermal or hybrid electrochemical); thermodynamic analysis of the cycle; technical feasibility of the cycle, including the kinetics and conversion yield of each reaction, and possible deactivation of the solid reactants; expected energy efficiency of the cycle; cost and availability of process chemicals; corrosiveness of the process media and availability/cost of reaction vessel materials; existence of nonstationary solid reactants; environmental safety and health issues in the cycle; type and availability/cost of implementation of the separation step.

Primarily, two- and three-step cycles were selected for their ease of implementation, which implies favorable economics. These cycles involve few reactions and separations, thereby mitigating the inefficiencies associated with heat transfer and product separation. They also involve available and safe materials and a heat input temperature compatible with solar thermal energy. About 30 cycles were selected, including the iron oxide and ZnO processes. In a more recent paper reported by the same group, Charvin et al.[60] emphasized that the nonvolatile iron oxide based cycle is particularly attractive since it involves less complex chemical steps and reactants, uses noncorrosive materials, involves solid−gas reactions, and avoids the problem of recombination during quenching encountered with volatile metal oxides such as zinc oxide.

Because the very high reduction temperature required for the Fe_3O_4/FeO and ZnO/Zn redox pairs creates an engineering challenge, any possibility of lowering the reduction temperature is desirable. For the iron oxide process, mixed solid solutions between the redox system Fe_3O_4/FeO and M_3O_4/MO are expected to reduce the reaction temperatures required from that for the Fe_3O_4/FeO system. There is the possibility of combining good H_2 yields thermodynamically in the Fe_3O_4/FeO system with the low reduction temperature in a M_3O_4/MO (M = Mn, Co, Mg) system.[1,50] Partial substitution of iron in Fe_3O_4 by Mn, Co, or Mg is possible to form mixed metal oxides $(Fe_{1-x}M_x)_3O_4$. The mixed oxide may be reducible at a lower temperature than that required for the reduction of Fe_3O_4, whereas the reduced phase $(Fe_{1-x}M_x)_{1-y}O$ is still capable of a hydrolysis reaction. Recently, Allendorf et al.[61] performed detailed thermodynamic analyses for mixed metal iron oxides or ferrites of MFe_2O_4, where M = Co, Ni, or Zn. Their results indicate that these three ferrites make the thermal reduction step thermodynamically more favorable in comparison to pure iron oxide, Fe_3O_4. Their thermodynamic calculations indicate that, of the three ferrites and Fe_3O_4, nickel ferrite has the most favorable combination of thermal reduction and hydrolysis reactions. The metal oxide processes via solutions between Fe_3O_4/FeO and M_3O_4/MO are known as "ferrite processes".

2.2. Iron-Based Oxide Processes

2.2.1. Ferrite Process

Figure 9a shows the equilibrium composition of a 1 mol of Fe_3O_4 + 100 mol of air system at 1 bar as a function of temperature. In air, the FeO phase forms at temperatures around 2500 K, but it is in the liquid phase because FeO melts at about 1650 K at 1 bar. There is significant formation of FeO and Fe vapor at around 2900 K. Tofighi et al.[53,62−64] produced solar thermal reduction of Fe_3O_4 experimentally. Thermal reduction of Fe_3O_4 was demonstrated on a small focal spot (<2 cm diameter) using a 2 kW solar concentrator. The reduction of magnetite in air at the 2 kW focal point was about 40%. In an inert atmosphere, complete decomposition was achieved. However, because of the high temperature of the treatment (>2100 K), thermal decomposition of the Fe_3O_4 occurred with concomitant strong vaporization. In this case, FeO vapor forms and is then oxidized back to Fe_3O_4 during the cooling process. Thus, it is necessary to

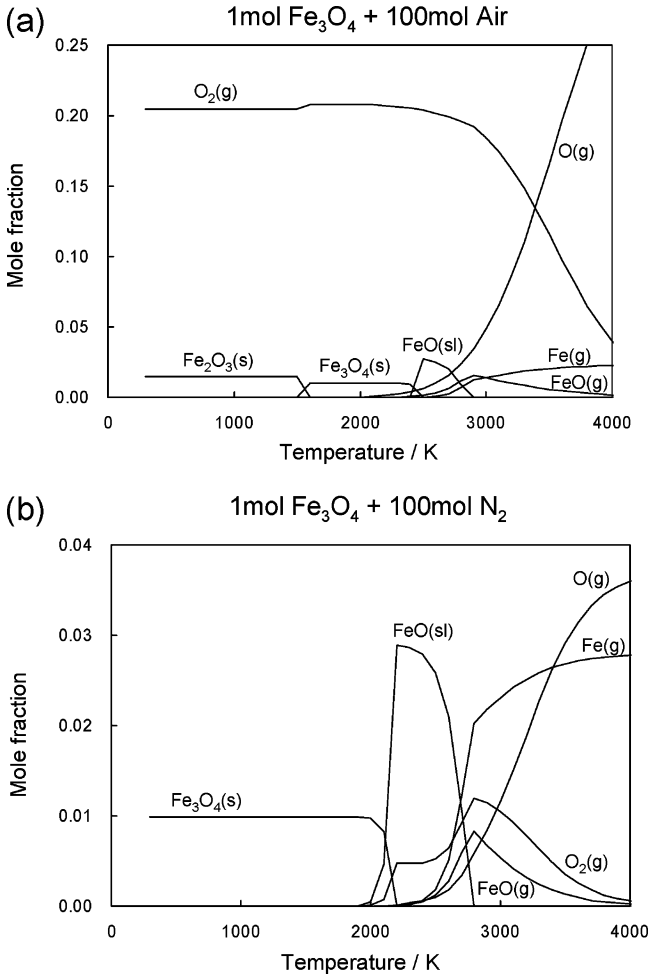

Figure 9. Equilibrium compositions of the systems of (a) 1 mol of Fe_3O_4 + 100 mol of air and (b) 1 mol of Fe_3O_4 + 100 mol of N_2 at 1 bar as a function of temperature.

quench the product to avoid reoxidation, which introduces irreversibility.

Nakamura[36] first estimated the efficiency of the iron oxide process in which the first thermal reduction proceeds at 2500 K and the subsequent hydrolysis reaction occurs at 450 K. From these estimated thermodynamic data, the schematic in Figure 10 showing heat flows of the iron oxide process is derived. As the temperature for the thermal reduction exceeds the melting points of Fe_3O_4 (1870 K) and FeO (1650 K), liquid Fe_3O_4 is thermally reduced to liquid FeO as the first step in the process. In the second step, the hydrolysis reaction, solid FeO reacts with steam to generate hydrogen and solid Fe_3O_4 at 450 K. The energy required to heat solid Fe_3O_4 at 450 K to liquid Fe_3O_4 at 2500 K is very large (140 kcal/mol of Fe_3O_4) because it includes the heat of fusion of Fe_3O_4 (33 kcal). The second hydrolysis reaction is exothermic, releasing 15 kcal of heat, which is enough to generate the necessary amount of steam at 450 K from liquid water at ambient temperature (11.1 + 0.63 = 11.7 kcal). Here efficiency (referred to as "HHV efficiency" in this paper) is defined using a higher heating value of the product hydrogen:

$$\eta_{\mathrm{HHV}} = \frac{-\Delta H_{\mathrm{f}}}{Q_{\mathrm{heat}} + W/\eta_{\mathrm{e}}} \tag{13}$$

ΔH_{f} is the enthalpy change of $H_2 + {}^1/_2O_2 = H_2O(l)$ at ambient temperature and 1 bar, and the $-\Delta H_{\mathrm{f}}$ value

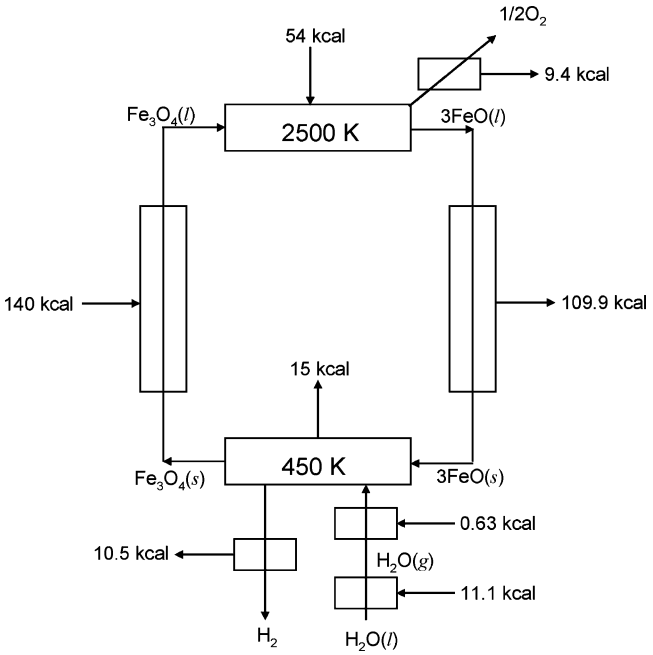

Figure 10. Schematic showing heat flows of an ideal Fe_3O_4 cycle operating between 450 and 2500 K.

corresponds to a higher heating value of H_2 (68.3 kcal/mol of H_2). Q_{heat} is the heat required from the heat source, W is the actual compression work, and η_{e} is the efficiency of the heat engine providing the necessary compression work. The following assumptions are made by Nakamura:[36]

- Because hydrogen can be generated at pressures higher than 1 bar in the second hydrolysis reaction at 450 K, the pumping work can be very small in the second step.
- The steam coexisting with the hydrogen condenses when cooling, enabling easy separation of hydrogen from water.
- If temperatures >2500 K are available for the thermal reduction step, the pressure of the oxygen produced is >1 bar, indicating a very small amount of pumping work in the first step.

The recoverable heat [the sensible heat of the high-temperature products (O_2 and FeO) and the latent heat of the liquid FeO] is very large (109.9 + 9.4 = 119.3 kcal). Therefore, the HHV efficiency, η_{HHV}, of the iron oxide process depends strongly upon the effectiveness of the heat recovery. Without heat recovery, the HHV efficiency is estimated to be 68.3/(140 + 54) = 35%. If the heat recovery is 70%, then the η_{HHV} exceeds 60%. Recently, Diver et al.[65] estimated the efficiency in a similar manner for an iron oxide process operating between 600 and 2300 K. They assumed that 100% of the Fe_3O_4 was converted to FeO and that the water/wustite reaction went to completion, although those are unrealistically optimistic assumptions at those temperatures and pressures. Without heat recovery, in which the exothermic heat from the hydrolysis reaction is also rejected, the HHV efficiency was reported to be 36%. In the case where the exothermic heat from the hydrolysis is used to generate steam at 600 K, the HHV efficiency is 39%. If the round-trip reaction extent of Fe_3O_4 to FeO and back is a more realistic 35%, then the efficiency is estimated to range from 16 to 17% in both cases. Also, Diver et al. estimated that the heat recovery could substantially reduce the heat required from the heat source. They reported that a maximum HHV efficiency of 74% was possible with heat recovery, without recovering the sensible heat in the product oxygen.

Steinfeld et al.[66] reported a second-law analysis of the iron oxide process in more detail. They pointed out that Nakamura's study did not account for the solar energy absorption efficiency and considered neither equilibrium composition nor the effect of heating and quenching air. Their analysis, in which a mixture of 1 mol/s of Fe_3O_4(s) and x mol/s of air are fed into the process at 298 K and 1 bar, accounts for these constraints. Several other conditions were different from those used in Nakamura's analysis. The products are quenched from the solar reactor temperature to ambient temperature, and FeO reacts exothermically with water in the hydrolysis reaction at ambient conditions. The exothermic heat of the hydrolysis reaction was rejected. The complete process was assumed to be carried out at constant pressure, and no pumping work was taken into account. They defined efficiency on the basis of the theoretical maximum available work as

$$\eta_W = \frac{W_G}{Q_{solar}} \tag{14}$$

where W_G is the $-\Delta G$ value for $H_2 + {}^1/_2O_2 = H_2O$(l) at ambient conditions and Q_{solar} is the total power coming from the solar concentrator. In one case, they assumed that 100% conversion of Fe_3O_4 to FeO proceeds at 2300 K without air. In this case, they obtained an η_W value of 20%, and from their data, the HHV efficiency (based on eq 13) is estimated to be 25%. In other cases, they considered equilibrium compositions and the effect of heating and quenching air. Solar reactor temperature ranges from 1900 to 2500 K and air/Fe_3O_4 molar ratios of 0, 1, and 10 were used for their estimation; they discovered that η_W values were <8% (HHV efficiency of <10% in our estimation using eq 13). The reason for such lower efficiencies is obviously the large amount of energy needed to heat the Fe_3O_4 and air to the solar reactor temperatures above 1900 K and the subsequent quenching to avoid reoxidation of FeO in air. However, as described below (section 2.2.4. Solar Reactors), if reactant Fe_3O_4 is directly irradiated by concentrated solar high fluxes to heat it to the thermal reduction temperature, it is not necessary to heat the air to such high temperatures (>1900 K)—only the temperature of the reactant Fe_3O_4 surface needs to reach the thermal reduction temperature required. This solar reactor concept will improve efficiency by reducing the energy needed to heat the air to the very high thermal reduction temperatures.

In these energy efficiency estimations, low efficiencies are also caused by the large amount of heat required to heat iron oxide to an extremely high temperature (>1900 K). The formation temperature of FeO, however, varies with the partial pressure of oxygen in the atmosphere. Figure 11 is the iron—oxygen phase diagram by Darken and Gurry.[67] It shows that the FeO phase can be formed at 1350 °C if the oxygen partial pressure in the atmosphere ranges from about 10^{-7} to 10^{-10} bar. This indicates that the Fe_3O_4-to-FeO thermal decomposition of eq 9 can proceed at around 1350 °C if it is performed under an oxygen partial pressure lower than 10^{-7} bar. Figure 9b shows the equilibrium composition of a 1 mol of Fe_3O_4 + 100 mol of nitrogen system at 1 bar as a function of temperature. The formation of liquid FeO proceeds significantly above 2000 K and is maximized below 2500 K in a nitrogen atmosphere. It is clear that reducing the thermal reduction temperature of the iron oxide process while keeping the equilibrium conversion of Fe_3O_4 to FeO

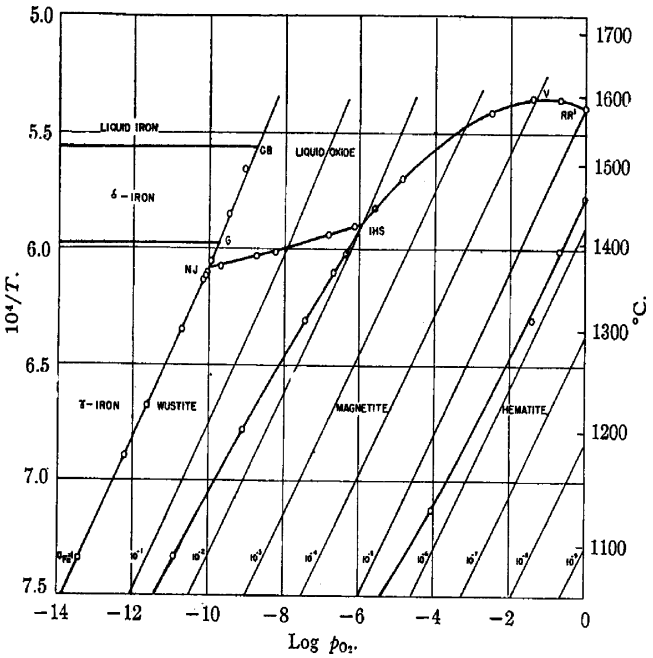

Figure 11. Oxygen partial pressure—reaction temperature diagram for liquid oxide, magnetite, wustite, and hematite. (Reprinted with permission from ref 67. Copyright 1946 American Chemical Society.)

high enough improves process efficiency. Oxygen gas is generated with FeO formation, but if the thermal reduction is carried out under nitrogen gas flow, then the oxygen and FeO can be separated by sweeping oxygen from the solar reactor. This eliminates the necessity of quenching the products in the thermal reduction, and, as discussed above,[66] the iron oxide process is not practical if a quench is used. However, the quenching is required to avoid reoxidation of FeO if the thermal reduction is carried out in air. Therefore, to avoid the reoxidation of FeO in air and to eliminate the quenching from the process, a reaction atmosphere with a low oxygen partial pressure is required for the iron oxide thermal reduction process. However, producing such a low oxygen partial pressure requires other large energy inputs and results in a large process cost. Because of this, mixed solid solutions (Fe_3O_4/FeO with M_3O_4/MO) are being investigated extensively to increase the required oxygen partial pressure of the atmosphere for thermal reduction—for the same reaction temperature, mixed solid solutions or ferrites can thermodynamically increase the oxygen partial pressure required, in comparison to pure Fe_3O_4.[61]

Another critical issue for the water-splitting cycle with Fe_3O_4/FeO that must be considered is the deactivation of the reactant iron oxide in the high-temperature cyclic reaction. FeO fusion may occur if the temperature is high. For example, at temperatures >1400 °C under a low oxygen partial pressure ($\sim 10^{-8}$), the liquid iron oxide phase is formed. The liquid FeO solidifies at the lower temperature of the hydrolysis reaction. In practice, alternating fusion and solidification of FeO will occur, which enhances the coagulation and sintering of iron oxide, resulting in a rapid decrease of the iron oxide surface area. As a result, the reactant of iron oxide particles will be deactivated very rapidly in the repetitive cycle. Recently, Patrice et al.[60,68] demonstrated the thermal reduction of iron oxide in a laboratory-scale solar furnace and a subsequent hydrolysis reaction by a solar-produced FeO. A pellet sample of Fe_2O_3 was placed on a water-cooled holder and heated by direct concentrated solar

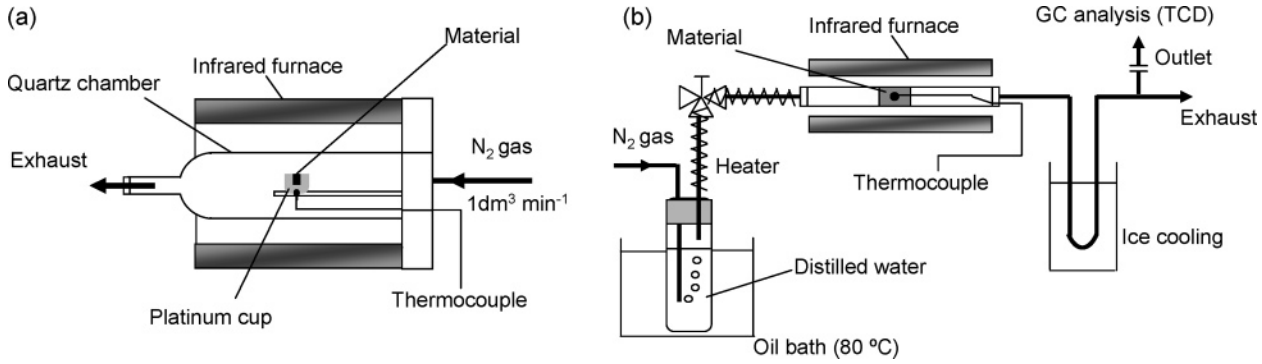

Figure 12. Experimental setups of (a) thermal reduction step and (b) hydrolysis step for iron-based oxide powders.

radiation in either air or a nitrogen atmosphere. Sample quenching was obtained by rapidly withdrawing the device from the focus of the concentrator of the solar furnace. Because of the high solar power supply, overheating of the sample occurred and fusion was observed. The temperature of the sample reached the Fe_3O_4 melting point of 1870 K in a few minutes under an N_2 atmosphere. Complete conversion into FeO occurred under N_2 at 0.1 bar in 2 min. It was impossible to attain complete conversion in air. The reoxidation of the FeO formed in air during quenching was responsible for the formation of Fe_3O_4. The inert N_2 atmosphere prevented the FeO formed from being reoxidized in air. However, it was necessary to mill the solar-reduced sample into a fine power in order to perform the subsequent hydrolysis in a tubular fixed-bed reactor placed in a vertical electric furnace. Only 7% chemical conversion was observed for the iron oxide sample with a particle size of 100−125 μm at 673 °C, whereas 54% conversion was obtained for particles 30−50 μm in size, even at 575 °C. The thermal reduction of Fe_3O_4 powder under a low oxygen partial pressure ($<10^{-7}$ bar) at 1400 °C was also examined in a laboratory-scale experiment in our laboratory.[69] Approximately 1 g of Fe_3O_4 powder was placed in a platinum cup in a quartz reaction chamber (Figure 12a) and heated to 1400 °C in an infrared furnace while N_2 gas was passed through the reactor to thermally reduce the Fe_3O_4. The Fe_3O_4 powder was converted to a nonporous, dense, hard mass in the platinum cup by thermal reduction. It was likely that the material melted at high temperature and solidified again when cooled. It was difficult to pulverize this hard mass by manual grinding using a mortar and pestle.

Thus, milling of the redox metal oxide into a fine powder is required in the iron oxide process, especially after the high-temperature thermal reduction step. This is because the subsequent reactions are mass transfer limited—reduced active surface area of the redox metal oxide results in a slower reaction rate and lower conversion. Many nonvolatile metal oxide processes must have the same problem. Therefore, an important challenge in the iron oxide process (and also in the ferrite process) is to develop the redox materials, the reaction devices, or a reactor setup in which the large active surface area of the metal oxide can be retained throughout high-temperature cyclic reactions.

As mentioned above, mixed solid solutions of Fe_3O_4/FeO and M_3O_4/MO can thermodynamically reduce the thermal reduction temperature required for the pure Fe_3O_4/FeO system. The problem of fusing FeO at temperatures above 1400 °C may be also alleviated in the mixed solid solutions involving MO having a higher melting point than FeO, such as NiO, MnO, and MgO. We also tested $Ni_{0.35}Fe_{2.65}O_4$ and $NiFe_2O_4$ powder samples in a manner similar to the Fe_3O_4 powder.[69] For $Ni_{0.35}Fe_{2.65}O_4$ and $NiFe_2O_4$, porous pellets were formed after the thermal reduction, resembling pellets of sintered fine particles. They were easily pulverized using a mortar and pestle. For the nickel(II) ferrites, Ni-doped wustite ($Ni_yFe_{1-y}O$) was formed instead of pure FeO in the thermal reduction, as corroborated by XRD analysis. The solid solutions of NiO and FeO (or $Ni_yFe_{1-y}O$) are expected to have a higher melting point than pure FeO because NiO has a much higher melting point (1998 °C) than FeO (1370 °C). The higher melting point of $Ni_yFe_{1-y}O$ is believed to be responsible for preventing the wustite phase from fusing during the thermal reduction at 1400 °C. In comparison to $Ni_{0.35}Fe_{2.65}O_4$, the $NiFe_2O_4$ sample yielded more porous and brittle pellets. Using the thermally reduced $NiFe_2O_4$ sample pulverized in a mortar, the hydrolysis reaction was performed in a quartz tube reactor (Figure 12b) at 1000 °C.[69] After the hydrolysis reaction, the ferrite sample underwent thermal reduction in a quartz reaction chamber (Figure 12a). The alternating two-step processes were repeated six times in this manner. Low amounts of hydrogen were produced in the repeated runs, but the amount varied from run to run—the small yield of hydrogen indicates that only 3−10% of the $NiFe_2O_4$ served as a reactant. After the hydrolysis reaction, the reflection peaks due to the wustite ($Ni_yFe_{1-y}O$) became slightly less intense in the XRD. In contrast, as described below, for *m*-ZrO_2-supported $NiFe_2O_4$, the wustite peak nearly disappeared after hydrolysis. These results suggest that the reduced phase of the unsupported nickel(II) ferrite was less reactive than that of $NiFe_2O_4$/*m*-ZrO_2 in the hydrolysis reaction. This is believed to result from the severe sintering of the unsupported ferrite particles.

Aoki et al.[70] also reported in 2004 a two-step water splitting with a $NiFe_2O_4$ system, but they used a very high temperature (1800 K) in air for thermal reduction of $NiFe_2O_4$. They performed the two-step reaction using only one cycle and showed that the thermal reduction of $NiFe_2O_4$ can proceed to form a wustite phase even in air if the temperature is very high (>1800 K). The reduced $NiFe_2O_4$ was able to decompose steam at 1123 K. However, if an air atmosphere is used for the thermal reduction of ferrite, the reduced ferrite must be prevented from being reoxidized in air, by quenching or by use of an inert gas or steam, when it is cooled for the subsequent hydrolysis step.

Eherensberger et al.[71,72] studied the Mn_3O_4−Fe_3O_4 system and reported that at atmospheric pressure, steam with a partial pressure of about 4200 Pa was able to oxidize $(Fe_{1-x}Mn_x)_{1-y}O$ ($x = 0.0$, 0.1, and 0.3) to $(Fe_{1-x'}M_{x'})_3O_4$ with $x' < x$, forming hydrogen at temperatures ranging from 773 to 1173 K. The partial substitution of iron for manganese at 10 and 30 mol

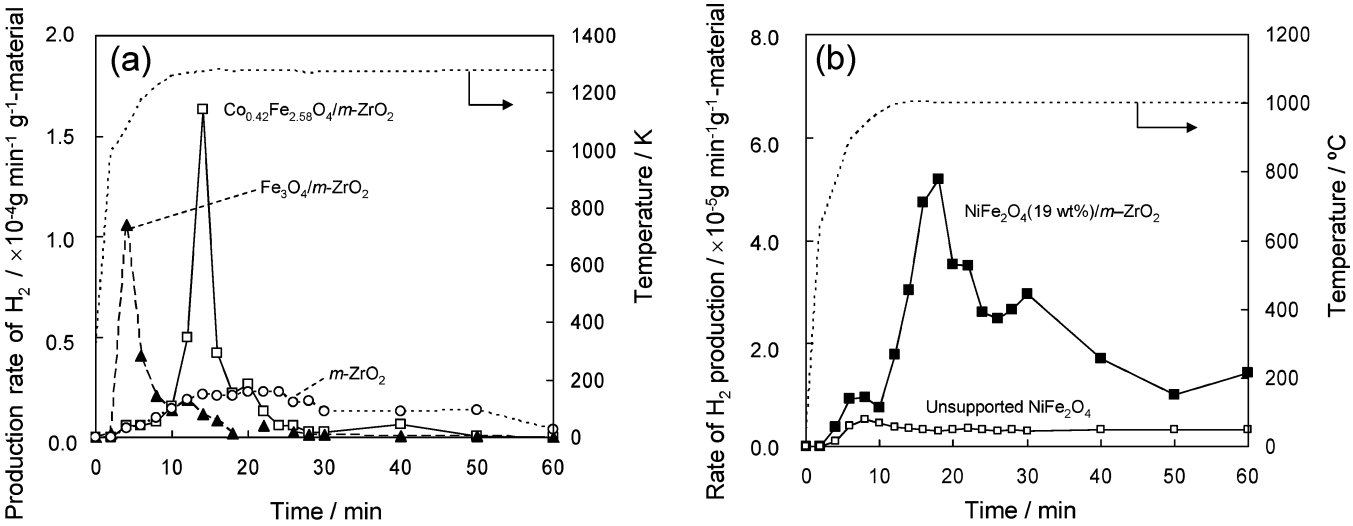

Figure 13. Time variations of the hydrogen production rate per weight of material (including ferrite and *m*-ZrO_2) during the hydrolysis step: (a) Fe_3O_4/*m*-ZrO_2, $Co_{0.42}Fe_{2.58}O_4$/*m*-ZrO_2, and *m*-ZrO_2; (b) unsupported $NiFe_2O_4$ and $NiFe_2O_4$/*m*-ZrO_2. The samples were thermally reduced at 1400 °C and used for the hydrolysis step at 1000 °C. The typical temperature profile of the sample in the hydrolysis step is also shown as a dotted curve in this figure.

% in the wustite phase did not lower the total amount of hydrogen formed per mole of transformed oxide in the hydrolysis reaction, but did slow the kinetics of the process significantly.

Kaneko et al.[73] investigated the thermal reduction of Zn ferrite or $ZnFe_2O_4$ by concentrated solar radiation. They used a stainless steel reactor having a window composed of a quartz glass plate (sandwich reactor) with the 15 kW solar dish concentrator at Australia National University. A flat layer of zinc ferrite powder was directly irradiated by concentrated solar radiation throughout the transparent quartz window of the reactor. The temperature of the zinc ferrite layer reached 1773 K in a few minutes, and zinc ferrite was decomposed to $Zn_xFe_{3-x}O_4$, Zn(g), and O_2. Chemical analysis of the thermally reduced zinc ferrite showed that the Fe^{2+}/Fe_{total} molar ratio of the ferrite was 0.130. From this Fe^{2+}/Fe_{total} value, we re-estimated the *x* value for $Zn_xFe_{3-x}O_4$ in the thermally reduced sample and found that about 13% of Fe^{3+} ions in the $ZnFe_2O_4$ were reduced to Fe^{2+} ions in the ferrite to produce $Zn_{0.7}Fe_{2.3}O_4$ in the ferrite phase. In the XRD pattern of the thermally reduced ferrite, significant peaks due to ZnO also appeared together with the peaks for $Zn_xFe_{3-x}O_4$ and metallic Zn, indicating that the vapor-phase Zn formed, recombined with the O_2 gas released, and deposited as ZnO on the surface of the inner wall of the reactor. There have also been many other reports by the same research group concerning the zinc ferrite process.[74−76]

Of the several other kinds of metal-doped iron oxides or ferrites tested for thermal reduction and/or hydrolysis reaction, none have demonstrated high activity and good repeatability of cyclic two-step water splitting using conventional or unsupported ferrite particles. However, we first demonstrated a repeatable two-step water splitting by highly active, ZrO_2-supported ferrite particles in 2003.[77] The supporting ZrO_2 alleviated the coagulation and/or sintering of the iron oxides; as a result, the cyclic reaction could be repeated with relatively good activity in the temperature range from 1000 to 1400 °C.[69,77−78]

The ZrO_2-supported magnetite was prepared by coating monoclinic ZrO_2 (*m*-ZrO_2) particles with magnetite using an aerial oxidation method of aqueous suspension of iron(II) hydroxide.[69,77−79] The *m*-ZrO_2-supported magnetite (20 wt % of Fe_3O_4 loading) was tested for reactivity toward two-step water splitting using a quartz reactor chamber (Figure 12a) and a fixed-bed reactor (Figure 12b). Figure 13a shows the hydrogen evolution profiles during the hydrolysis reaction with Fe_3O_4/*m*-ZrO_2 and a pure *m*-ZrO_2 support that had been thermally reduced at 1400 °C. The hydrogen production rates (grams per minute) per weight of material used (including the ferrite phase and *m*-ZrO_2 support) are plotted with respect to time of reaction. The pure *m*-ZrO_2 support produced a very small amount of hydrogen in the hydrolysis,[79] whereas the Fe_3O_4/*m*-ZrO_2 produced a much larger amount. The XRD pattern of the thermally reduced Fe_3O_4/*m*-ZrO_2 showed that the reflection peaks due to magnetite became less intense in comparison to those in the original Fe_3O_4/*m*-ZrO_2, and small XRD peaks due to wustite appeared along with strong peaks due to the *m*-ZrO_2 support (Figure 14). This wusite peak disappeared after the hydrolysis reaction, and the peaks due to magnetite became intense again, indicating that the wustite phase formed in the thermal reduction was completely reoxidized with steam to the magnetite phase on the *m*-ZrO_2 support.

As discussed above, other metal doping into the ferrite phase, such as Mn and Co, to produce $M_xFe_{3-x}O_4$ may thermodynamically improve the reactivity of the thermal reduction of the magnetite, thus improving the two-step water-splitting reactivity. Thus, other ZrO_2-supported ferrites (cobalt ferrites, nickel ferrites, etc.) were also prepared and tested for reactivity toward the two-step reactions using similar experimental procedures.[69,79,80] The ferrite/*m*-ZrO_2 samples tested are listed in Table 1. As shown in Figure 13a, with $Co_{0.4}Fe_{2.6}O_4$/*m*-ZrO_2 thermally reduced at 1400 °C, a larger hydrogen evolution peak appeared than for Fe_3O_4/*m*-ZrO_2. Figure 13b shows the hydrogen production profile of the hydrolysis reaction with $NiFe_2O_4$/*m*-ZrO_2, where the hydrogen production rate per weight of used material (including the ferrite phase and *m*-ZrO_2 support) is compared to that of unsupported $NiFe_2O_4$. The hydrogen production rate with $NiFe_2O_4$/*m*-ZrO_2 is significantly greater than that with unsupported $NiFe_2O_4$, although only 20% by weight of the ferrite phase was contained in $NiFe_2O_4$/*m*-ZrO_2 in comparison to the unsupported material. A similar hydrogen evolution profile was observed in the hydrolysis reaction of

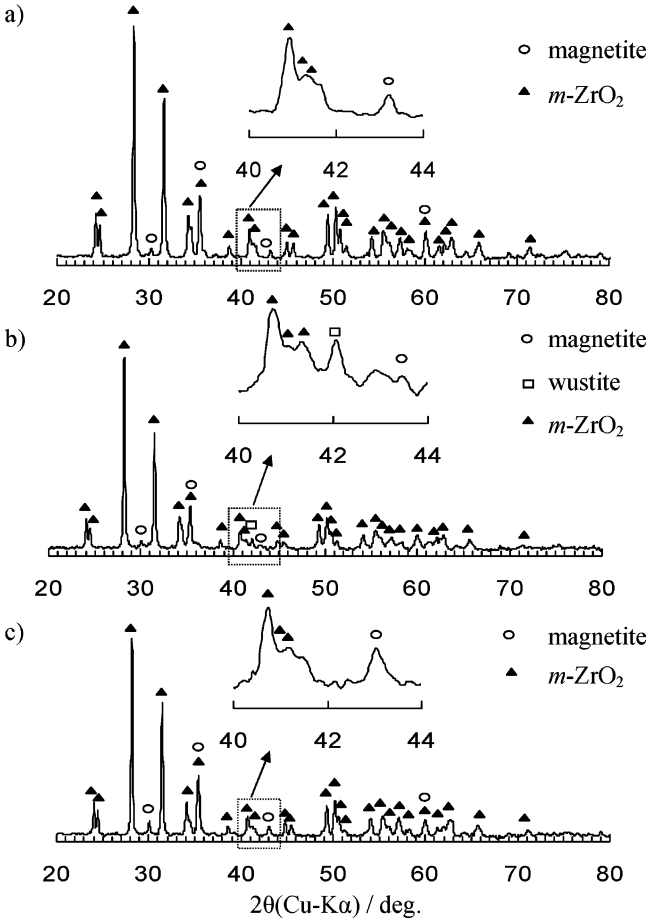

Figure 14. XRD patterns of $Fe_3O_4/m\text{-}ZrO_2$: (a) initial sample; (b) after the thermal reduction step at 1400 °C; (c) after the subsequent hydrolysis step at 1000 °C. (Reprinted with permission from ref 79. Copyright 2005 Elsevier.)

Table 1. Compositions and Loadings of the *m*-ZrO_2- or YSZ-Supported Ferrites Tested

notation	composition	loading/wt %
nondoped	$Fe_3O_4/m\text{-}ZrO_2$	20.0
Mn04	$Mn_{0.36}Fe_{2.64}O_4/m\text{-}ZrO_2$	17.0
Mn07	$Mn_{0.69}Fe_{2.31}O_4/m\text{-}ZrO_2$	19.0
Mn10	$MnFe_2O_4/m\text{-}ZrO_2$	19.0
Mg02	$Mg_{0.19}Fe_{2.81}O_4/m\text{-}ZrO_2$	17.0
Mg06	$Mg_{0.56}Fe_{2.44}O_4/m\text{-}ZrO_2$	18.8
Co02Mn05	$Co_{0.19}Mn_{0.48}Fe_{2.33}O_4/m\text{-}ZrO_2$	19.4
Co04Mn01	$Co_{0.39}Mn_{0.10}Fe_{2.51}O_4/m\text{-}ZrO_2$	16.8
Co04Mn03	$Co_{0.39}Mn_{0.30}Fe_{2.31}O_4/m\text{-}ZrO_2$	15.7
Co04Mn05	$Co_{0.39}Mn_{0.52}Fe_{2.09}O_4/m\text{-}ZrO_2$	15.5
Co06Mn02	$Co_{0.56}Mn_{0.16}Fe_{2.28}O_4/m\text{-}ZrO_2$	18.0
Co04	$Co_{0.42}Fe_{2.58}O_4/m\text{-}ZrO_2$	16.7
Co07	$Co_{0.67}Fe_{2.33}O_4/m\text{-}ZrO_2$	20.2
Co10	$CoFe_2O_4/m\text{-}ZrO_2$	20.1
Ni10	$NiFe_2O_4/m\text{-}ZrO_2$	19.2
Fe-3YSZ	Fe_3O_4/YSZ (3mol%-Y_2O_3)	20.3
Fe-8YSZ	Fe_3O_4/YSZ (8mol%-Y_2O_3)	18.0
Fe10-YSZ	Fe_3O_4/YSZ (10mol%-Y_2O_3)	17.2

the sixth run, demonstrating good reproducibility for the cyclic reactions. Figure 15 shows the amount of hydrogen produced in the hydrolysis reactions of the repeated water-splitting cycles using ferrite/*m*-ZrO_2 samples such as Fe_3O_4 and cobalt, manganese, magnesium, nickel, and cobalt−manganese ferrites.[80] For each sample, the average amount of hydrogen produced, per cycle and per sample weight (the ferrite phase + *m*-ZrO_2 support), is listed in Table 2. The activity was greatly promoted by Ni-doping into the ferrite phase. About twice the yield of hydrogen could be obtained

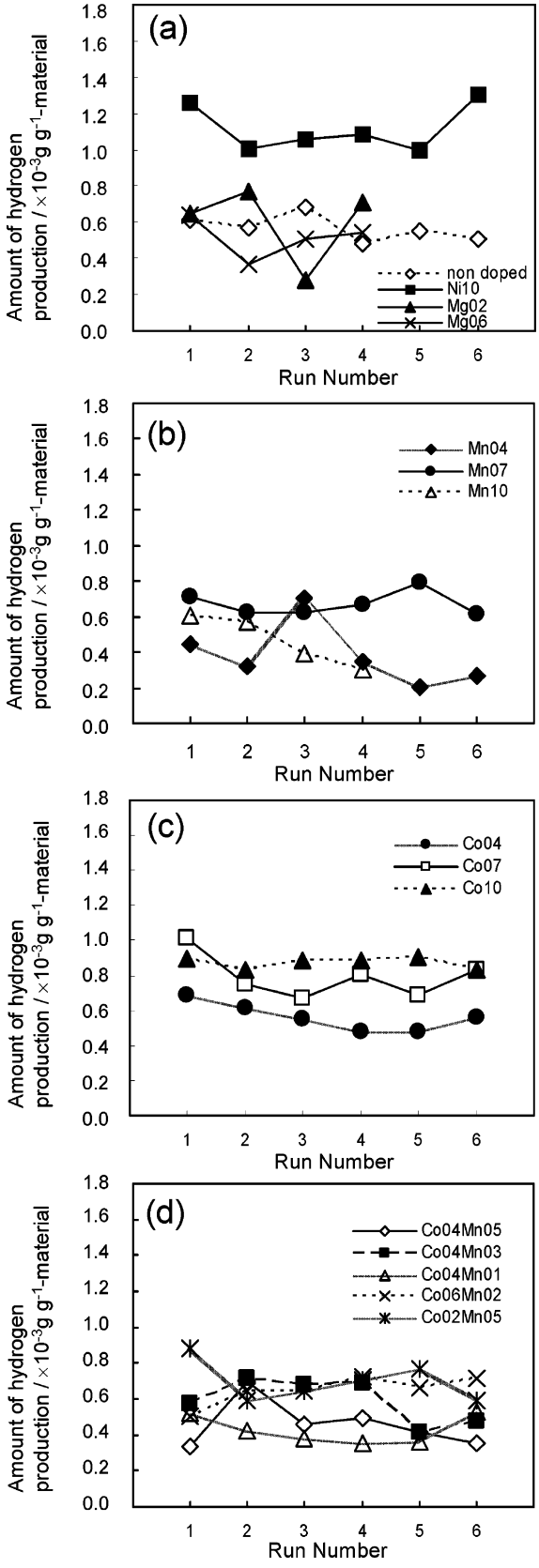

Figure 15. Amounts of hydrogen evolved in the repeated water-splitting cycles using the ferrite/*m*-ZrO_2 power samples when performing the thermal reduction step at 1400 °C and the hydrolysis step at 1000 °C: (a) Fe_3O_4, $NiFe_2O_4$, and $Mg_xFe_{3-x}O_4$ ($x = 0.2$ and 0.6); (b) $Mn_xFe_{3-x}O_4$ ($x = 0.4$, 0.7, and 1.0); (c) $Co_xFe_{3-x}O_4$ ($x = 0.4$, 0.7, and 1.0); (d) $Co_xMn_yFe_{3-x-y}O_4$. The weight of the hydrogen evolved per weight of material (ferrite + *m*-ZrO_2) is plotted for each cycle.

Table 2. Hydrogen Productions and Ferrite Conversions of the ZrO_2- or YSZ-Supported Ferrites

notation	runs of cyclic reaction	av. of H_2 production/ 10^{-4} g g^{-1} of material	ferrite conversion[a]/%
nondoped	6	5.7	33
Mn04	6	3.9	26
Mn07	6	6.7	41
Mn10	4	4.7	28
Mg02	4	6.0	40
Mg06	4	5.1	29
Co02Mn05	6	7.0	42
Co04Mn01	6	4.3	30
Co04Mn03	6	5.9	44
Co04Mn05	6	4.6	34
Co06Mn02	6	6.5	42
Co04	6	5.6	39
Co07	6	8.0	46
Co10	6	8.7	51
Ni10	6	11.0	69
Fe-3YSZ	7	4.5	26
Fe-8YSZ	6	4.7	31
Fe10-YSZ	6	4.6	31

[a] The ferrite conversion in the thermal reduction step was defined by a fraction of reduced Fe^{3+} ions in ferrite to Fe^{2+}, which was estimated from the hydrogen amount evolved in the subsequent hydrolysis step by assuming that the Fe^{2+} ions formed in the thermally reduced step were all oxidized back to Fe^{3+} via the water decomposition in the hydrolysis step. The thermal reduction steps were performed at 1400 °C.

by $NiFe_2O_4/ZrO_2$ in comparison to undoped Fe_3O_4/ZrO_2.

The conversion from ferrite to wustite on *m*-ZrO_2 in the thermal reduction step was estimated from the amount of hydrogen produced in the subsequent hydrolysis reaction, assuming that the wustite phase formed in the thermal reduction was completely reoxidized to ferrite via the subsequent hydrolysis reaction. The estimated ferrite conversion, averaged over the repeated cycles, is also listed in Table 2. The ferrite conversion reached about 69% with $NiFe_2O_4$/*m*-ZrO_2. After all thermal reduction steps, a reflection due to wustite appeared in the XRD pattern of $NiFe_2O_4$/*m*-ZrO_2, which then disappeared after the subsequent hydrolysis reaction, thus implying that the reduced phase of wustite is almost completely oxidized to the ferrite phase on the *m*-ZrO_2 support. The BET surface area of the initial $NiFe_2O_4$/*m*-ZrO_2 sample was 13.8 m^2 g^{-1} and then significantly reduced to 0.4 m^2 g^{-1} after the first run of the repeated cycle. Then, the surface area remained on the same order of magnitude (0.9 m^2 g^{-1}) until even after the sixth run. This indicates that pulverization using a mortar and pestle was enough to prevent the sample from sintering severely.

2.2.2. Nonstoichiometric Ferrite Process

Tamaura et al.[81] studied the nickel−manganese ferrite system using a solar furnace at around 1000 K for two-step water splitting. They found that the two-step process consisted of the formation of a nonstoichiometric ferrite phase with cation excess at temperatures >1073 K and a hydrolysis reaction with cation excess ferrite at temperatures <1073 K:

$$Ni_{0.5}Mn_{0.5}Fe_2O_4 \rightarrow Ni_{0.5}Mn_{0.5}Fe_2O_{4-\delta} + {}^{\delta}/_{2}O_2 \text{ at } >1073 \text{ K} \quad (15)$$

$$Ni_{0.5}Mn_{0.5}Fe_2O_{4-\delta} + \delta H_2O \rightarrow Ni_{0.5}Mn_{0.5}Fe_2O_4 + \delta H_2 \text{ at } <1073 \text{ K} \quad (16)$$

In this cycle, the phase transition between ferrite and wustite does not occur in the solid phase, and the ferrite retains its spinel-type structure in the crystal. Water splitting is reported to accompany the formation of nonstoichiometry, δ, in the spinel-type structure. This cycle requires more moderate reaction temperatures than those required for the wate-splitting cycles using normal wustite/ferrite redox pairs (normal ferrite processes). However, the amount of hydrogen evolved in this system is very limited because water splitting was caused by the small magnitude of nonstoichiometry in the spinel-type ferrite as compared to that accompanying the Fe_3O_4-to-FeO phase transition in the normal ferrite processes.

2.2.3. Iron-Containing Zirconia Process

As mentioned above, it was shown in our previous papers[69,77,79,80] that the transformation between Fe_3O_4 and FeO crystals occurs on the surface of a "monoclinic" ZrO_2 support and is associated with the redox reaction step of the solid phase. In 2004, however, we first found that Fe_3O_4 reacts with "cubic" zirconia stabilized by the doping of yttrium, calcium etc., to form a very reactive Fe-containing cubic zirconia that is capable of serving as a redox working material for a two-step water-splitting cycle below 1400 °C.[82] We used the yttrium- or calcium-stabilized cubic ziriconia (YSZ and CSZ, respectively) as the support, instead of *m*-ZrO_2, and found that a new redox reaction, different from the transformation between Fe_3O_4 and FeO crystals on *m*-ZrO_2, occurred.[82−85] For example, when YSZ (doped with 3 mol % of Y_2O_3) was used as the support for Fe_3O_4, XRD studies indicated that a new cyclic reaction proceeds as follows:[82,83]

$${}^{x}/_{3}Fe_3O_4 + Y_{0.06}Zr_{0.94}O_{1.97} \rightarrow Fe^{2+}{}_{x}Y_{0.06}Zr_{0.94}O_{1.97+x} + {}^{x}/_{6}O_2 \quad (17)$$

$$Fe^{2+}{}_{x}Y_{0.06}Zr_{0.94}O_{1.97+x} + {}^{x}/_{3}H_2O \rightarrow {}^{x}/_{3}Fe_3O_4 + Y_{0.06}Zr_{0.94}O_{1.97} + {}^{x}/_{3}H_2 \quad (18)$$

For Fe_3O_4 supported on YSZ with 3 mol % of Y_2O_3, FeO crystals do not form, but Fe^{2+} enters into the stabilized cubic ZrO_2 crystal in the thermal reduction at 1400 °C under an inert atmosphere to form Fe^{2+}-containing YSZ (Fe^{2+}-YSZ)—previous reports by other researchers have demonstrated the high-temperature synthesis of a cubic zirconia containing Fe in the lattice.[86−88] In the subsequent hydrolysis reaction, Fe_3O_4 crystals are deposited when the Fe^{2+}-YSZ reacts with steam to generate hydrogen according to eq 18. This reaction mechanism was confirmed by XRD studies on the Fe_3O_4/YSZ associated with the cyclic reactions.

If YSZ doped with >8 mol % of Y_2O_3 is used as the support for Fe_3O_4, the reaction mechanism of the hydrolysis changes, and the two-step water-splitting cycle proceeds as[84,85]

$$Fe^{2+}{}_{x}Y_yZr_{1-y}O_{2-y/2+x} + {}^{x}/_{2}H_2O \rightarrow Fe^{3+}{}_{x}Y_yZr_{1-y}O_{2-y/2+3x/2} + {}^{x}/_{2}H_2 \quad (19)$$

$$Fe^{3+}{}_{x}Y_yZr_{1-y}O_{2-y/2+3x/2} \rightarrow Fe^{2+}{}_{x}Y_yZr_{1-y}O_{2-y/2+x} + {}^{x}/_{4}O_2 \quad (20)$$

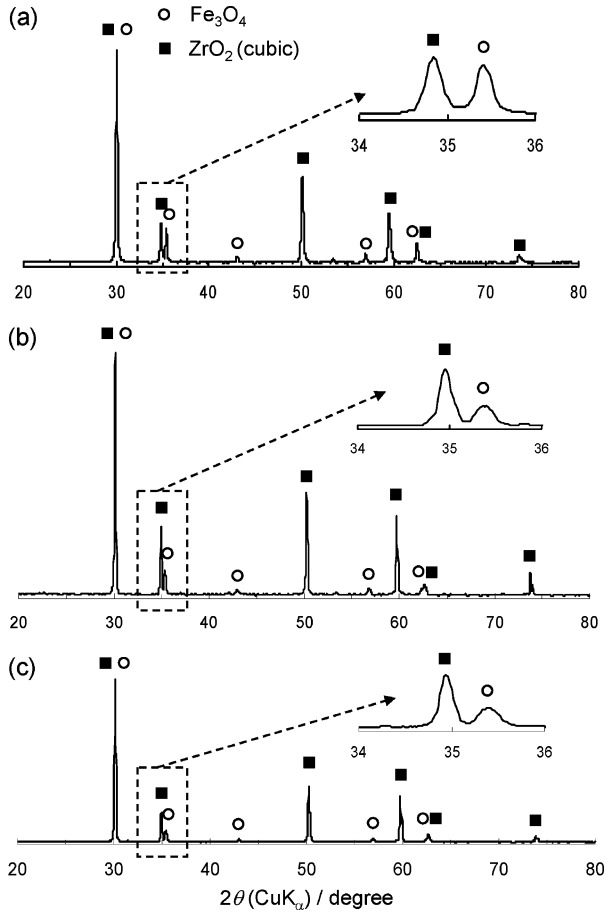

Figure 16. XRD patterns of (a) Fe_3O_4/YSZ doped with 10 mol %-Y_2O_3 original (Fe_3O_4/10YSZ), (b) that after the thermal reduction step, and (c) that after the hydrolysis step.

where $y \geq 0.15$. The Fe^{2+}-YSZ is first formed by a high-temperature reaction between the YSZ and Fe_3O_4 supported on the YSZ (1400 °C, inert atmosphere):

$$^{x}/_{3}Fe_3O_4 + Y_yZr_{1-y}O_{2-y/2} \rightarrow Fe^{2+}{}_xY_yZr_{1-y}O_{2-y/2+x} + {}^{x}/_{6}O_2 \quad (21)$$

The x value of eqs 19−21 for YSZ with 8 mol % of Y_2O_3 ($y = 0.15$) was determined to be 0.08 by chemical analysis.[84,85]

Figure 16 shows a typical change in the XRD pattern of Fe_3O_4/YSZ with >8 mol % of Y_2O_3 in the YSZ. In the original Fe_3O_4/YSZ, reflection peaks due to the Fe_3O_4 are observed along with strong XRD peaks from the YSZ support. After the first heat treatment at 1400 °C under an N_2 atmosphere, the Fe_3O_4 peaks become less intense and the cubic YSZ peaks become more intense. Peaks due to the reduced iron oxide phase of FeO are not observed in the XRD pattern. During the heat treatment, a significant oxygen evolution peak was observed by mass spectroscopy. After the thermal reduction, the Fe_3O_4/YSZ underwent hydrolysis at 1000 °C, and significant hydrogen evolution was observed; however, the XRD pattern of the oxidized Fe_3O_4/YSZ remained unchanged when compared with the thermally reduced product. Following the formation of Fe^{2+}-YSZ, the reactions shown in eqs 19 and 20 are alternately repeated, associated with a redox transition from Fe^{2+} to Fe^{3+} in the cubic zirconia lattice, as corroborated by XRD analysis.

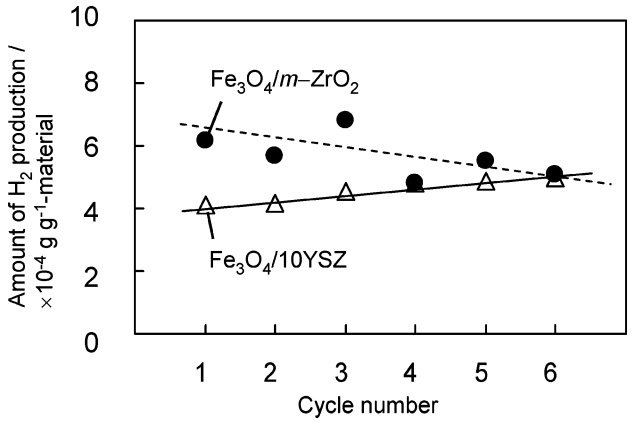

Figure 17. Amounts of hydrogen evolved in the repeated water-splitting cycles using Fe_3O_4/*m*-ZrO_2 and Fe_3O_4/YSZ with 10 mol %-Y_2O_3 (Fe_3O_4/10YSZ) when performing the thermal reduction step at 1400 °C and the hydrolysis step at 1000 °C. The weight of the hydrogen evolved per weight of material (ferrite + *m*-ZrO_2 or YSZ) is plotted for each cycle.

In the above reaction mechanisms involving Fe^{2+}-YSZ, it is possible to alleviate coagulation or sintering of the FeO phase at 1400 °C because the melting FeO phase is not appreciably formed in these systems. These systems also prevent the reactant FeO crystals from being scaled off of the YSZ support because the reactant Fe^{2+} ions are in the YSZ lattice. In addition, stabilized ZrO_2 is more stable as a support than the nonstabilized material in the cyclic reaction with a high-temperature step. The nonstabilized ZrO_2 may transform between monoclinic and tetragonal crystal forms during this temperature swing, whereas stabilized cubic ZrO_2 does not change crystal form.[89] Furthermore, in the new redox mechanism involving the Fe_3O_4/YSZ doped with >8 mol % of Y_2O_3 in the YSZ support, there exists an advantage—prevention from severe sintering of the Fe_3O_4 at high temperatures and scaling off of Fe_3O_4 from the support, resulting in improved repeatability of the cyclic reaction − due to the reactant Fe^{3+} ions remaining in the stable YSZ lattice during the hydrolysis reaction. This difference originates from the fact that the encased Y^{3+} ions in the zirconia stabilize the Fe^{3+} ions in the cubic lattice so that the Fe^{2+} ions can be converted into Fe^{3+} ions at the lattice sites of the YSZ. This new redox material (Fe-containing YSZ) is promising as a working material for the thermochemical two-step water splitting cycle.

The chemical compositions and reactivities of the Fe_3O_4/YSZ samples, doped with 3, 8, and 10 mol % of Y_2O_3 in the YSZ supports, are also listed in Tables 1 and 2.[82−85] Similar reactivities to Fe_3O_4 supported on *m*-ZrO_2 were observed. The stability of the reactivity was, however, much improved with Fe_3O_4/YSZ doped with 10 mol % of Y_2O_3 in the YSZ support. Figure 17 shows a comparison of the variation of amount of hydrogen evolved in repeated cycles between the Fe_3O_4/*m*-ZrO_2 and Fe_3O_4/YSZ samples. The reactivity of the Fe_3O_4/YSZ increased with increasing run number of the repeated cycle, whereas that of the Fe_3O_4/*m*-ZrO_2 gradually decreased with increased run number.

In 2005, Ishihara et al.[90] reported that the calcination of a mixture of YSZ balls and $NiFe_2O_4$ powder produced Ni- and Fe-containing YSZ at 1873 K. They showed that the material split steam for 10 cycles via a two-step reaction involving thermal reduction at 1773 K in an Ar stream and a hydrolysis reaction at 1473 K.

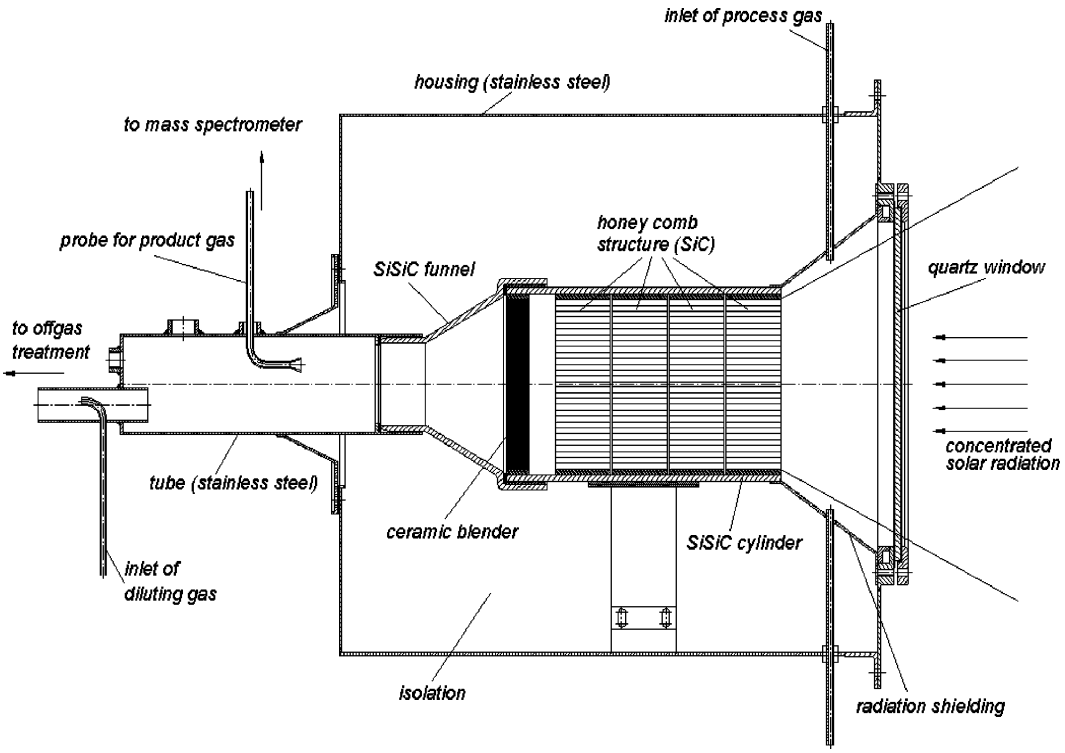

Figure 18. Solar reactor with multichanneled honeycomb ceramic support proposed by DLR Cologne Germany. (Reprinted with permission from ref 92. Copyright 2006 American Society of Mechanical Engineers.)

2.2.4. Solar Reactors

In concert with basic research on active redox working materials such as ZrO_2-supported ferrites, a new chemical reactor system needs to be developed to realize two-step water splitting using concentrated solar radiation as the energy source. The first endothermic step of thermal reduction of iron-based oxides requires a very high temperature (around 1400 °C) even if it is carried out in an inert gas atmosphere. One effective way to reach and retain such high temperatures in a solar chemical reactor is by direct irradiation by high fluxes of concentrated solar radiation. From this perspective, several solar reactor concepts have been proposed and/or demonstrated for two-step water splitting by redox materials composed of iron-based oxides.

In Germany, the German Aerospace Center (DLR) has proposed the use of multichanneled honeycomb ceramic supports coated with an active redox material of ferrite powder in a solar receiver−reactor system, in a configuration similar to that encountered in automobile exhaust catalytic converters.[91−94] The structure of the reactor is illustrated in Figure 18. The ferrite-coated SiC-based honeycombs are directly irradiated by concentrated solar radiation through a quartz window and heated to 1200−1300 °C in order to perform the thermal reduction step while N_2 gas is passed through it. Steam is passed through the reactor to perform the hydrolysis step while the amount of solar power input is reduced because of the lower temperature of the hydrolysis step than of the thermal reduction step. Such a reactor concept allows the continuous removal of the evolved oxygen and hydrogen gases from the stationary solid redox materials, eliminating the quenching process required for volatile metal oxide processes. A honeycomb monolithic reactor was constructed and tested in the solar furnace in Cologne, Germany. Seven coated honeycombs were tested—four of them loaded with zinc−manganese ferrites and the other three with pure iron oxides. Solar thermochemical water splitting was reportedly successfully demonstrated several times. For example, a SiSiC monolith coated with iron oxide performed six cycles at 1073 K (solar hydrolysis reaction) and at 1473 K (solar thermal reduction). The η_{HHV} efficiency of the hydrogen production was reported to be 4.4% (assuming $W = 0$ and Q_{heat} is the solar power input for eq 13.), but the reactor was very small scale, and neither the reactor nor the redox material was optimized.[94] Such a design is hindered by the fact that iron oxide is not chemically inert to SiC at high temperatures. At high temperatures (∼1073−1473 K), iron oxide will react with the SiC matrix to form an undesired compound. Therefore, the SiC matrix must be completely coated and covered with an inert material such as zirconia.

Recently, we have examined ceramic foams coated with Fe-containing YSZ (Fe_3O_4/YSZ) particles in thermochemical water-splitting devices for use in a directly solar-irradiated receiver−reactor system.[95] Ceramic foams were selected as the matrix of the water-splitting device because there exist the following advantages in comparison to the ceramic honeycomb matrix: higher loading of the reactive working materials (due to high surface area) in comparison to the honeycomb matrix; more effective absorption of solar radiation because of the larger geometric surface area of the foam matrix than the honeycomb matrix per volume of the device.

Higher temperatures will be realized on the foam than on the honeycomb if solar flux densities irradiating the devices are the same. Although a higher temperature may increase the re-radiation loss, it can thermodynamically and kinetically favor the thermal reduction of metal oxide.

We chose the Fe_3O_4/YSZ particles with >8 mol %-Y_2O_3 in the YSZ as the coating material. If Fe_3O_4 (or other metal-doped ferrite) particles coat the ceramic matrix (foam or honeycomb), an alternating phase transition between Fe_3O_4 and FeO crystals occurs on the ceramic support during

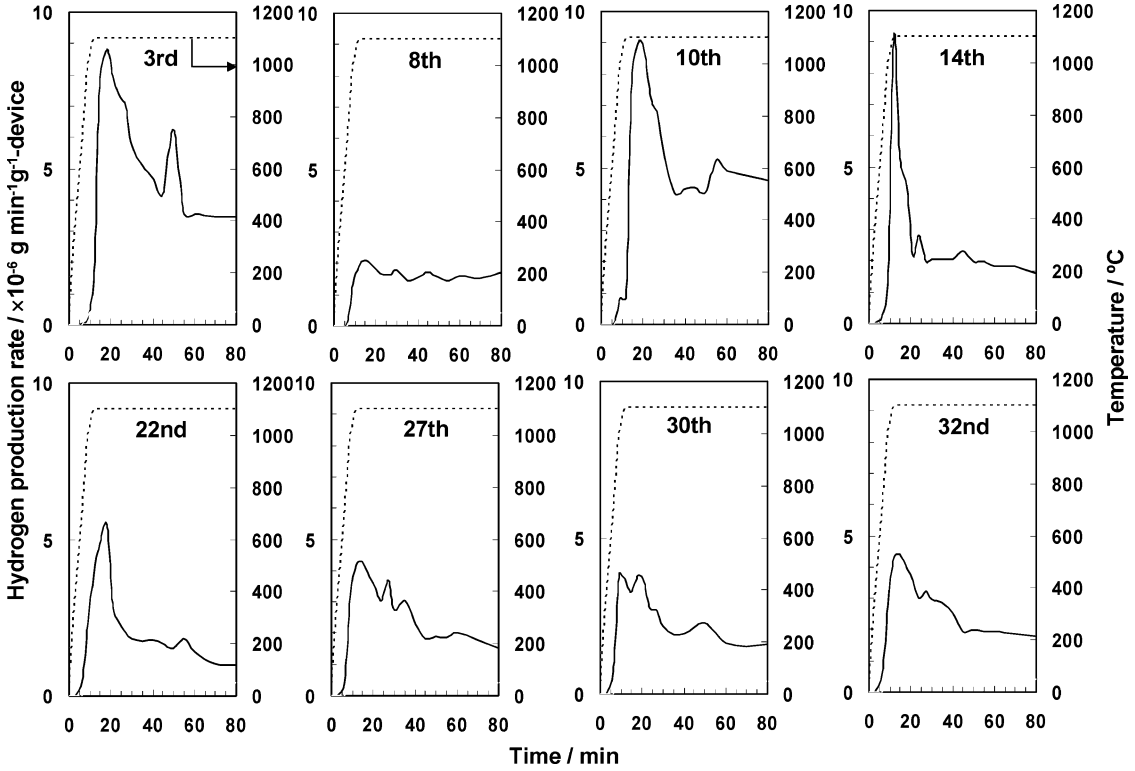

Figure 19. Hydrogen evolution profiles in the repeated water-splitting cycles with Fe_3O_4/YSZ-coated foam device for the 3rd, 8th, 10th, 14th, 22nd, 27th, 30th, and 32nd cycles. Hydrogen production rates per weight of device are plotted against time. The foam device was thermally reduced at 1400 °C and then reacted with steam at 1100 °C to produce hydrogen. The typical temperature profiles of the foam device are also shown as a dotted curve.

repeated water-splitting cycles. A cyclic volume change due to the transition between Fe_3O_4 and FeO crystals naturally occurs, which may cause scaling of the iron oxide particles from the ceramic support matrix. On the other hand, for coating with the Fe_3O_4/YSZ particles, the reactant Fe^{2+} and Fe^{3+} ions remain in the YSZ lattice throughout the repeated two-step cycles, and a phase transition between Fe_3O_4 and FeO crystals does not occur on the support. In addition, the stabilized cubic YSZ crystal is generally stable when undergoing temperature changes between 1000 and 1400 °C. The Fe-YSZ particles were coated on a Mg partially stabilized zirconia foam disk, and the foam device was tested in a two-step water-splitting cycle being performed at temperatures alternating between 1100 and 1400 °C. In a laboratory-scale receiver−reactor system, the foam device was irradiated by concentrated visible light from a sun simulator at a peak flux density of 1000 kW m^{-2} and an average flux density of 470 kW m^{-2} in an N_2 gas stream and, then, was reacted with steam at 1100 °C while heating by an infrared furnace in another quartz tube reactor.[95] Typical profiles of hydrogen evolution from the repeated cycles by the Fe_3O_4/YSZ-coated foam device are shown in Figure 19. Figure 20 shows the amount of hydrogen evolved per gram of the device in repeated cycles. The Fe_3O_4 and YSZ loadings on the foam device were 10.5 and 4.0 wt %, respectively. There was considerable variation in the amount of hydrogen evolved among the first 11 runs of the cycle. The concentrated visible light irradiation period was then prolonged from 30 to 60 min after the 12th run, which resulted in stable hydrogen evolution. Figure 20 also shows the Fe_3O_4 conversion in the thermal reduction step for the Fe_3O_4 loaded on the device. In the Fe_3O_4/YSZ-coated foam device, 20−26% of the Fe_3O_4 conversion was obtained after the 12th run of the cycle. Unfortunately, the foam device

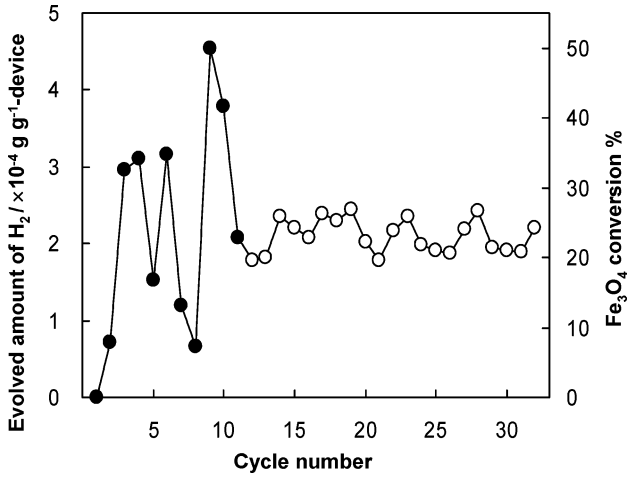

Figure 20. Evolved amounts of hydrogen and Fe_3O_4 conversions in the repeated water-splitting cycles with Fe_3O_4/YSZ-coated foam device. Weight of evolved hydrogen per weight of device was plotted against cycle number. The foam device was thermally reduced at 1400 °C and then reacted with steam at 1100 °C to produce hydrogen. The irradiation periods by solar-simulated light in the thermal reduction step were 30 min for the 1st through the 11th cycles (solid circles) and 60 min after the 12th cycle (open circles).

had cracks and broke after the 32nd run of the cycle. This was due to the fact that the thermal shock resistance of the Mg partially stabilized zirconia foam was not high enough for the heat cycles. The Mg partially stabilized zirconia foam has a monoclinic and tetragonal eutectic crystal form, whereas YSZ has a cubic crystal form. As described above, YSZ does not change its crystal form between 1100 and 1400 °C, whereas Mg partially stabilized zirconia foam does. Thus, YSZ foam should be more suitable as the matrix than Mg

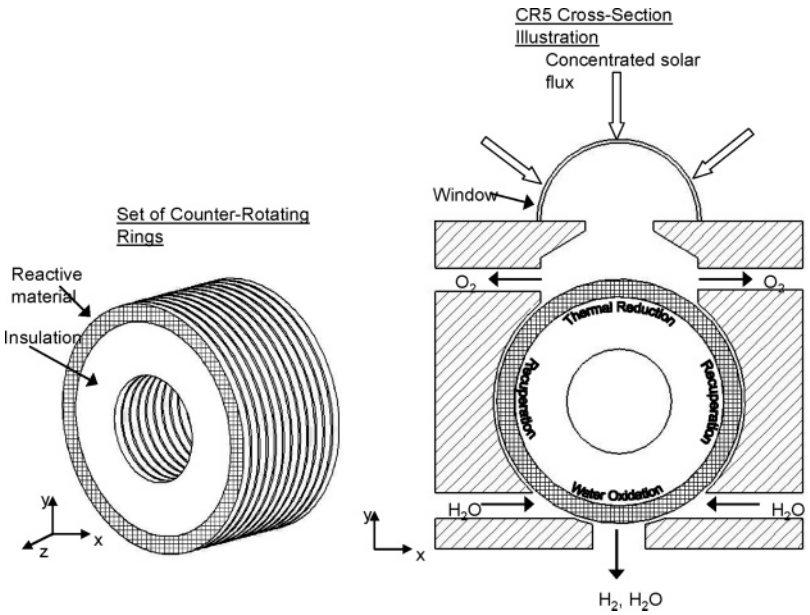

Figure 21. Illustrations of the CR5 and the solar interface of counter-rotating rings. (Reprinted with permission from ref 65. Copyright 2006 American Society of Mechanical Engineers.)

partially stabilized zirconia foam. We are now trying to prepare YSZ foams, to coat the YSZ foam with Fe_3O_4, and to perform the water-splitting cycle using the Fe_3O_4-coated YSZ foam device. The results will be published elsewhere. Otherwise, as in the DLR monolithic honeycomb reactor, SiC-based foams, which have higher thermal shock resistance, should be used as the matrix of the water-splitting device. However, it must be remembered that iron oxide is not chemically inert to SiC at high temperatures. Therefore, again, the SiC matrix must be completely coated with an inert material layer such as zirconia before Fe_3O_4 is applied to the matrix.

In 2006, researchers at the Tokyo Institute of Technology reported the details of a rotary-type reactor for two-step water splitting using a nickel−manganese ferrite as the working material.[96] It is a dual-cell reactor, having two different types of reaction rooms: one is for thermal reduction, and another is for the hydrolysis reaction. Argon was passed through the reaction cell for the thermal reduction. The rotary cylinder containing the reactive ferrite was rotated 180° every 10 min. Successive evolutions of oxygen and hydrogen were observed in the thermal reduction and hydrolysis reaction cells, respectively.

In the United States, a new reactor concept is in development at Sandia National Laboratories (SNL), which is the Counter-Rotating-Ring Receiver/Reactor/Recuperator or "CR5".[65,97,98] The concept utilizes two sets of moving beds of ferrite reactant material in close proximity, moving in opposite directions to overcome a major impediment to achieving high efficiency by enabling thermal recuperation between solids in efficient counter−counter arrangements. The concept also provides inherent separation of the product hydrogen and oxygen. An illustration of the CR5 is shown in Figure 21. The CR5 uses a stack of counter-rotating rings or disks with fins along the perimeter. The fins contain the ferrite reactant on a support. Each ring rotates in the opposite direction of its nearest neighbor at a rotational speed on the order of 1 rpm. At the top of the reactor, the rings are directly irradiated by concentrated solar radiation through a transparent window, performing the thermal reduction of the ferrite. The temperature of the fins having reactive ferrite material reaches 1600 °C. At the bottom of the reactor, the rings are subjected to steam flowing at about 1100 °C to perform the hydrolysis step. Between the top and bottom of the reactor, the counter-rotating rings exchange heat in what is known as the recuperator section. The project began in 2004 with the conception of the general idea for the CR5, and then an appropriate reactive material was identified. This work involved a literature survey combined with experimental validation of prospective materials, finally selecting cobalt ferrite ($Co_{0.67}Fe_{2.33}O_4$)[79] supported on YSZ in a 1:3 ratio by mass as their baseline material. The SNL researchers produced prototypes of the ferrite fins using a SNL-developed rapid prototyping technique called "Robocasting" that is capable of manufacturing monolithic ceramic structures with complex three-dimensional geometries.[97] A small three-dimensional monolithic lattice structure composed of a cobalt ferrite/zirconia mixture was produced and tested in the water-splitting cycle involving thermal reduction at 1400 °C (heating rate = 50 °C/min) and subsequent hydrolysis at 1100 °C using an electric furnace. Six cycles were carried out, and hydrogen continued to be produced at 7−11 N cm^3 [(6−9) × 10^{-4} g] per gram of ferrite per cycle. After the six cycles, a small crack formed in the structure.

However, it must be pointed out that such reactor concepts—the DLR monolithic reactor, our foam reactor, the rotary-type reactor, and the CR5—have a disadvantage in that the mass of the redox materials to be loaded onto the support is very limited and, therefore, only a small amount of the redox material, coated on the restricted surface area of the support, can contribute to the chemical reactions. The active surface area of the redox metal oxide is very limited due to the small loading of the material in the reactor. Therefore, a small mass of hydrogen will be produced by "one run" of the cyclic reaction in the reactor. To realize a large mass production of hydrogen by such reactor concepts, a very large number of runs of the cyclic reaction are required. The solar period of time each day, of course, is limited; thus, to realize the very large number of run for the limited period of time, very high reaction kinetics are required for the limited surface area of the meal oxide in the reactor. In other words, the metal oxide must realize a

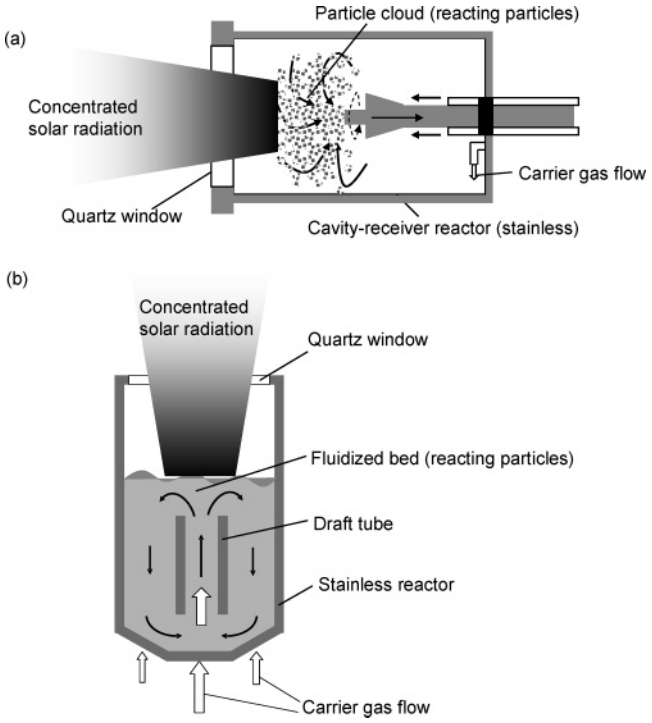

Figure 22. Schematics of solar reactor concepts using (a) a particle cloud and (b) an internally circulating fluidized bed of reacting particles.

very high "turnover number". However, as discussed above, the kinetics of the hydrolysis step strongly depends on the active surface area of the ferrite; thus, the large surface area will be required to realize the high reaction kinetics. As a result, to allow the reactor concept to be scaled up to multi-megawatt size, a cluster of the reactors must be constructed at the top of a solar tower.[92]

The idea of a volumetric gas particle solar receiver−reactor has been examined for more than two decades.[99−109] The reactor concept is based on direct solar irradiation of either "suspension of reacting particles in a gas stream" or "falling particles", providing efficient heat transfer directly to a large mass of reacting particles. Fine metal oxide particles have a larger surface area than metal oxide devices such as a metal oxide coated honeycomb or foam. Thus, this type of reactor can be expected to demonstrate greater hydrogen productivity than reactors with metal oxide devices. The falling particles concept has been experimentally demonstrated for methane splitting,[106−109] but not yet for water-splitting cycles by metal oxide particles. On the other hand, for the concept using a suspension of reacting particles, several reactors have been demonstrated as mentioned below.[104,105] The difficulty in this concept is how to prevent the solar-heated particle suspension from contacting the transparent quartz window. Provided that the reactor is combined with a conventional solar concentrating system such as a solar tower, solar high flux must enter horizontally or upward into the reactor housing through a side window (Figure 22a). In this case, conventional fluidized beds of reacting particles cannot be utilized in the solar reactor, but, rather, a "cloud" of the reacting particles needs to be created by more vicious gas streams in the reactor to avoid contact between the particle suspension and the window,[104,105] as shown in Figure 22a. Several reactors using a gas-particle vortex flow confined in a solar cavity receiver with a window have been demonstrated.[104,105] Recently, however, it has been proposed that a solar chemical reactor, such as a solar reformer, be combined with the newly developed solar reflective tower with beam-down optics.[20−27,110] As a reminder, the optical path of the beam-down comprises a heliostat field illuminating a hyperboloidal reflector that is placed on a tower and directs the beams downward. This beam-down setup has an advantage over normal tower-top arrangements of reactor in that it allows a large-scale reactor to be built on the ground, with the solar radiation entering the reactor housing through a window in the ceiling. In such a reactor design, conventional fluidized beds of the reacting particles can be applied because an interspacing gap can easily be produced between the fluidized particle bed and the window to prevent their contact, as shown in Figure 22b. With this in mind, we have developed a novel design concept for a two-step water-splitting reactor using an internally circulating fluidized bed of reacting particles.[80,111] In this reactor concept, the cylindrical reactor body is made of steel, but a transparent quartz window is installed in the ceiling of the reactor. A draft tube is centrally inserted into the fluidized bed region. Gases are introduced into the draft tube and annulus regions of the beds separately. The concentrated solar radiation passes downward through the window and directly heats the internally circulating fluidized bed of reacting particles. In this system, the particles are always transported upward in the draft tube and move downward in the annulus sections. This solid circulation within the reactor provides solar energy transfer from the top of the fluidized bed to the bottom because directly solar-heated particles in the top region always move to the bottom region. This creates a more uniform temperature distribution throughout the solar-irradiated fluidized bed when compared with a normal solar-irradiated fluidized bed. Another advantage is that the internally circulating bed reactor requires a rapid gas flow only in a small region (solely in the draft tube), reducing the total gas flow compared to a traditional fluidized bed reactor. This reduces the energy required for gas flowing to the reactor extensively.

This novel reactor concept was experimentally demonstrated using two kinds of laboratory-scale reactors—a "quartz tube" reactor (Figure 23a) and a "windowed stainless tube" reactor (Figure 23b)—for the thermal reduction of a ferrite/zirconia particle bed as part of the two-step water-splitting cycle.[80,111] The $NiFe_2O_4$/*m*-ZrO_2 particles were selected as the reacting particles because they had the greatest reactivity among the ferrite/zirconia powder samples tested (Table 2). By preheating the reactor to 900 °C, 20−35 g of the $NiFe_2O_4$/*m*-ZrO_2 particle bed was internally fluidized by passing N_2 gas through from the bottom of the reactor. Then, the particle bed was irradiated for 15 min by about 1 kW of concentrated visible light from a sun simulator. The bed temperature reached about 1200 °C. After the irradiation, the thermally reduced particles were transferred to another fixed-bed reactor (Figure 12b) and were reacted with steam at 1000 °C. With either of the two kinds of reactors, about 45% of the $NiFe_2O_4$ on the *m*-ZrO_2 support was converted to the reduced phase, which was completely reoxidized with steam at 1000 °C to produce hydrogen, whereas only a few percent of the ferrite conversion was obtained by the thermal reduction of the particles ($NiFe_2O_4$/*m*-ZrO_2) in a normal fluidized bed reactor without a draft tube. With this system, pulverization of the $NiFe_2O_4$/*m*-ZrO_2 particles is not needed following thermal reduction; similar levels of hydrolysis reactivity were obtained either with or without pulverizing the particles.[111] This implies that the thermal reduction and

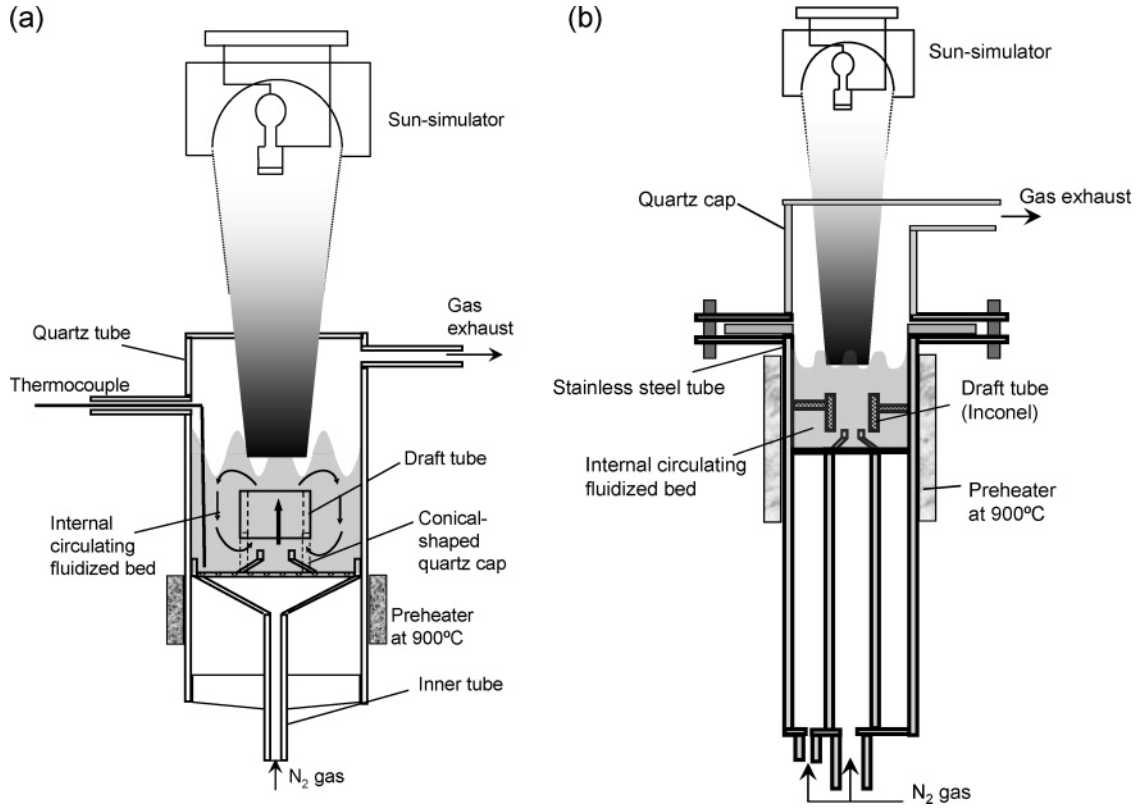

Figure 23. Schematics of experimental setups for an internally circulating fluidized bed laboratory-scale reactor: (a) a "quartz tube" reactor; (b) a "windowed stainless steel tube" reactor.

hydrolysis steps may be conducted in a single reactor of this type by switching the feed gas between inert gas (nitrogen) and steam. However, under the current experimental conditions, the thermal reduction kinetics of the ferrite in the internally circulating bed were too slow to yield an energy efficiency of interest. The main reason for the slow kinetics is the fact that the power of the concentrated visible light input was too small, and thus, the bed temperature could not reach the temperature required for thermal reduction of ferrite (>1400 °C). This problem will probably be solved by increased input power.

2.3. ZnO Process

ZnO/Zn is also a potential candidate for a working redox pair in two-step thermochemical water splitting. This system has been extensively examined and developed,[55−59,112−122] mainly by the Paul Scherrer Institute (PSI) in Switzerland. A good review of the area was written by Steinfeld of the PSI.[58] The redox cycle proceeds according to eqs 11 and 12. The products, zinc vapor and oxygen, eventually must be separated or quenched to avoid recombination. Palumbo et al.[55] reported that the two-step water-splitting cycle has the potential to achieve energy conversion efficiencies exceeding 50%. Steinfeld[57] carried out a more detailed analysis for the theoretical maximum energy conversion efficiency of the solar thermochemical process. It was assumed that the first thermal reduction step was performed at 2300 K using concentrated solar radiation as the source of process heat, that the Zn vapor was quenched to 298 K without any change of the chemical composition, and that the Zn was sent to the hydrolyzer reactor at 298 K to react exothermally with water in a non solar process step. The complete process was assumed to be carried out at a constant pressure of 1 bar; in practice, pressure drops will occur, and pumping work is required. The energy efficiency, η_W, based on the Gibbs free energy change of the product hydrogen oxidation, was reported to be 29 and 36% for fluxes of concentrated solar radiation incident into the solar reactor at 5000 and 10000 kW m^{-2}, respectively. The HHV efficiencies, defined by eq 13 with $W = 0$, are 36 and 45%, respectively. The major sources of irreversibility are associated with re-radiation losses from the solar reactor and the quenching of products—32 and 26% of the input solar power is lost by re-radiation and by quenching, respectively.

In practice, the Zn yield strongly depends on the kinetics of dissociation and the technical feasibility of quenching the gaseous products quickly enough to avoid recombination.[113] Early solar experiments conducted by the PSI using argon circulation resulted in up to 75% zinc molar content in the condensed vapors, but no zinc was observed in a static air atmosphere.[51] The solar experiments, in which ZnO pellets in an argon flow were directly exposed to a solar flux density of 4000 kW m^{-2}, yielded as high as 90% zinc in the recovered products, depending in part on the dilution ratio and quenching surface temperature.[55]

A directly irradiated rotary reactor is now under development to decompose ZnO particles into Zn vapor and oxygen using concentrated solar radiation as the energy source of the process heat.[114,119−123] The 10- kW solar reactor prototype is shown in Figure 24. The main component of the reactor is a rotating drum composed of a cylindrical cavity. The cavity is built from metallic hafnium and has a thin inner HfO_2 layer. The rotational movement along the horizontal axis generates a centripetal acceleration that forces ZnO particles to cover the cavity wall. The reactor has a dynamic feeder that extends and contracts within the cavity, enabling even spreading of solid ZnO along the entire cavity wall. Argon gas is passed into the reactor to sweep the gaseous

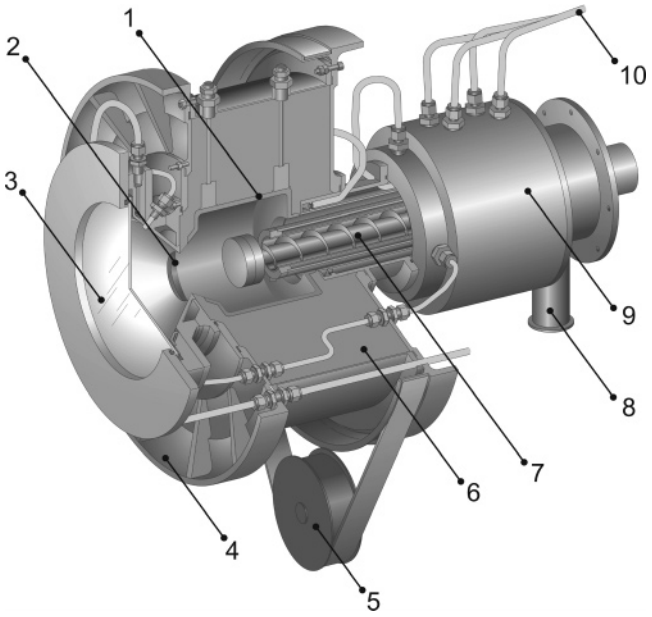

Figure 24. Ten kilowatt solar reactor prototype for thermal decomposition of ZnO: 1, cavity; 2, aperture; 3, quartz window; 4, rotating drum; 5, actuation; 6, insulation; 7, dynamic feeder; 8, product outlet port; 9, rotary joint; 10, cooling fluids. (Reprinted with permission from ref 122. Copyright 2007 Elsevier Ltd.)

products (Zn vapor and O_2) to the quenching zone at the exit of the cavity. The water-cooled walls and the injection of cold Ar promote the quenching of zinc vapor to solid zinc. In a solar demonstration of the thermal reduction of ZnO, 2.35 kg of ZnO was decomposed in the course of 44 feeds, but the solid products collected contained only 61% Zn on average. Mechanical stability problems were observed with the insulating and cavity materials.

For the hydrolysis reaction of eq 12, another reactor system must be developed. It has been pointed out that the hydrolysis reaction needs to be operated at a temperature above the melting point of zinc because of the reaction kinetics.[115] However, when molten zinc is made to react with steam, a ZnO(s) layer is formed, and it floats on top of the melt, preventing further reaction.[115] Recently, Wegner et al.[59] reported a new combined process for the hydrolysis of Zn with steam that encompasses the formation of Zn nanoparticles, followed by their in situ hydrolysis for H_2 generation. The combined process was experimentally demonstrated using a tubular aerosol flow reactor featuring Zn evaporation, steam quenching, and Zn/H_2O reaction zones. The maximum chemical conversion of Zn to ZnO was reported to be 83% when the Zn evaporation was operated at 1023 K. The ZnO particles were deposited on a stainless steel bar placed into the reaction zone and collected by simply scraping off.

2.4. Other Metal Oxide Processes

A manganese oxide based cycle has been proposed for solar thermochemical water splitting.[125,126] It consists of three steps but, in practice, is carried out in four:

$$^1/_2Mn_2O_3(s) \rightarrow MnO(s) + {}^1/_2O_2 \text{ at } >1835 \text{ K} \quad (22)$$

$$MnO(s) + NaOH(l) \rightarrow NaMnO_2(s) + {}^1/_2H_2 \text{ at } 900 \text{ K} \quad (23)$$

$$NaMnO_2(s) + ({}^1/_2 + x)H_2O(l) \rightarrow {}^1/_2Mn_2O_3(s) + NaOH{-}H_2O \text{ at } 373 \text{ K} \quad (24)$$

$$NaOH{-}H_2O \rightarrow NaOH(s) + xH_2O \text{ at } 298 \text{ K} \quad (25)$$

Equation 22 is the solar thermal reduction of Mn_2O_3 to MnO. The reaction is endothermic and proceeds in air at temperatures above 1835 K. In the slightly exothermic second step, hydrogen is produced by the reaction of MnO and NaOH(l) at temperatures between 900 and 1100 K. The $NaMnO_2(s)$ produced is hydrolyzed with H_2O to produce $Mn_2O_3(s)$ and an $NaOH{-}H_2O$ solution. Mn_2O_3 has to be separated from the $NaOH{-}H_2O$ solution for use in the first solar step. NaOH is separated from H_2O for reuse in the second step. Sturzenegger and Nüesch[125] reported that the maximum theoretical efficiency was 74%. The process flow sheet using solar thermal energy input was designed by Weimer et al.[126] The key disadvantages[126] are, however, the corrosive nature of NaOH, the difficulty of separating Mn_2O_3 from NaOH, and the fact that multiple oxide species (i.e., MnO, Mn_2O_3, $NaMnO_2$) are involved in the process, complicating separation and recovery.

Kaneko et al.[127−129] proposed the following three-step cycle with $Na_2CO_3/MnFe_2O_4/Fe_2O_3$:

$$2MnFe_2O_4 + 3Na_2CO_3 + (1 + 6\delta)H_2O \rightarrow Na(Mn_{1/3}Fe_{2/3})O_{2+\delta} + 3CO_2 + (1 + 6\delta)H_2 \text{ at } 1073 \text{ K} \quad (26)$$

$$6Na(Mn_{1/3}Fe_{2/3})O_{2+\delta} + 3Fe_2O_3 \rightarrow 2MnFe_2O_4 + 6NaFeO_2 + (1 + 6\delta)/2O_2 \text{ at } 1273 \text{ K} \quad (27)$$

$$6NaFeO_2 + CO_2 \rightarrow Na_2O_3 + Fe_2O_3 \text{ at } 873 \text{ K} \quad (28)$$

It involves solid−solid reaction steps at 1073 and 1273 K. However, the complete industrial-scale solid−solid reaction generally requires many difficult reaction conditions, such as homogeneous mixture of the reactant solids, use of milled small solid particles, and intimate contact between the solids by making pellets—complicated and costly procedures in the overall process. In addition, the process needs solid−solid separation of Fe_2O_3 from the $MnFe_2O_4/Na_2CO_3/Fe_2O_3$ mixture before $MnFe_2O_4$ and Na_2CO_3 are reused for the first hydrogen generation step. This solid−solid separation is impossible in industrial use.

A cerium oxide process has been recently reported by Abanades and Flamant.[130] The process uses a CeO_2/Ce_2O_3 redox pair and proceeds in two steps:

$$2CeO_2(s) \rightarrow Ce_2O_3(s) + {}^1/_2O_2(g) \text{ at } 2000\ ^\circ\text{C} \quad (29)$$

$$Ce_2O_3(s) + H_2O(g) \rightarrow 2CeO_2(s) + H_2(g) \text{ at } 400{-}600\ ^\circ\text{C} \quad (30)$$

The thermal reduction step in eq 29 was performed using a CeO_2 pellet in a solar furnace under inert gas (N_2) at 2000 °C and 100−200 mbar. At high temperature (>1950 °C), the CeO_2 sample was reduced during melting—the melting point data of CeO_2 varies in the literature from 1950 to 2400 °C according to the source.[130] The reduced solid material was then pounded into a powder in a mortar. Then, the hydrolysis step in eq 30 was performed in a fixed-bed reactor using an electric furnace. The authors state that the cycle

based on CeO_2/Ce_2O_3 shows significant advantages over the other two-step cycles investigated, such as ZnO/Zn, Fe_3O_4/FeO, and oxygen-deficient ferrites. One of the reasons is that the cerium process does not require any product quenching because the solar step proceeds in the liquid phase as soon as the material's melting point has been reached. However, as mentioned above, many ferrite processes do not require product quenching if an inert gas can be used for the thermal reduction step. For example, the thermal reduction of $NiFe_2O_4$ proceeds at temperatures lower than its melting point in an inert atmosphere.[69] Another advantage of the cerium process the authors emphasize is that the particle size does not interfere with the efficiency of the hydrolysis. However, in their experiments, only solid particles ranging from 100 to 300 μm in size are used for the hydrolysis. The particle size range tested is too narrow to conclude that the particle size does not interfere with the efficiency of the hydrolysis. To make such a conclusion requires experimental evidence from detailed kinetic studies using solid samples with particle sizes encompassing a much wider range (e.g. from centimeters to micrometers).

2.5. Economic Evaluation

There have been a few economic assessments of hydrogen production by metal oxide processes. One of them was for the ZnO process, made by Steinfeld in 2002.[57] He assumed a "beam down system" for solar power concentration.[20−23] The reactor was placed on the ground with a CPC on top, eliminating the need for a massive and expensive tower, piping, and frequent personnel access to the tower top. The solar plant size was assumed to be one that delivers 90 MW of concentrated solar power to the reactor. The recycling of an inert gas for quenching was not included in the cost calculation. Hydrogen production rates were 61 and 75 million kWh/year for solar concentration factors of 5000 and 10000, respectively. The solar hydrogen cost was calculated to be 0.14−0.15 $/kWh based on the LHV, depending on the solar concentration factor. The heliostat field was the source of the largest cost, responsible for 44% of the total investment cost of the entire plant. Because, for a fixed hydrogen production rate, the solar reactor efficiency dictates the size of the heliostat field, a high solar reactor efficiency is critical for reducing cost. However, Steinfeld also pointed out that the solar hydrogen cost would be doubled if N_2 gas was used for inert quenching to avoid the recombination of Zn and O_2.

Recently, the DLR estimated the solar hydrogen cost produced by a solar plant using clusters of their monolithic reactor.[92] They assumed that a cluster of reactors was constructed at the top of a solar tower. Six clusters of reactors were located along the six sides of the hexagonal tower top. The solar reactor efficiency was assumed to be 40%, defined by a ratio of the HHV of the hydrogen produced and the solar power input to the reactor. The solar plant was assumed to be sited in Almería, Spain, and to produce 65.5 GWh annually, based on LHV. The reactions were performed at 1473 and 1073 K for the thermal reduction and hydrolysis steps, respectively. A 7-fold surplus of nitrogen was used for the thermal reduction step. Using these conditions, the hydrogen production cost was estimated to be 0.18 euro/kWh of hydrogen based on LHV. The major potential parameters for a reduction in the production cost were reduction of the metal oxide, enhancement of reaction characteristics, operation at temperatures lower than 1473 K, reduction of the necessary amount and purity of nitrogen, and potential cogeneration of hydrogen and electric power.

The DLR researchers concluded that there is the potential to reduce the production cost of hydrogen to 0.10−0.20 euro/kWh (LHV).

3. Multistep Water-Splitting Cycles with More than Three Steps, and Hybrid Cycles, Capable of Working below 1200 K

3.1. Introduction

Thermodynamic analysis by Abraham and Schreiner[48] indicates that the minimum number of reaction steps for thermochemical cycles operating between 298 and 1000 K is three, as inferred from the required entropy change. In fact, there have been a number of multistep thermochemical water-splitting cycles with more than three steps, which are capable of working below 1200 K. Most of them have been developed with the goal of using as their thermal energy source a high-temperature gas-cooled reactor (HTGR), that is, nuclear heat.[28,131] As the maximum temperature of the nuclear heat from an HTGR is restricted to about 1200 K for safety reasons, most of these thermochemical cycles were forced to operate under this temperature limit. Some of them are not pure thermochemical cycles but, rather, hybrid electrochemical−thermochemical cycles including a two-step cycle. Many of these thermochemical and hybrid cycles have been tested at bench scale.

Recently, to provide the thermal energy required for the endothermic reactions to proceed, the use of thermal heat from concentrated solar radiation has been extensively examined. Good reviews of these thermochemical and hybrid cycles capable of working below 1200 K as "solar" water-splitting cycles have been published, for example, by Serpone et al.,[132] Funk,[133] and Perkins and Weimer.[134] This section gives a brief review of some of the promising multistep thermochemical water-splitting cycles and the hybrid electrochemical−thermochemical cycles, which are capable of working below 1200 K.

3.2. Mark 1 and Fe–Cl Family

Scientists at the European Joint Research Center (JRC), in Ispra, Italy, have performed many studies on multistep water-splitting cycles capable of working below 1200 K. In 1986, Beghi[135] published a summary of a decade of the Ispra research program. The first phase of the research program was focused on the "Mark 1" cycle, which proceeds as follows:[135]

$$CaBr_2 + 2H_2O \rightarrow Ca(OH)_2 + 2HBr \text{ at } 1050\ K \quad (31)$$

$$2HBr + Hg \rightarrow HgBr_2 + H_2 \text{ at } 450\ K \quad (32)$$

$$HgBr_2 + Ca(OH)_2 \rightarrow CaBr_2 + HgO + H_2O \text{ at } 450\ K \quad (33)$$

$$HgO \rightarrow Hg + {}^1/_2O_2 \text{ at } 900\ K \quad (34)$$

Experimental tests were performed on each of the chemical reactions. The studies on Mark 1 concluded that thermochemical water splitting was feasible, but was not suited for large-scale industrial applications due to the presence of mercury. The copper cycle (Mark 1C), the manganese cycle

(Mark 2), the vanadium cycle (Mark 3), etc., were explored, trying to avoid the use of mercury; however, the more promising cycles were those using mercury. Study of Mark 1 and these first exploratory cycles was stopped because another family of cycles appeared using more common elements, iron and chlorine, in the second phase of the research program.

The Fe−Cl family of cycles, for instance, the Mark 15 cycle, was studied during the second phase of the Ispra research program.[135] The Mark 15 proceeds as follows:

$$3FeCl_2 + 4H_2O \rightarrow Fe_3O_4 + 6HCl + H_2 \text{ at } 650-700\ ^\circ C \quad (35)$$

$$Fe_3O_4 + 8HCl \rightarrow FeCl_2 + 2FeCl_3 + 4H_2O \text{ at } 200-300\ ^\circ C \quad (36)$$

$$2FeCl_3 \rightarrow 2FeCl_2 + Cl_2 \text{ at } 280-320\ ^\circ C \quad (37)$$

$$Cl_2 + H_2O \rightarrow 2HCl + {}^1/_2O_2 \text{ at } 600-700\ ^\circ C \quad (38)$$

For eq 35, a bench-scale, semicontinuous moving-bed reactor having a 5 cm inner diameter was successfully operated. A high conversion of $FeCl_2$ (80−90%) was obtained. However, the moving-bed reactor is unsuitable for large-scale operation, as it leads to excessive column diameters. The greatest problem exists in the thermal decomposition of ferric chloride (eq 37). The chemical equilibrium is unfavorable, and the chemical conversion lies around 10%. The thermal efficiency was calculated to be about 20% due to the large energy demand for the thermal decomposition of ferric chloride. The corrosivity of the chemicals involved was also critical. Modification of the processes and various alternatives for the thermal decomposition of $FeCl_3$ were examined—use of selective membranes, electrolysis of $FeCl_3$ in aqueous media or in fused salts, the introduction of a supplementary chemical reaction, etc.—but no suitable solution was found.

3.3. Sulfur Family

The sulfur family of cycles was studied in the third phase of the program.[135] The primary reaction involved in the sulfur family of cycles is the decomposition of sulfuric acid. The process proceeds in three stages as follows:

$$H_2SO_4{-}H_2O \rightarrow H_2SO_4 + H_2O \text{ at } 600\ K \quad (39a)$$

$$H_2SO_4 \rightarrow H_2O + SO_3 \text{ at } 600-1000\ K \quad (39b)$$

$$SO_3 \rightarrow SO_2 + {}^1/_2O_2 \text{ at } >1100\ K \quad (39c)$$

After concentration of the sulfuric acid (eq 39a), it vaporizes and decomposes into SO_3 and H_2O at temperatures ranging from 600 to 1000 K, and by further heating (to over 1100 K) in the presence of solid catalyst, SO_3 decomposes into SO_2 and O_2. These are all endothermic reactions. In practice, these processes can be performed as one heating step. Thus, the overall reaction, with the total endothermic heat, can be given by

$$H_2SO_4\ (aq, inf) \rightarrow H_2O + SO_2 + {}^1/_2O_2 \quad \Delta H^o = 371\ kJ \quad (40)$$

where "aq, inf" means an aqueous solution of infinite dilution.

3.3.1. Westinghouse Cycle (Mark 11)

The Westinghouse cycle (Mark 11 in the Ispra scheme) combines the decomposition of sulfuric acid (eq 40) with a subsequent electrochemical process, to make a "hybrid" two-step cycle:[136−145]

$$2H_2O + SO_2 \rightarrow H_2SO_4 + H_2 \text{ at } 80\ ^\circ C \text{ (electrolysis)} \quad (41)$$

The process consists of four major components: the electrolyzer, the acid decomposer, the concentrator, and the separation system.[139] The Westinghouse cycle can practically proceed in "two steps"; however, it is not a pure thermochemical but a hybrid electrochemical−thermochemical cycle. Electrical power is required in the electrolysis step, but the electrolysis of a mixture of sulfur dioxide and water can theoretically be conducted at a much lower potential ($E^o = -0.17$ V) than a direct water electrolysis ($E^o = -1.23$ V). Therefore, the electrical power required is theoretically reduced. However, in practice, overpotential and cell losses can significantly increase the energy required, and there are large gaps between the theoretical and experimental electrode potentials for the electrolysis process of a mixture of sulfur dioxide and water.[137,138] Jeong et al.[139] reported that if the efficiency is defined by the $-\Delta H$ value for $H_2 + {}^1/_2O_2 = H_2O(g)$ at 298 K (LHV of 1 mol of H_2) divided by the total energy input from a "nuclear reactor" (assuming thermal to electrical efficiency is 45%), then the maximum energy efficiency with an actual electrode potential is about 47% (55% if based on HHV) (conditions: 1200 K, 10 bar, 60 mol % [H_2SO_4] for decomposer, 70 wt % [H_2SO_4] for electrolyzer), whereas the ideal efficiency with a theoretical electrode potential is about 74% under identical conditions. When using concentrated solar radiation as the thermal energy source instead of an HTGR, the energy efficiencies of the solar collector and solar receiver/reactor must be considered as well.

In Jeong's report,[139] it was indicated that the major factor affecting efficiency is the electrode overpotential. The efficiency gained by reducing the overpotential would be possible through the development of advanced electrolysis materials and configurations, because there are still large gaps between the theoretical and experimental values of the electrode potential. This cycle has been experimentally investigated at the Research Center in Jülich, Germany, in cooperation with the JRC in Ispra.[139] For the electrochemical step, construction of a three-compartment electrolytic cell for the cathodic production of 10 L/h of hydrogen and the anodic oxidation of SO_2 was undertaken. The cell was operated at pressures up to 15 bar at 80 °C, and a 600 h test run was successful. The cell voltage was about 0.6 V at 100 mA/cm^2 and 0.8 V at 200 mA/cm^2. With an improved tungsten carbide coated cathode, reductions of the cell voltage of 0.05 and 0.1 V, respectively, were obtained. In the hybrid thermochemical−electrochemical cycles of the Westinghouse and Mark 13 cycles (detailed below), the most important criterion is the minimum voltage for electrochemical step efficiency. There is always a compromise between acid concentration and cell voltage.

The other key process of the Westinghouse cycle is the high-temperature thermal decomposition of sulfuric acid, which poses severe challenges for materials due to the corrosivity of sulfurous acid at high temperature. This is a common critical problem to cycles of the sulfur family, such as the Mark 13 and S−I cycles (detailed below). Extensive study of sulfuric acid decomposition was performed in the Ispra program, with various contracts to industrial companies and universities.[135] Many tests were performed to verify the influences of various parameters: temperature in the range

of 900−1200 K, type of catalyst, pressure up to 3 bar, and long exposure at high temperature. A laboratory test facility working under steady-state conditions was built and operated successfully. However, for a large-scale industrial plant, the metallic materials corrosion problem must be solved economically for the steps involving concentration, evaporation, and decomposition of H_2SO_4, particularly when metallic materials are required for the heat exchangers. Commercial materials that can withstand those conditions are not yet available.

In early versions of the sulfur family of cycles, such as the Westinghouse Mark 11 cycle and the Mark 13 cycle, the decomposition of sulfuric acid (eq 40) was carried out in tube and shell heat exchangers. Later, in the Ispra research program, hot air was used as a vector, and energy was transferred by direct contact between the hot air vector and reactants; this scheme was called the Cristina process.[135,140−142] The air is superheated and brought into direct contact with a liquid solution of H_2SO_4, so that the three endothermic steps (concentration, evaporation, and decomposition) can be carried out in adiabatic reactors, which can be constructed of acid-resistant bricks. It is basically an application of an industrial process used for sulfuric acid synthesis. No exchangers constructed of metallic materials need contact corrosive reactants. Using the operating conditions of the Cristina process, long-term corrosion tests were started in a corrosive atmosphere having a composition corresponding to the H_2SO_4 decomposition using an acid gas/hot air mixture in the Ispra program. Afterward, a new Cristina process was proposed and evaluated by Bilgen et al.,[140,142] in which hot oxygen was used as a vector instead of hot air to improve efficiency and reduce cost. The HHV efficiency of the Westinghouse cycle (Mark 11) with the new Cristina process was calculated to be 38% when the overall conversion efficiency of the process heat to electricity in the main power plant was assumed to be 38%, and the conversion efficiencies from recovered heat to electricity within the process were estimated for Rankine cycles (3.95−9.81%).[140]

Material selection for the acid decomposition step is still challenging as is electrode selection for the electrochemical step.[135,137] Materials such as silicon, silicon carbide, silicon nitride, and silicide-coated Incoloy 800A have shown resistance to highly corrosive sulfuric acid at elevated temperatures. However, these materials are brittle in most cases, and therefore their use is limited to designs having low tensile stresses. The European HYTHEC program, started in 2004, is a European collaboration to develop promising CO_2-free thermochemical cycles, primarily the S−I cycle, and, to a lesser extent, the Westinghouse cycle, to investigate their potential for massive hydrogen production.[143,144] This program deals with the development of the thermal decomposition of sulfuric acid at high temperatures including the material selection.

In the current U.S. DOE Hydrogen Program,[44] the Nuclear Hydrogen Initiative (NHI), sponsored by the Office of Nuclear Energy (NE), is conducting research into developing commercial-scale production of hydrogen using nuclear heat. In the area of thermochemical cycles, the NHI is investigating the sulfur-based S−I and Westinghouse cycles. In this project, Sandia National Laboratories (SNL) is developing and testing the H_2SO_4 decomposition section.[146] The H_2SO_4 decomposition was first demonstrated in an apparatus using superalloys for the high-temperature regions. They reported acid decomposition experiments successfully performed up to 875 °C and 11 bar. Their recent work has focused on a more robust and integrated configuration based on ceramic materials (SiC) in the high-temperature regions and glass- or Teflon-lined steel in the low-temperature areas. The new configuration uses a bayonet heat exchanger with SiC components as an integrated vaporizer, superheater, and decomposer, mitigating the corrosion and complexity issues of previous systems. In the design, the acid boiler and decomposer are incorpoated into a single SiC-based unit, which also provides heat recuperation between the reactor effluent and incoming liquid acid stream. The acid conversion fraction was approximately 65% at 850 °C under ambient pressure.

It has been proposed that the high-temperature thermal decomposition step (eq 40) be carried out using concentrated solar radiation as the energy source instead of nuclear heat; therefore, a "solar" Cristina process was designed and evaluated.[141] In the process, to avoid a shutdown of operations at night in the solar hydrogen production plant, a process was devised in which SO_2 is produced during the daytime hours and the decomposer is operated in reverse as a sulfuric acid synthesizer using a small portion of the stored SO_2 to produce process heat during nighttime operation. During night operation, the last two processes of the acid decomposition, eqs 39b and 39c, are reversed, using oxygen from the air. In this manner, the heat generated is supplied to the chemical process itself to keep the equipment at a nearly constant operating temperature, reducing thermal inertia and startup problems. The Cristina system with hot air as a vector was conceived to produce 10^6 mol of SO_2/h, coupled to a central receiver solar system producing 10^6 GJ of heat/year. The Westinghouse cycle (Mark 11) with the solar Cristina process was assumed to produce 0.67×10^6 GJ of hydrogen/year using electric energy supplied from the outside. With this assumption, the total cost of production was estimated to be $68/GJ of hydrogen (1986).[141] Some problems were pointed out for this solar process: expensive materials (Incoloy 800 and stainless steel) for the heat recuperators, which are in contact with corrosive fluids at mild and high temperatures, discharging a trace amount of SO_2 to the atmosphere, etc. In addition, the solar receiver must contain the reactors, which must be developed.

Later, the Westinghouse cycle (Mark 11) with the new Cristina process using oxygen as a vector was also adapted to utilize a solar heat source.[142] A 10^6 GJ/year central receiver solar system was assumed, along with the Cristina process producing SO_2 at 10^6 mol/h and the plant producing 0.63×10^6 GJ of hydrogen/year. The overall HHV efficiency was calculated to be 37.79%, defined as the HHV of the hydrogen produced divided by the total thermal energy input to the process, assuming the conversion efficiency of thermal energy to electricity was 38%, and therefore not including the energy efficiencies of the solar collector and receiver. The solar hydrogen cost, including the costs of the Cristina process, the central receiver solar system, and the electrochemical process, was estimated to be from $15 to $70 per GJ of hydrogen (1988), depending on the cost parameters. The solar hydrogen cost was most sensitive to the process heat cost. The typical hydrogen cost was $33/GJ for a 15% capital charge rate, $10/GJ for solar thermal energy, and $0.02/kWh for electrical energy. This result can be compared to the cost result recalculated for the same conditions with the solar Cristina-Mark process:[141] $53/GJ. The typical solar

hydrogen cost of $33/GJ can be also compared to that of nuclear hydrogen—about $10/GJ.[140]

In the European HYTHEC program,[143,144] researchers at the DLR analyzed and evaluated the Westinghouse cycle with regard to its potential for coupling to a solar central tower and receiver system in a large-scale hydrogen production plant.[145] They selected a solar-only powered plant and first calculated the heat balance and the solar field geometry. The process flow sheet was designed by assuming operation only in the daytime, without expensive, demanding thermal or chemical storage. Two different sizes of solar-only plant were taken into consideration—the smaller one providing an annual power average of 50 MW_{th}, and the larger one, 300 MW_{th} as thermal power entering the chemical part of the plant. About 150 and 840 MW_{th} energy inputs are required for the entire plant, respectively. In their concept, a solar central tower is used as the solar concentrating system, and the acid decomposition takes place in the solar receiver at a temperature of 1200 °C; the equilibrium conversion of the acid to sulfur trioxide is more favorable if the temperature is higher, and a temperature of 1200 °C is achievable with the solar central receiver system. Six clusters of receivers were assumed to be located along the six sides of the hexagonal tower top. Average tower heights were 215 and 370 m for the 50 and 300 MW_{th} plants, respectively. Assuming an efficiency of 75% for the heat exchangers, a 38% HHV efficiency was reported. However, it is not clear whether the theoretical or experimental electrode potential was used in their evaluation of the electrochemical step efficiency, and, as discussed above, this can strongly affect the efficiency.

In the DLR solar plant concept, the H_2SO_4 evaporation and decomposition processes are planned to take place in the solar receiver. However, to date, no sufficient or efficient technology has been developed to carry out these processes using concentrated solar radiation. Therefore, the DLR researchers are developing a solar direct absorbing volumetric receiver−reactor in which a porous absorber is used.[144,145] Liquid sulfuric acid is injected into a solar-heated ceramic porous absorber located behind a quartz window in the reactor. The porous absorber is directly irradiated by concentrated solar radiation through the quartz window to evaporate and decompose the sulfuric acid. The temperature of such a volumetric absorber can reach up to 1300 °C; therefore, a catalyst is not necessary. This point is very important because catalysts for sulfur splitting are very short-lived. Because different temperature levels are required for the evaporation (600−1000 K) and the decomposition of SO_3 to SO_2 (>1100 K), two porous absorbers are implemented to meet the required temperature levels individually. The evaporation occurs in a foam with a large inner surface area located behind the window, and the decomposition takes place in a honeycomb structure located behind the foam. A solar demonstration was carried out in a solar furnace. The largest chemical conversion was about 55%, and the efficiency of the reactor was in the range of 5−15%.

3.3.2. Mark 13 Cycle

The Mark 13 cycle is also a hybrid process, coupling eq 40 with the following two reactions, including one electrochemical step:[135,138,147,148]

$$2H_2O + Br_2 + SO_2 \rightarrow H_2SO_4 + 2HBr \text{ at } 27\ ^\circ C \quad (42)$$

$$2HBr \rightarrow H_2 + Br_2 \text{ at } 100\ ^\circ C \text{ (electrolysis)} \quad (43)$$

The minimum theoretical potential of the electrolysis of eq 43 is 0.56 V.[138] The efficiency of the overall process was given as 37.3% at a cell potential of 0.8 V.[147] The first ever demonstration of a complete thermochemical water splitting was performed by the Mark 13 in 1978 using a bench-scale continuous process.[135] The plant was constructed mainly of glass and quartz equipment connected with PTFE tubing, and at atmospheric pressure, it could be successfully operated at 100 L/h for over 150 h.

An assessment of solar hydrogen production using the Mark 13 cycle was evaluated by Bilgen and Joels.[148] A central tower cavity receiver was used, and the helium heat transfer fluid was assumed to leave at 900 °C from the solar receiver, enter the SO_3 decomposer, and return at 800 °C to the receiver. The central receiver system was assumed to receive 1.4 GJ $\times$ 10^6 GJ/year. The receiver had an overall efficiency of 90%. The plant scale was 0.912 $\times$ 10^6 GJ/year of hydrogen. The SO_3 decomposition temperature was assumed to be 1083 K, and the electrolytic cell voltage for the HBr electrolyzer was assumed to be 0.7 V at 373 K, with an electrolyzer efficiency of 98%. A flow sheet of the solar process based on the Mark 13 cycle was developed to operate using an intermittent heat supply (daytime only) from the central tower system and a continuous electric energy supply from outside (24 h). The overall efficiency of the process was reported to be 37% excluding solar energy collection (21% including it) for 2000 kWh m^{-2} $year^{-1}$ total irradiance at normal incidence (the solar field was about 1.5 $\times$ 1.5 km). The solar hydrogen cost was estimated to be $52/GJ of hydrogen (1985).

3.3.3. S–I (I–S) Process (GA Process or Mark 16)

The sulfur-iodine (S−I) or iodine-sulfur (I−S) process is a pure thermochemical cycle with three steps, combining eq 40 with the following steps:[135,149−172]

$$2H_2O + xI_2 + SO_2 \rightarrow H_2SO_4 + 2HI_x \text{ at } 100\ ^\circ C \text{ (Bunsen reaction)} \quad (44)$$

$$2HI_x \rightarrow xI_2 + H_2 \text{ at } 300-500\ ^\circ C \quad (45)$$

HI_x represents a mixture of several polyiodides formed in solution in eq 44. This cycle is Mark 16 in the Ispra scheme. Because General Atomics (GA) of San Diego, CA, has done a great deal of development on this cycle, the cycle is also known as the "GA process". Compared to Mark 13, the decomposition of HI_x requires much less energy than the corresponding decomposition of HBr, whereas the acid formation of eq 44 in the S−I process becomes more difficult than that of eq 42 in Mark 13. This reaction is called the "Bunsen reaction", producing two acids, hydriodic acid and sulfuric acid, from water, sulfur dioxide, and iodine in an aqueous solution. The Bunsen reaction requires surplus water to proceed. One of the difficulties of this cycle lies in the separation of the two acids in this step. In the Mark 13 cycle, HBr and H_2SO_4 can be easily separated by distillation of the $HBr/H_2SO_4/H_2O$ solution. However, separation by simple distillation cannot be applied to an $HI/H_2SO_4/H_2O$ solution, because HI is oxidized by SO_2, which can be formed by the reverse Bunsen reaction as the acid concentration increases. Many kinds of separation processes have been proposed and tested on the $HI/H_2SO_4/H_2O$ solution. After separation of the two acids, generally they are purified, concentrated, and decomposed in separate reactors in the gaseous phase.

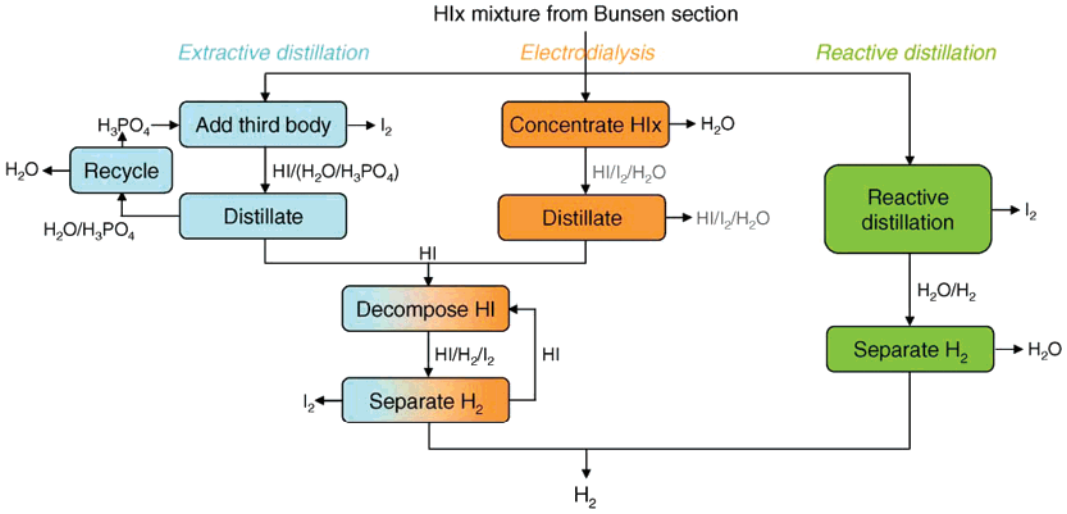

Figure 25. Schematic representation of the main options for the HI section in the S−I cycle. (Reprinted with permission from ref 170. Copyright 2006 Elsevier Ltd.)

Extensive research programs were conducted on the S−I process from the mid 1970s through the mid 1980s. In addition to GA, this process has been studied by the JRC Ispra, Rheinisch Westfälische Technishe Hochschule (RWTH) in Aachen, le Commissariat à l'Engergie Atomique (CEA) in France, and the Japanese Atomic Energy Agency (JAEA). Some studies included bench-scale tests of the process.[149,153−155] The JAEA has successfully demonstrated "continuous" hydrogen production at a rate of about 32 L/h for 20 h.[154,155]

In the JAEA bench-scale demonstration,[154,155] H_2SO_4 and HI_x were separated by gravity because the acid solutions are virtually immiscible. The upper phase contains almost all of the H_2SO_4, and the lower phase contains most of the HI_x—the separated hydriodic acid phase dissolves the iodine and is denoted as the HI_x phase. After purification, hydriodic acid was separated from iodine by distillation. The HI was then decomposed to produce hydrogen. Similarly, the separated sulfuric acid phase was purified, concentrated, vaporized, and decomposed to produce oxygen. However, the hydrogen production efficiency in the bench-scale demonstration was less than 10%; efficient separation of HI from the HI_x solution and enhancement of HI conversion were required to improve the hydrogen production efficiency.[159] In the Ispra Mark 16, it was planned to separate HI from the HI_x solution using liquid SO_2 as an extracting agent—HI is soluble in liquid SO_2 but H_2SO_4 is not.[135,149,151] Different approaches have been also tested to solve this difficulty, for example, the addition of other substances of inorganic or organic compounds and the use of membranes.[135,152,158,159] Three main routes are currently being considered for the separation of the HI_x solution from the Bunsen reaction, as Vitart et al.[170] have summarized (Figure 25): extractive distillation,[153] electrodialysis,[158,159,161] and reactive distillation.[172] The reactive distillation was proposed by RWTH Aachen,[172] in which HI_x distillation and HI decomposition are carried out in the same reactor at 350 °C. A liquid−gas equilibrium is obtained in the middle of the column. I_2 is dissolved in the lower liquid phase, and a mixture of gaseous H_2 and water is recovered at the top of the column.

The energy efficiency of the hydrogen production is affected by the apparatus selection. Norman et al.[153] first evaluated an efficiency of 47%, based on a flow sheet in which H_2SO_4 was separated from water by a constant-pressure, multieffect distillation, and HI was separated from HI_x using phosphoric acid that had to be regenerated. Brown et al.[156] and Goldstein et al.[157] investigated the heat/mass balance of the flow sheet featuring reactive distillation of the HI_x solution. Goldstein et al.[157] found an upper bound of the HHV efficiency of 0.51, defined by eq 13 with $W = 0.5$. They indicated that the separation between water and sulfuric acid, on the one hand, and water, HI, and iodine, on the other hand, seems to be the most energy consuming. The best estimate of the efficiency was found to be between 33 and 36%. The JAEA has developed the I−S process using an EED (electro-electrodialysis) cell for HI concentration and a hydrogen permselective membrane reactor for decomposition of HI.[158,159,161] They developed its flow sheet and estimated the upper bound of thermal HHV efficiency to be 57%, assuming electricity generation efficiency of 40%. The efficiency based on more realistic parameters from experimental results was determined to be 34%.

As mentioned above, the JAEA currently has great research and development activity in the I−S cycle. Their bench-scale study was completed in the middle of 2005, and pilot-scale tests are planned for a hydrogen production rate of about 30 Nm^3/h.[160] The S−I cycle is also the main target of the European HYTHEC project[143,144] that started in 2004, as described above. The HYTHEC project aims to conduct flow-sheeting, industrial scale-up, and safety- and cost-modeling and to improve the fundamental knowledge and efficiency of the S−I cycle's H_2 production step.

Corrosive chemicals such as H_2SO_4, HI, and I_2 are used at high temperatures in the S−I process and, thus, corrosion-resistant materials are necessary. Corrosion tests for material selection have been carried out,[159,160,166−170] and candidate materials studied by the JAEA are presented in ref 159.

The JAEA roughly estimated the hydrogen production cost of their I−S cycle and compared the cost with that produced by conventional steam re-forming with fossil fuel.[155] The hydrogen cost by the I−S cycle coupled to an HTGR was 1.6 times higher than that by the steam re-forming process. If a CO_2 fixation cost (21 ¥/kg of CO_2) is taken into consideration, the hydrogen cost from the I−S cycle is somewhat lower than that from steam re-forming.

As described above, in the U.S. NHI, the S−I cycle is a major target of development in the area of thermochemical cycles for nuclear hydrogen production.[146] The objectives

are as follows: evaluate the potential of the S−I cycle for hydrogen production using nuclear energy, perform an integrated laboratory-scale experiment to demonstrate closed-loop operation of the S−I cycle, and provide the technical basis for scaleup decisions on a 500 kW pilot-scale experiment. This project is being performed as part of the U.S. DOE, French-CEA International Nuclear Energy Research Initiative agreement. As mentioned above, the SNL is developing and testing the H_2SO_4 decomposition section. The CEA is designing and testing the Bunsen reaction section, and GA is developing and testing the HI decomposition section. The development of HI decomposition is based on an extractive distillation approach, which allows I_2 be separated from the HI_x solution feed stream before decomposition. The experiments have focused on the liquid−liquid extraction step, where H_3PO_4 strips the HI and water from the HI_x feed solution. The optimum H_3PO_4 concentrations are currently being identified. The HI and H_2SO_4 sections, developed in the United States, will be integrated with the French CEA Bunsen section and assembled into an integrated experiment late in 2007. Integrated laboratory-scale experiments are planned for 2008.

As for the solarization of the S−I cycle, the HYTHEC project[143−145] is investigating a solar primary energy source for the H_2SO_4 decomposition step of the S−I and Westinghouse cycles, as mentioned above. Huang and T-Raissi[171] also started to analyze the S−I cycle for solar hydrogen production. They conducted a flow sheet analysis on the acid decomposition process and, on the basis of the results, provided revised flow sheets of the S−I cycle that present better processes to couple with inherently transient heat sources such as solar energy.

3.4. UT-3 Cycle

The UT-3 cycle is a purely thermochemical process consisting of the following four steps developed at University of Tokyo:[173−179]

$$CaBr_2(s) + H_2O(g) \rightarrow CaO + 2HBr(g) \text{ at } 700-760\ ^\circ C \quad (46)$$

$$CaO(s) + Br_2(g) \rightarrow CaBr_2(s) + 0.5O_2(g) \text{ at } 500-600\ ^\circ C \quad (47)$$

$$Fe_3O_4(s) + 8HBr(g) \rightarrow 3FeBr_2(s) + 4H_2O(g) + Br_2(g) \text{ at } 200-300\ ^\circ C \quad (48)$$

$$3FeBr_2(s) + 4H_2O(g) \rightarrow Fe_3O_4(s) + 6HBr(g) + H_2(g) \text{ at } 550-650\ ^\circ C \quad (49)$$

The reactions in eqs 46 and 49 are endothermic. All of the reaction steps of the UT-3 cycle are gas−solid reactions. The process contains four reactors and can be carried out in a gas cyclic mode by transferring the gaseous reactant from one reactor to another reactor while the solid reactants remain in the same reactor. However, the reactions in the reactors have to be switched (for example, eq 46 → 47, eq 48 → 49) by reversing the direction of the gas cycle. Kinetics studies, bench-scale tests, development of the solid reactant, and engineering evaluations have been extensively carried out.[173−179] The bench-scale test plant, called MASCOT, was constructed in 1982. This plant was designed to produce 3 L/h of hydrogen. Hydrogen was produced smoothly during the operation of 11 cycles.[175] A commercial-size plant was conceptually designed and its hydrogen production cost evaluated, for an output of 20000 Nm^3/h with an HTGR primary energy source.[173,178] The HHV efficiency of the commercial-size plant was calculated to be >40%, defined as the HHV of hydrogen divided by the thermal energy supplied from the HTGR, if the power generation efficiency of the net recovered heat was >0.25.[173,178] The flow sheet of the UT-3 plant using a membrane gas separator was later proposed, which showed the possibility that more than about 45% of the HHV efficiency was obtained if the power generation efficiency was >0.25.[177] The cost of the produced hydrogen was estimated to be 47.8 ¥/Nm^3 of hydrogen (1997), with no membrane application, and 44.5−47.7 ¥/Nm^3 with membrane application, depending on the heat recovery rate.

A new UT-3 process was reported later in which all four reactions are carried out adiabatically using a heat carrier vector (steam or an inlet gas).[175] If the plant produces hydrogen at 30000 Nm^3/h, the HHV efficiency was improved to 47% by the adiabatic UT-3 process. The efficiency of the adiabatic UT-3 process increased to 49% with credit to excess thermal energy.

Recently, however, Teo et al.[180] presented a critical assessment of the actual energy efficiency that could be realized in the UT-3 cycle. They made the following points regarding Sakurai's calculations:[177]

- The low-temperature waste heat (550 K) in Sakurai's calculation should be converted to electricity with an efficiency of 17% to generate 1.35 MW of power. However, Sakurai used 100% efficient compressors in the calculation. Teo calculated that 1.75 MW was required for the three compressors of the UT-3 cycle if a practical compressor efficiency of 75% was used. Thus, 0.45 MW of additional power has to be generated. This reduces the HHV efficiency (with a power generation efficiency of 45%) to 44%.
- It was found that the H_2 production step (eq 49) has the greatest impact on the process efficiency. With 100% conversion assumed in Sakurai's calculation, the gas-phase composition from the reactor for eq 49 is inconsistent with thermodynamic equilibrium. The hydrogen concentration assumed for 726−833 K can be approached only when the temperature approaches 1000 K. Such an operating temperature is not feasible because $FeBr_2$ sublimes above 850 K.
- The gaseous HBr and H_2 effluent from the reactor (eq 49) is separated using a suitable membrane or bubbled through water for the dissolution of HBr, forming hydrobromic acid. It was found that the UT-3 process is viable only if high-temperature membrane separation of hydrogen in the presence of HBr proves to be possible. Even in this case, additional energy would be required to drive the hydrogen recompression, reducing the HHV efficiency to 30%.
- After the completion of one cycle, the reaction in the reactors has to be switched, and the gas flow is reversed. When the gas flow is reversed, the piping in the vicinity of the reactors undergoes great temperature changes. To reduce the time required to reach steady state after flow reversal, additional heat may be necessary. This reduces the upper bound of the HHV efficiency from 30% to around 15%.

Thus, Teo et al.[180] pointed out that when using nuclear heat as the energy source, the HHV efficiency is <15% (13% with respect to LHV). Also, Lemont et al.[181,182] recently conducted a physicochemical and thermodynamic investigation, as well as technological and chemical assessment of the UT-3 cycle. They suggest that the physicochemical

properties of the solid and gaseous reactants would make the operation of an industrial process very difficult.

Bromide and bromide compounds are corrosive in the presence of H_2O, and cost-effective corrosion-resistant materials are necessary for industrial large-scale applications. The toxicity of the reactants also must be taken into consideration.

The solar UT-3 thermochemical cycle was also evaluated. Sakurai et al.[183] assumed two different operational modes:

- The thermochemical process is run in a cyclic manner, consisting of both day and night operations. During the daytime, high-temperature solar heat is used to produce some intermediate chemicals, which are stored. The stored chemicals are used during night operation.
- The thermochemical process is run continuously. During the daytime, high-temperature solar heat is used directly in the chemical process and is also stored in a thermal storage system. At night, thermal energy is supplied to the process from the thermal storage system.

A central tower receiver system was used for the evaluation. For cyclic operation, it was concluded that there are several disadvantages: a one cycle per day operation requires large equipment; steam is necessarily condensed; an aqueous solution of HBr is stored for night operation; and a chemical heat pump system using hydrogen from the UT-3 process is coupled to improve the efficiency, increasing cost. For continuous operation, the HHV efficiency was evaluated to be 47% with and 50% without credit to excess thermal energy. However, the energy efficiencies of the solar collector and receiver must also be considered. The continuous operation case is ideal, because no sufficient technology has been developed for such a high-temperature thermal storage system (>1033 K) on an industrial scale.

Teo et al.[180] also made a critical assessment of the actual energy efficiency for the solar UT-3 cycle. They also took into account the combined efficiency of the solar furnace/central receiver system (29−56%) and the thermal energy storage (98.8%). As discussed above, they calculated the upper bound of the HHV efficiency for the UT-3 process to be around 15%, and, thus, that for the solar UT-3 process should be <8%, which is less than the reference range of 8−13% for PV followed by water electrolysis.[180,184−186]

3.5. Hybrid Copper Chloride Cycle

The hybrid copper chloride cycle[187] proceeds as follows:

$$2Cu(s) + 2HCl(g) \rightarrow H_2 + 2CuCl(s) \text{ at } 425\ ^\circ C \quad (50)$$

$$4CuCl(s) \rightarrow 2Cu(s) + 2CuCl_2(s) \text{ (electrochemical)} \quad (51)$$

$$2CuCl_2(s) + H_2O \rightarrow Cu_2OCl_2(s) + 2HCl(g) \text{ at } 325\ ^\circ C \quad (52)$$

$$Cu_2OCl_2(s) \rightarrow 2CuCl(s) + {}^1/_2O_2 \text{ at } 550\ ^\circ C \quad (53)$$

The idealized efficiency of the cycle was estimated to be about 40% based on LHV. However, critical thermodynamic data must be determined experimentally, such as the enthalpy of formation of Cu_2OCl_2 and its heat capacity as a function of temperature. Fabrication of batch and continuous electrochemical cells for the reaction in eq 51 is underway at both Argonne National Laboratory (ANL) and the Gas Technology Institute (GTI) in the United States. In addition, the optimum operational parameters for the reactions in eqs 52 and 53 must be identified, which are not as well understood as the reactions in eqs 50 and 51.

4. Summary

Thermochemical water-splitting cycles producing hydrogen are reviewed, emphasizing those that have promise to be coupled with concentrated solar high-temperature heat available in "sunbelt regions". There are solar peculiarities in comparison to conventional thermochemical processes: high thermal flux density and frequent thermal transitions because of the fluctuating insolation. Therefore, conventional industrial thermochemical processes are generally not suitable for solar-driven processes. Thus, adaptation of the process to solar high-temperature heat is required.

A chemical process should be operated most efficiently without interruption. However, the solar high-temperature heat supply is intermitten; that is, it is interrupted during the night and by cloud passage during the day. To solve this problem, it is ideal to store solar high-temperature heat in a thermal storage system and use the stored thermal energy continuously (24 h a day) for the process. However, thermal storage at temperatures above 1000 K is very difficult to achieve on an industrial scale.

Generally speaking, even for a solar thermochemical process that is planned to be operated only during daytime, chemical engineers are not in agreement as to whether the chemical process can be stopped, for example, for 30 min by cloud passage, and then operated effectively again.[141] The thermal inertia problems and startup difficulties in an intermittently operated system will be more severe if the chemical plant is larger, with larger heat capacities of the reactors, separators, piping, etc. It is also difficult for a complicated process with a number of steps (e.g. reaction, separation, and concentration) to be effectively operated with quick response to an intermittent heat supply from concentrated solar radiation. From this perspective, for the development of an effective solar thermochemical process, the solar reactor should have a quick response to the intermittent heat supply, and there should be as few steps as possible in the process.

Section 2 reviews two-step water-splitting processes involving redox metal oxides. The chemistry of the processes is well discussed. The reactions are very simple, as the process contains only a few separation steps in which technical difficulty does not lie. However, the two-step thermochemical cycle requires heat above 1500 K, minimum. This presents a challenge to solar reactor concepts and has resulted in the research and development of several types of windowed solar reactors. Direct irradiation of the redox working material enables the reactor to respond very quickly to the intermittent heat supplied by concentrated solar radiation. For iron-based oxide processes, several types of windowed solar reactors are currently being developed—monolithic, foam, rotary-type, CR5, and internally circulating fluidized bed reactors. In these reactors, both the thermal reduction and hydrolysis steps are planned to be carried out in a single reactor. However, basic kinetic studies on the thermal reduction and hydrolysis reactions are not yet sufficient to prove the feasibility of the reactor. The kinetics of the reactions must be an important key factor for each reactor. Thus, further development of active redox materials and devices will have a very large impact on the improvement of these reactors. Further investigation of the kinetics of the reactions in the iron oxide based processes is urgently

needed. For the ZnO process, the kinetics of the reactions are being investigated well. However, two reactors are required in the current operational concept: one for the thermal reduction of ZnO and one for the hydrolysis of Zn. The hydrolysis reactor still requires temperatures above 1023 K for Zn evaporation.[59] In addition, the volatile oxide process requires an additional product quenching system. In the case of the ZnO process, the product recombination of zinc vapor and oxygen severely decreases the chemical conversion in the absence of efficient quenching.

Some of the reactor concepts must use solar thermal energy for the hydrolysis step as well as for the thermal reduction step if the hydrolysis step requires high-temperature operation, and heat recovery from the high-temperature thermal reduction step is insufficient. The hydrolysis step in the metal oxide two-step cycles is exothermic, but, generally, the heat released is not particularly great. Heat losses are increased at higher temperature, and heating the steam feed to a higher temperature requires a higher temperature heat supply. This solar-driven hydrolysis step results in the heliostat field being utilized partially by the hydrolysis process. Normally, as heliostats make up well over 50% of the capital cost in a solar thermal hydrogen plant, this has a major effect on economics. Therefore, lower temperature operation of the hydrolysis step is an important factor. If the hydrolysis temperature is high, the heat recovery from the higher temperature thermal reduction step to the hydrolysis step must be efficiently conducted, as in the CR5 concept.[65]

The reactor concepts may be successful for a small-scale solar plant, for example, with a few hundred kilowatts of hydrogen production, although fundamental research, such as into active redox materials or device development, is still required in addition to engineering work on the reactor design and operation. However, in scaling up to multi-megawatts size, other engineering difficulties may be found, for example, in making a cluster of the reactors at the top of a solar tower. The scale of one reactor must be limited by the size limitations imposed by its quartz window and, thus, a cluster of the reactors will be required for multi-megawatt scaled application.

Section 3 reviews multistep water-splitting cycles capable of working below 1200 K. They are thermochemical cycles with more than three steps and thermochemical−electrochemical hybrid cycles with more than two steps. However, the promising cycles all suffer from the use of corrosive reactants and difficulties in the separation steps. For cycles with more than three reaction steps, the efficiency may be extensively reduced when coupled to concentrated solar high-temperature heat, instead of nuclear heat. The case of the UT-3 process is a good example, as pointed out by Teo et al.[180] From this point of view, the "two-step" Westinghouse cycle is the most promising process among the multistep water-splitting cycles capable of working below 1200 K, although it is not a pure thermochemical cycle. In hybrid cycles, an important criterion is the minimum voltage for electrochemical step efficiency. There is always a compromise between acid concentration and cell voltage. Material selection for the acid decomposition step of the Westinghouse cycle is also still challenging, as well as the electrode selections for the electrochemical step. The DLR is developing a solar direct absorbing volumetric receiver−reactor, which may have quick response to the intermittent heat supply. However, to allow the reactor concept to be upscaled to multi-megawatts scale, a cluster of the reactors is required at the top of a solar tower because the reactors are windowed.

5. References

(1) Kodama, T. *Prog. Energy Combust. Sci.* **2003**, *29*, 567.
(2) Johnston, G.; Lovegrove, K.; Luzzi, A. *Solar Energy* **2003**, *74*, 133.
(3) Mills, D. *Solar Energy* **2004**, *76*, 19.
(4) Kalogirou, A. S. *Prog. Energy Combust. Sci.* **2004**, *30*, 231.
(5) Meinecke, W.; Bohn, M. *Solar Energy Concentrating Systems, Applications and Technologies*; Becker, M., Gupta, B., Eds.; Müller Verlag: Heidelberg, Germany, 1995.
(6) Tyner, C.; Kolb, G.; Meinecke, W.; Trieb, F. *J. Phys. IV* **1999**, *9*, Pr3−17.
(7) Becker, M.; Meinecke, W. *J. Phys. IV* **1999**, *9*, Pr3−23.
(8) Geyer, E.; Schiel, W.; Zaraza, E.; González-Aguilar, R.; Nava, P. EUROTROUGH−a new parabolic trough collector with advanced light weight structure. In *Solar Thermal 2000, Proceedings of the 10th SolarPACES International Symposium on Solar Thermal Concentrating Technologies*; Kreetz, H., Lovegrove, K., Meike, W., Eds.; The Meeting Manager Pty Ltd: Sydney, Australia, 2000; p 45.
(9) Frier S. D.; Cohen, G. E.; Cable, R. G. An overview of the Kramer Junction parabolic trough solar electric system. In *Proceedings of ANZES 36th Annual Conference*, Christchurch, New Zealand, 1998; p 547.
(10) Price, H.; Lüpfert, E.; Kearney, D.; Zarza, E.; Cohen, G.; Gee, R.; Mahoney, R. *Sol. Energy Eng., ASME* **2002**, *124*, 109.
(11) Stuetzle, T.; Blair, N.; Mitchell, J. W.; Beckman, W. A. *Solar Energy* **2004**, *76*, 187.
(12) Tyner, C.; Kolb, G.; Praire, M.; Weinrebe, G.; Valverde, A.; Sanchez, M. Solar power tower development: recent experiences. In *Solar Thermal Concentrating Technologies, Proceedings of the 8th International Symposium*, Köln, Germany, 1996; Müller Verlag: Heidelberg, Germany, 1997; Vol. 1, p 193.
(13) Pacheco, J. E.; Reilly, H. E.; Kolb, G. J.; Tyner, C. E. Summary of the solar two test and evaluation program. In *Solar Thermal 2000, Proceedings of the 10th SolarPACES International Symposium on Solar Thermal Concentrating Technologies*; Kreetz, H., Lovegrove, K., Meike, W., Eds.; The Meeting Manager Pty Ltd: Sydney, Australia, 2000; p 1.
(14) Schmitz-Goeb, M.; Finker, A. The PHOEBUS solar power tower. In *Solar Thermal Concentrating Technologies, Proceedings of the 8th International Symposium*, Köln, Germany, 1996; Müller Verlag: Heidelberg, Germany, 1997; Vol. 1, p 269.
(15) Osuna, R.; Fernández, V.; Romero, M.; Blanco, M. PS10: A 10 MW solar tower power plant for southern Spain. In *Solar Thermal 2000, Proceedings of the 10th SolarPACES International Symposium on Solar Thermal Concentrating Technologies*; Kreetz, H., Lovegrove, K., Meike, W., Eds.; The Meeting Manager Pty Ltd: Sydney, Australia, 2000; p 13.
(16) Osuna, R.; Fernández, V.; Romero, S.; Romero, M.; Sánchez, M. PS10: a 11.0-MW solar tower power plant with saturated steam receiver. In *Proceedings of 12th SolarPACES International Symposium*, Oaxaca, Mexico, 2004; Carlos, R., Huacuz, J., Eds.; Electrical Research Institute: Mexico City, Mexico, 2004.
(17) Osuna, R.; Olavarría, R.; Morillo, R.; Sánchez, M.; Cantero, F.; Fernández-Quero, V.; Robles, R.; López Del Cerro, T.; Esteban, A.; Cerón, F.; Talegón, J.; Romero, M.; Téllez, F.; Marocas, M.; Martínez, D.; Valverde, A.; Monterreal, R.; Pitz-Paal, R.; Brakmann, G.; Ruiz, V.; Silva, M.; Menna, P. PS10, construction of a 11MW solar thermal tower plan in Seville, Spain. In *Proceedings of 13th International Symposium on Concentrated Solar Power and Chemical Energy Technologies*, Seville, Spain; Romero, M., Martínez, D., Ruiz, V., Silva, M., Brown, M., Eds; CIEMAT: Madrid, Spain, 2006.
(18) Heller, P.; Baumüller, A.; Schiel, W. EURODISH−the next milestone to decrease the costs of dish/stirling systems towards competitiveness. In *Solar Thermal 2000, Proceedings of the 10th SolarPACES International Symposium on Solar Thermal Concentrating Technologies*; Kreetz, H., Lovegrove, K., Meike, W., Eds.; The Meeting Manager Pty Ltd: Sydney, Australia, 2000; p 33.
(19) Luzzi, A. "Showcase" project: 2 MWe solar thermal demonstration power plant. In *Solar Thermal 2000, Proceedings of the 10th SolarPACES International Symposium on Solar Thermal Concentrating Technologies*; Kreetz, H., Lovegrove, K., Meike, W., Eds.; The Meeting Manager Pty Ltd: Sydney, Australia, 2000; p 83.
(20) Yogev, A.; Kribus, A.; Epstein, M.; Gogan, A. *Int. J. Hydrogen Energy* **1998**, *23* (4), 239.
(21) Segal, A.; Epstein, M. *J. Phys. IV* **1999**, *9*, Pr3−53.
(22) Segal, A.; Epstein, M. *Solar Energy* **1999**, *65* (4), 207.
(23) Segal, A.; Epstein, M. *Solar Energy* **2000**, *69* (Suppl.), 229.

(24) Frommherz, U.; Kräupl, S.; Wieckert, C.; Epstein, M.; Guillot, E.; Olalde, G.; Osinga, T.; Palumbo, R.; Robert, J.; Santen, S.; Semrau, G.; Steinfeld, A.; Vishnevetsky, I. Design of a pilot scale solar reactor for the carbothermic reduction of ZnO. In *Proceedings of 12th SolarPACES International Symposium*, Oaxaca, Mexico 2004; Carlos, R., Huacuz, J., Eds.; Electrical Research Institute: Mexico City, Mexico, 2004.

(25) Segal, A.; Epstein, M. Practical considerations in designing large scale "beam down" optical systems. In *Proceedings of 13th International Symposium on Concentrated Solar Power and Chemical Energy Technologies*, Seville, Spain; Romero, M., Martínez, D., Ruiz, V., Silva, M., Brown, M., Eds.; CIEMAT: Madrid, Spain, 2006.

(26) Epstein, M.; Odalde, G.; Santén, S.; Steinfeld, A.; Wieckert, C. Towards an industrial solar carbothermic production of zinc. In *Proceedings of 13th International Symposium on Concentrated Solar Power and Chemical Energy Technologies*, Seville, Spain; Romero, M., Martínez, D., Ruiz, V., Silva, M., Brown, M., Eds.; CIEMAT: Madrid, Spain, 2006.

(27) Tamaura, Y.; Utamura, M.; Kaneko, H.; Hasuike, H.; Domingo, M.; Relloso, S. A novel beam-down system for solar power generation with multi-ring central reflectors and molten salt thermal storage. In *Proceedings of 13th International Symposium on Concentrated Solar Power and Chemical Energy Technologies*, Seville, Spain; Romero, M., Martínez, D., Ruiz, V., Silva, M., Brown, M., Eds.; CIEMAT: Madrid, Spain, 2006.

(28) Yalçcin, S. *Int. J. Hydrogen Energy* **1989**, *14 (8*), 551.

(29) Funk, J. E.; Reinstrom, R. M. Energy requirements in the production of hydrogen from water. *Ind. Eng. Chem. Process Design Dev.* **1966**, *5*, 336.

(30) Sizmann, R. *CHIMIA* **1989**, *43*, 202.

(31) Lakshmanan, S.; Manasse, F.; Mathur, V. Production of fuels from high temperature solar thermal synthesis—economic analysis. In *Fundamentals and Applications of Solar Energy*; Farag, I., Melsheimer, S., Eds.; AIChE Symposium Series 198; AIChE: New York, 1998; Vol. 76, p 156.

(32) Grasse, W.; Tyner, C.; Steinfeld, A. *J. Phys. IV* **1999**, *9*, Pr3−9.

(33) Fletcher, E.; Moen, R. *Science* **1977**, *197*, 1050.

(34) Fletcher, E., *J. Minn. Acad. Sci.* **1984**, *49* (2), 30.

(35) Steinfeld, A.; Schubnell, M. *Solar Energy* **1993**, *50* (1), 19.

(36) Nakamura, T. *Solar Energy* **1977**, *19*, 467.

(37) Ihara, S. *Int. J. Hydrogen Energy* **1978**, *3*, 287.

(38) Ihara, S. *Int. J. Hydrogen Energy* **1980**, *5*, 527.

(39) Diver, R.; Fletcher, E. *Energy* **1979**, *4*, 1139.

(40) Diver, R. B.; Pederson, S.; Kappauf, T.; Fletcher, E. A. *Energy* **1983**, *12*, 947.

(41) Kogan, A. *Int. J. Hydrogen Energy* **1998**, *23* (2), 89.

(42) Lédé, J.; Villemaux, J.; Ouzane, R.; Hossain, M. A.; Ouahes, R. *Int. J. Hydrogen Energy* **1987**, *12*, 3.

(43) Olalde, G.; Gauthier, D.; Vialaron, A. *Adv. Ceramics* **1988**, *24*, 879.

(44) http://www.hydrogen.energy.gov/.

(45) Perret, R.; Chen, Y.; Besenbruch, G.; Diver, R.; Weimer, A.; Lewandowski, A.; Miller, E. DOE Hydrogen Program, 2005 Annual Progress Report, U.S. Department of Energy, IV.I.1 "Solar Hydrogen Generation Research; 2005; pp 377; available online at http://www.hydrogen.energy.gov/.

(46) Carty, R. H.; Mazumder, M. M.; Schreider, J. D.; Panborn, J. B. *Thermochemical Hydrogen Production*; GRI-80/0023; Gas Research Institute for the Institute of Gas Technology: Chicago, IL, 1981; Vol. 1−4.

(47) McQuillan, B. W., et al. High Efficiency Generation of Hydrogen Fuels Using Solar-Thermochemical Splitting of Water: Annual Report, Oct 1, 2003, through Sept 30, 2004, to be published as GA-A24972, San Diego, CA.

(48) Abraham, B. M.; Schreiner, F. *Ind. Eng. Chem. Fundam.* **1974**, *13* (4), 305.

(49) Yamauchi, S. *Netsu Sokutei* **1985**, *12* (3), 142.

(50) Lundberg, M. *Int. J. Hydrogen Energy* **1993**, *18* (5), 369.

(51) Bilgen, E.; Ducarroir, M.; Foex, M.; Sebieude, F.; Trombe, F. *Int. J. Hydrogen Energy* **1977**, *2*, 251.

(52) Abanades, S.; Charvin, P.; Flamant, G.; Neveu, P. *Energy* **2006**, *31*, 2805.

(53) Sibieude, F.; Ducarroir, M.; Tofighi, A.; Ambriz, J. *Int. J. Hydrogen Energy* **1982**, *7* (1), 79.

(54) Steinfeld, A.; Kuhn, P.; Reller, A.; Palumbo, R.; Murray, J.; Tamaura, Y. *Int. J. Hydrogen Energy* **1998**, *23* (9), 767.

(55) Palumbo, R.; Lédé, J.; Boutin, O.; Elorza Ricart, E.; Steinfeld, A.; Möller, S.; Weidenkaff, A.; Fletcher, E. A.; Bielicki, J. *Chem. Eng. Sci.* **1998**, *53* (14), 2503.

(56) Steinfeld, A.; Palumbo, R. Solar thermochemical process technology. In *Encyclopedia of Physical Science and Technology*; Meyer, R. A., Ed.; Academic Press: San Diego, CA, 2001; Vol. 15, p 237.

(57) Steinfeld, A. *Int. J. Hydrogen Energy* **2002**, *27*, 611.

(58) Steinfeld, A. *Solar Energy* **2005**, *78*, 603.

(59) Wegner, K.; Ly, H. C.; Weiss, R. J.; Pratsinis, S. E.; Steinfeld, A. *Int. J. Hydrogen Energy* **2006**, *31*, 55.

(60) Charvin, P.; Abanades, S.; Flamant, G.; Lemort, F. *Energy* **2007**, *32* (*7*), 1124.

(61) Allendorf, M. D.; Diver, R. B., Jr.; Miller, J. E.; Siegel, N. P. Thermodynamic analysis of mixed-metal ferrites for hydrogen production by two-step water splitting. In *Proceedings of the ASME International Solar Energy Conference, Solar Engineering 2006*, Denver, CO; Morehouse, J. H., Krarti, M., Eds.; ASME: New York, 2006.

(62) Tofighi, A.; Sibieude, F.; Ducarrior, M.; Benezech, G. *Rev. Int. Hautes Temp. Refract*. **1978**, *15*, 7.

(63) Tofighi, A.; Sibieude, F. *Int. J. Hydrogen Energy* **1980**, *5*, 375.

(64) Tofighi, A.; Sibieude, F. *Int. J. Hydrogen, Energy* **1984**, *9* (4), 293.

(65) Diver, R. B.; Miller, J. E.; Allendorf, M. D.; Siegel N.; Hogan, R. E. Solar thermochemical water-splitting ferrite-cycle heat engine. In *Proceedings of the ASME International Solar Energy Conference, Solar Engineering 2006*, Denver, CO; Morehouse, J. H., Krarti, M., Eds.; ASME: New York, 2006.

(66) Steinfeld, A.; Sanders, S.; Palumbo, R. *Solar Energy* **1999**, *65* (1), 43.

(67) Darken, L. S.; Gurry, R. W. *J. Am. Chem. Soc.* **1946**, *63*, 798.

(68) Patrice, C.; Stéphane, A.; Florent; Gilles, F. Experimental evalutaion of promising solar thermochemical cycles for hydrogen production. In *Proceedings of 13th International Symposium on Concentrated Solar Power and Chemical Energy Technologies*, Seville, Spain; Romero, M., Martínez, D., Ruiz, V., Silva, M., Brown, M., Eds.; CIEMAT: Madrid, Spain, 2006.

(69) Kodama, T.; Gokon, N.; Yamamoto, R., Thermochemical two-step water splitting by ZrO_2-supported $Ni_xFe_{3-x}O_4$ for solar hydrogen production. *Solar Energy* **2007**, doi:10.1016/j.solener.2007.03.005 (available online at http://www.sciencedirect.com).

(70) Aoki, H.; Kaneko, H.; Hasegawa, N.; Ishihara, H.; Takahashi, Y.; Suzuki, A.; Tamaura, Y. Two-step water splitting with Ni-ferrite system for solar H_2 production using concentrated solar radiation. In *Engineering 2004, Proceedings of the International Solar Energy Conference*, Portland, OR, 2004; ASME International: New York, 2004.

(71) Ehrensberger, K.; Frei, A.; Kuhn, P.; Oswald, H.; Hug, P. *Solid State Ionics* **1995**, *78*, 151.

(72) Ehrensberger, K.; Kuhn, P.; Shklover, V.; Oswald, H. *Solid State Ionics* **1996**, *90*, 75.

(73) Kaneko, H.; Kodama, T.; Gokon, N.; Tamaura, Y.; Lovegrove, K.; Luzzi, A. *Solar Energy* **2004**, *76*, 317.

(74) Tamaura, Y.; Kojima, N.; Hasegawa, N.; Inoue, M.; Uehara, R.; Gokon, N.; Kanako, H. *Int. J. Hydrogen Energy* **2001**, *26* (9), 917.

(75) Kaneko, H.: Kojima, N.; Hasegawa, N.; Inoue, M.; Uehara, R.; Gokon, N.; Tamaura, Y.; Sano, T. *Int. J. Hydrogen Energy* **2002**, *27*, 1023.

(76) Kaneko, H.; Aoki, H.; Hasegawa, N.; Ishihara, H.; Takahashi, Y.; Suzuki, A.; Tamaura, Y. Oxygen gas releasing of Zn-ferrite in air at 1800 K for solar H_2 production. In *Proceedings of 12th SolarPACES International Symposium*, Oaxaca, Mexico 2004; Carlos, R., Huacuz, J., Eds.; Electrical Research Institute: Mexico City, Mexico, 2004.

(77) Kodama, T.; Kondoh, Y.; Kiyama, A.; Shimizu, K.-I. Hydrogen production by solar thermochemical water-splitting/methane-reforming process. In *Proceedings of ASME International Solar Energy Conference (ISEC)*, Hawaii, 2003; Thornbloom, M. D., Jones, S. A., Eds.; ASME: New York, 2003.

(78) Kodama, T.; Shimizu, T.; Satoh, T.; Nakata, M.; Shimizu, K.-I. *Solar Energy* **2002**, *73* (5), 363.

(79) Kodama, T.; Kondoh, Y.; Yamamoto, R.; Andou, H.; Satoh, N. *Solar Energy* **2005**, *78*, 623.

(80) Gokon, N.; Mizuno, T.; Takahashi, S.; Kodama, T. A two-step water splitting with ferrite particles and its new reactor concept using an internally circulating fluidized-bed. In *Proceedings of the ASME International Solar Energy Conference, Solar Engineering 2006*, Denver, CO, 2006; Morehouse, J. H., Krarti, M., Eds.; ASME: New York, 2006.

(81) Tamaura, T.; Steinfeld, A.; Kuhn, P.; Ehrensberger, K. *Energy* **1995**, *20* (4), 325.

(82) Kodama, T.; Nakamuro, Y.; Mizuno, T.; Yamamoto, R. A two-step thermochemical water splitting by iron-oxide on stabilized zirconia. In *Engineering 2004, Proceedings of the International Solar Energy Conference*, Portland, OR, 2004; ASME International: New York, 2004.

(83) Kodama, T.; Nakamuro, Y.; Mizuno, T. *J. Solar Energy Eng.* **2006**, *128*, 3.

(84) Gokon, N.; Mizuno, T.; Nakamuro, Y.; Kodama, T. Iron-containing YSZ (yttrium-stabilized zirconia) system for a two-step thermochemical water splitting. In *Proceedings of 13th International Symposium on Concentrated Solar Power and Chemical Energy*

Technologies; Romero, M., Martínez, D., Ruiz, V., Silva, M., Brown, M., Eds.; Seville, Spain, 2006.
(85) Gokon, N.; Mizuno, T.; Nakamuro, Y.; Kodama, T. Iron-containing YSZ (yttrium-stabilized zirconia) system for a two-step thermochemical water splitting. *J. Solar Energy Eng.* **2007**, in press.
(86) Wen-Xiang, W.; Zheng, L.; Fan, L. *J. Solid State Chem.* **1993**, *107*, 201.
(87) Liu, Z.; Dong, Q.; Chen, Y. *Mater. Chem. Phys.* **1998**, *53*, 67.
(88) Štefanić, G.; Grźeta, B.; Nomura, K.; Trojko, R.; Musić, S. *J. Alloys Compounds* **2001**, *327*, 151.
(89) Arroyave, R.; Kaufman, L.; Eager, T. *CALPHAD: Comput. Coupling Phase Diagrams Thermochem.* **2002**, *26* (1), 95.
(90) Ishihara, H.; Kanako, H.; Yokoyama, T.; Fuse, A.; Hasegawa, N.; Tamaura, Y. Hydrogen production through two-step water splitting using YSZ(Ni Fe) system for solar hydrogen production. In *Proceedings of 2005 ASME International Solar Energy Conference*, Orlando, FL; ASME: New York, 2005.
(91) Agrafiotis, C.; Roeb, M.; Konstandopoulos, A. G.; Nalbandian, L.; Zaspalis, V. T.; Sattler, C.; Stobbe, P.; Steele, A. M. *Solar Energy* **2005**, *79*, 409.
(92) Roeb, M.; Sattler, C.; Klüser, R.; Monnerie, N.; de Oliveira, L.; Konstandopoulos, A. G.; Agrafiotis, C.; Zaspalis, V. T.; Nalbandian, L.; Steele, A.; Stobbe, P. *J. Sol. Energy Eng.* **2006**, *128*, 125.
(93) Agrafiotis, C.; Lorentzou, S.; Ragkoura, C.; Kostoglou, M.; Konstandopoulos, A. G. Advanced monolithic reactors for hydrogen generation from solar water splitting. In *Proceedings of 13th International Symposium on Concentrated Solar Power and Chemical Energy Technologies*; Romero, M., Martínez, D., Ruiz, V., Silva, M., Brown, M., Eds.; Seville, Spain, 2006.
(94) Sattler, C.; Roeb, M.; Monnerie, N.; Graf, D.; Möller, S. Efficeint solar thermal processes from carbon based to carbon free hydrogen production. In *Proceedings of the ASME International Solar Energy Conference, Solar Engineering 2006*, Denver, CO; Morehouse, J. H., Krarti, M., Eds.; ASME: New York, 2006.
(95) Kodama, T.; Hasegawa, T.; Nagasaki, A.; Gokon, N. Reactive Fe-YSZ coated foam devices for solar two-step water splitting. In *Proceedings of the 2007 ASME Energy Sustainability Conference (ES2007*), Long Beach, CA; ASME: New York, 2007.
(96) Kaneko, H.; Fuse, A.; Miura, T.; Ishihara, H.; Tamaura, Y. Two-step water splittng with concentrated solar heat using rotary-type solar furnace. In *Proceedings of 13th International Symposium on Concentrated Solar Power and Chemical Energy Technologies*, Seville, Spain; Romero, M., Martínez, D., Ruiz, V., Silva, M., Brown, M., Eds.; CIEMAT: Madrid, Spain, 2006.
(97) Miller, J. E.; Evans, L. R.; Stuecker, J. N.; Allendorf, M. D.; Siegel, N. P.; Diver, R. B. Material developement for the CR5 solar thermochemical heat engine. In *Proceedings of the ASME International Solar Energy Conference, Solar Engineering 2006*, Denver, CO; Morehouse, J. H., Krarti, M., Eds.; ASME: New York, 2006.
(98) James, D. L.; Siegel, N. P.; Diver, R. B.; Boughton, B. D.; Hogan, R. E. Numerical modeling of solar thermo-chemical water-splitting reactor. In *Proceedings of the ASME International Solar Energy Conference, Solar Engineering 2006*, Denver, CO; Morehouse, J. H., Krarti, M., Eds.; ASME: New York, 2006.
(99) Hunt, A.; Ayer, J.; Hull, P.; Miller, F.; Noring, J.; Worth, D. *Solar Radiant Heating of Gas-Particle Mixtures*; LBL-22743; Lawrence Berkeley Laboratory, University of California: Berkeley, CA, 1986.
(100) Rightley, M.; Matthews, L.; Mulholland, G. *Solar Energy* **1992**, *48*, 363.
(101) Steinfeld, A.; Brack, M.; Ganz, J.; Haueter, P.; Imhof, A.; Meier, A.; Mischler, D.; Nater, E.; Seitz, T.; Schwarz, A.; Wuillemin, D. Particle-cloud reactor development for high-temperature solar chemistry. In *Proceedings of 7th International Symposium on Solar Thermal Concentrating Technologies*, Moscow, Russia, 1992; Vol. 4, p 888.
(102) Meier, A.; Ganz, J.; Steinfeld, A. *Chem. Eng. Sci.* **1996**, *51* (11), 3181.
(103) Ganz, J.; Meier, A.; Mischler, D.; Tschudi, H. Properties of volumetric gas-particle solar reactors. In *Solar Thermal Concentrating Technologies, Proceedings of the 8th International Symposium*, Köln, Germany, 1996; Müller Verlag: Heidelberg, Germany, 1997; Vol. 1, p 555.
(104) Steinfeld, A.; Brack, M.; Meier, A.; Weidenkaff, A.; Wuillemin, D. *Energy* **1998**, *23* (10), 803.
(105) Weidenkaff, A.; Brack, M.; Möller, S.; Palumbo, R.; Steinfeld, A. *J. Phys. IV* **1999**, *9*, Pr-313.
(106) Dahl, J. K.; Barocas, V. H.; Clough, D. E.; Weimer, A. W. *Int. J. Hydrogen Energy* **2002**, *27* (*4*), 377.
(107) Dahl, J. K.; Buechler, K. J.; Finley, R.; Stanislaus, T.; Weimer, A. W.; Lewandowski, A.; Bingham, C.; Smeets, A.; Schneider, A. *Energy* **2004**, *29*, 715.
(108) Dahl, J. K.; Buechler, K. J.; Weimer, A. W.; Lewandowski, A.; Bingham, C. *Int. J. Hydrogen Energy* **2004**, 29 (*7*), 725.
(109) Dahl, J. K.; Weimer, A. W.; Lewandowski, A.; Bingham, C.; Bruetsch, F.; Steinfeld, A. *Ind. Eng. Chem. Res.* **2004**, *43*, 5489.
(110) Segal, A.; Epstein, M. *Solar Energy* **2003**, *75*, 479.
(111) Gokon, N.; Takahashi, S.; Yamamoto H.; Kodama, T. New solar water-splitting reactor with ferrite particles in an internally circulating fluidized bed. In *Proceedings of the 2007 ASME Energy Sustainability Conference (ES2007)*, Long Beach, CA; ASME: New York, 2007.
(112) Palumbo, R. *J. Phys. IV* **1999**, *9*, Pr3−35.
(113) Weidenkaff, A.; Steinfeld, A.; Wokaun, A.; Auer, P.; Eichler, B.; Reller, A. *Solar Energy* **1999**, *65* (1), 59.
(114) Haueter, P.; Moeller, S.; Paloumbo, R.; Steinfeld, A. *Solar Energy* **1999**, *67* (1−3), 161.
(115) Weidenkaff, A.; Reller, A.; Wokaun, A.; Steinfeld, A. *Thermochem. Acta* **2000**, *359*, 69.
(116) Berman, A.; Epstein, M. *Int. J. Hydrogen Energy* **2000**, *25*, 957.
(117) Möller, S.; Palumbo, R. *Chem. Eng. Sci.* **2001**, *56*, 4505.
(118) Keunecke, M.; Meier, A.; Palumbo, R. *Chem. Eng. Sci.* **2004**, *59*, 2695.
(119) Palumbo, R.; Keuneck, M.; Möller, S.; Steinfeld, A. *Energy* **2004**, *29*, 727.
(120) Müller, R.; Haeberling, P.; Polumbo, R. D. *Solar Energy* **2005**, *80*, 500.
(121) Müller, R.; Schunk, L.; Meier, A.; Steinfeld, A. Solar thermal dissociation of zinc oxide in a directly-irradiated rotary reactor. In *Proceedings of 13th International Symposium on Concentrated Solar Power and Chemical Energy Technologies*, Seville, Spain; Romero, M., Martínez, D., Ruiz, V., Silva, M., Brown, M., Eds.; CIEMAT: Madrid, Spain, 2006.
(122) Müller, R.; Steinfeld, A. Band-approximated radiative heat transfer analysis of a solar chemical reactor for the thermal dissociation of zinc oxide. *Solar Energy* **2007**, doi:10.1016/j.solener.2006.12.006 (available online at http://www.sciencedirect.com).
(123) Müller, R.; Lipinski, W.; Steinfeld, A. Transient heat transfer in a directly-irradiated solar chemical reactor for the thermal dissociation of ZnO. *Appl. Thermal Eng.* **2007**, doi:10.1016/j.applthermaleng.2007.05.002 (available online at http://www.sciencedirect.com).
(124) Perkins, C. M.; Andowski, A. L.; Bingham, C.; Clichty, P.; Weimer, A. W. Zinc oxide decomposition as the solar step in a two-step thermochemical water splitting cycle: chemical reaction kinetics. In *Proceedings of 13th International Symposium on Concentrated Solar Power and Chemical Energy Technologies*, Seville, Spain; Romero, M., Martínez, D., Ruiz, V., Silva, M., Brown, M., Eds.; CIEMAT: Madrid, Spain, 2006.
(125) Sturzenegger, M.; Nüesch, P. *Energy* **1999**, *24*, 959.
(126) Weimer, A. W.; Francis, T.; Carney, C.; Wyss, J.; Martinek, J.; Kerins, M. 2006 Annual Progress Report, U.S. Department of Energy, II.I.2 "Fundamentals of a Solar-thermal Hydrogen Production Process Using a Metal-Oxide Based Thermochemical Water Splitting Cycle"; pp 216; available at http://www.hydrogen.energy.gov/.
(127) Kaneko, H.; Hosokawa, Y.; Gokon, N.; Kojima, N.; Hasegawa, N.; Kitamura, M.; Tamaura, Y. *J. Phys. Chem. Solids* **2001**, *62* (*7*), 1341.
(128) Kaneko, H.; Ochiai, Y.; Shimizu, K.; Hosokawa, Y.; Gokon, N.; Tamaura, Y. *Solar Energy* **2002**, *72* (4), 377.
(129) Tamaura, Y.; Ueda, Y.; Matsunami, J.; Hasegawa, N.; Nezuka, M.; Sano, T.; Tsuji, M. *Solar Energy* **1999**, *65* (1), 55.
(130) Abanades, S.; Flamant, G. *Solar Energy* **2006**, *80*, 1611.
(131) Nelson, P. F.; Flores, A.; François, J. L. *Nucl. Eng. Des.* **2007**, *237*, 219.
(132) Serpone, N.; Lawless, D.; Terzian, R. *Solar Energy* **1992**, *49* (4), 221.
(133) Funk, J. E. *Int. J. Hydrogen Energy* **2001**, *26*, 185.
(134) Perkins, C.; Weimer, A. W. *Int. J. Hydrogen Energy* **2004**, *29*, 1587.
(135) Beghi, G. E. *Int. J. Hydrogen Energy* **1986**, *11* (12), 761.
(136) Carty, R. H.; Conger, W. L. *Int. J. Hydrogen Energy* **1980**, *5*, 7.
(137) Lu, P. W. T. *Int. J. Hydrogen Energy* **1983**, *8* (10), 773.
(138) Weirich, W.; Knoche, K. F.; Behr, F.; Barnert, H. *Nucl. Eng. Des.* **1984**, *78*, 285.
(139) Jeong, Y. H.; Kazimi, M. S.; Hohnholt, K. J.; Yildiz, B. Optimization of the hybrid sulfur cycle for hydrogen generation. Massachusetts Institute of Technology Center for Advanced Nuclear Energy Systems, Cambridge, MA, 2005; available at http://web.mit.edu/canes/pdfs/reports/nes-004.pdf.
(140) Bilgen, E.; Bilgen, C. *Int. J. Hydrogen Energy* **1986**, *11* (4), 241.
(141) Bilgen, C.; Broggi, A.; Bilgen, E. *Solar Energy* **1986**, *36* (3), 267.
(142) Bilgen, E. *Solar Energy* **1988**, *41* (2), 199.
(143) Le Duigou, A.; Borgard, J.-M.; Larousse, B.; Doize, D.; Eysseric, C.; Allen, R.; Ewan, B. C. H.; Priestman, G.; Elder, R.; Cerri, G.; Salvine, C.; Giovannelli, A.; De Maria, G.; Robe, M.; Monneri, N.; Schmitz, M.; Sattler, Cl.; Buenaventura, A.; De Lorenzo, D.; Dechelotte, S.; Baudouin, O. Hytec: a search for a long term mossive hydrogen production rute. In *Proceedings International Hydrogen Energy Congress and Exhibition IHEC 2005*; Istanbul, Turkey, 2005; available online at http://www.kintecus.com.

(144) Le Duigou,; Borgard, J.-M.; Larousse, B.; Doize, D.; Allen, R., et al. *Int. J. Hydrogen* **2007**, *32* (10−11), 1516.
(145) Roeb, M.; Noglik, A.; Monneri, N.; Schmitz, M.; Sattler, C.; Gerri, G.; Maria, G. de; Giovannelli, A.; Orden, A.; Lorenzo, D. de; Cedillo, J.; LeDuigou, A.; Borgard, J.-M. Development and verification of process concepts for the splittng of sulphuric acid by concentrated solar radiation. In *Proceedings of 13th International Symposium on Concentrated Solar Power and Chemical Energy Technologies*, Seville, Spain; Romero, M., Martínez, D., Ruiz, V., Silva, M., Brown, M., Eds.; CIEMAT: Madrid, Spain, 2006.
(146) Pickard, P. S.; Gelbard, F.; Moore, B.; Vernon, M.; Parma, E. 2006 Annual Progress Report, U.S. Department of Energy, "II. G.2 Sulfur-Iodine Thermochemical Cycle"; pp 178; available online at http://www.hydrogen.energy.gov/.
(147) Broggi, A.; Joels, R.; Mertel, G.; Morbello, M. *Int. J. Hydrogen Energy* **1981**, *6*, 25.
(148) Bilegn, E.; Joels, R. K. *Int. J. Hydrogen Energy* **1985**, *10* (3), 143.
(149) O'Keefe, D.; Allen, C.; Besenbruch, G.; Brown, L.; Norman, J.; Sharp, R.; McCorkle, K. *Int. J. Hydrogen Energy* **1982**, *7* (5), 381.
(150) Onuki, K.; Shimizu, S.; Nakajima, H.; Fujita, S.; Ikezoe, Y.; Sato, S.; Machi, S. Studies on an iodine-sulfur process for thermochemical hydrogen production. In *Proceedings of the 8th World Hydrogen Energy Conference*, Hawaii, 1990; Vol. 2, p 547.
(151) Engels, H.; Knoche, K. F. *Int. J. Hydrogen* **1986**, *11*, 703.
(152) Sato, S.; Shimizu, S.; Nakajima, H.; Ikezoe, Y. *Int. J. Hydrogen Energy* **1983**, *8*, 15.
(153) Norman, J. H.; Besenbruch, G. E.; Brown, L. C.; O'Keefe, D. R.; Allen, C. L. *Thermochemical Water-Splitting Cycle. Bench-Scale Investigation and Process Engineering*; General Atomics Report GA-A 16713; 1982.
(154) Kubo, S.; Nakajima, H.; Kasahara, S.; Higashi, S.; Masaki, T.; Abe, H.; Onuki, K. *Nucl. Eng. Des.* **2004**, *233*, 347.
(155) Yamawaki, M.; Nishihara, T.; Inagaki, Y.; Minato, K.; Oigawa, H.; Onuki, K.; Hino, R.; Ogawa, M. *Int. J. Hydrogen Energy* **2007**, doi: 10.1016/j.ijhydene.2006.09.026 (available online at www.sciencedirect.com).
(156) Brown, L. C.; Besenbruch, G. E.; Lentsch, R. D.; Schultz, K. R.; Funk, J. F.; Pickard, P. S.; Marshall, A. C.; Showalter, S. K. *High Efficiency Generation of Hydrogen Fuel Using Nuclear Power*; General Atomics Report GA-A24285; 2003.
(157) Goldstein, S.; Borgard, J.-M.; Vitart, X. *Int. J. Hydrogen Energy* **2005**, *30*, 619.
(158) Kasahara, S.; Hwang, G.-J.; Akajima, H.; Choi, H.-S.; Onuki, K.; Nomura, M. *J. Chem. Eng. Jpn.* **2003**, *36*, 887.
(159) Kasahara, S.; Kubo, S.; Hino, R.; Onuki, K.; Nomura, M.; Nakao, S.-I. *Int. J. Hydrogen Energy* **2007**, *32* (4), 489.
(160) Kubo, S.; Kasahara, S.; Okuda, H.; Terada, A.; Tanaka, N.; Inaba, Y.; Ohashi, H.; Inagaki, Y.; Onuki, K.; Hino, R. *Nucl. Eng. Des.* **2004**, *233*, 355.
(161) Nomura, M.; Okuda, H.; Kasahara, S.; Nakao, S.-I. *Chem. Eng. Sci.* **2005**, *60*, 7160.
(162) Öztürk, I. T.; Hammache, A.; Bilgen, E. *Eng. Convers. Manag.* **1995**, *36* (1), 11.
(163) Onuki, K.; Ioka, I.; Futakawa, M.; Nakajima, H.; Shimizu, S. *Corrosion Eng.* **1997**, *46*, 141.
(164) Futakawa, M.; Onuki, K.; Ioka, I.; Nakajima, H.; Shimizu, S. *Corrosion Eng.* **1997**, *46*, 811.
(165) Ioka, I.; Mori, J.; Kato, C.; Futakawa, M.; Onuki, K. *J. Mater. Sci. Lett.* **1999**, *18*, 1497.
(166) Nishiyama, N.; Futakawa, M.; Ioka, I.; Onuki, K.; Shimizu, S.; Eto, M.; Oku, T.; Kurabe, M. *J. Soc. Mater. Sci. Jpn.* **1999**, *48* (7), 746.
(167) Futakawa, M.; Wakui, T.; Ioka, I.; Eto, M. *J. Eur. Ceramic Soc.* **2000**, *20*, 1135.
(168) Futakawa, M.; Kubo, S.; Wakui, T.; Onuki, K.; Shimizu, S.; Yamaguchi, A. *J. Jpn. Soc. Exp. Mech.* **2003**, *3* (2), 109.
(169) Wu, X.; Onuki, K. *Tsinghua Sci. Technol.* **2005**, *10* (2), 270.
(170) Vitart, X.; Le Duigou, A.; Carles, P. *Energy Conversion Manag.* **2006**, *47*, 2740.
(171) Huang, C.; T-Raissi. *Solar Energy* **2005**, *78*, 632.
(172) Roth, M.; Knoche, K. F. *Int. J. Hydrogen Energy* **1989**, *14*, 545.
(173) Aochi, A.; Tadokoro, T.; Yoshida, K.; Kameyama, H.; Nobue, M.; Yamaguchi, T. *Int. J. Hydrogen Energy* **1989**, *14* (7), 421.
(174) Yoshida, K.; Kameyama, H.; Aochi, T.; Nobue, M.; Aihara, M.; Amir, R.; Kondo, H.; Sato, T.; Tadokoro, T.; Yamaguchi, T.; Sakai, N. *Int. J. Hydrogen Energy* **1990**, *15* (3), 171.
(175) Sakurai, M.; Aihara, M.; Miyake, N.; Tsutsumi, A.; Yoshida, K. *Int. J. Hydrogen Energy* **1992**, *17* (8), 587.
(176) Sakurai, M.; Tsutsumi, A.; Yoshida, K. *Int. J. Hydrogen Energy* **1995**, *20* (4), 297.
(177) Sakurai, M.; Bilgen, E.; Tsutsumi, A.; Yoshida, K. *Int. J. Hydrogen Energy* **1996**, *21* (10), 865.
(178) Tadokoro, Y.; Kajiyama, T.; Sakai, N.; Kameyama, H.; Yoshida, K. *Int. J. Hydrogen Energy* **1997**, *22* (1), 49.
(179) Sakurai, M.; Miyake, Y.; Tsutsumi, A.; Yoshida, K. *Int. J. Hydrogen Energy* **1996**, *21* (10), 871.
(180) Teo, E. D.; Brandon, N. P.; Vos, E.; Kramer, G. J. *Int. J. Hydrogen Energy* **2005**, *30*, 559.
(181) Lemort, F.; Lafon, C.; Dedryvére, R.; Gondeau, D. *Int. J. Hydrogen Energy* **2006**, *31*, 906.
(182) Lemort, F.; Charvin, P.; Lafon, C.; Romnicianu, M. *Int. J. Hydrogen Energy* **2006**, *31*, 2063.
(183) Sakurai, M.; Bilgen, E.; Tsutsumi, A.; Yoshida, K. *Solar Energy* **1996**, *57* (1), 51.
(184) Stokes, R. A. Solar energy. In *Encyclopedia of Chemical Technologies*, 4th ed.; Kroschwitz, J. I., Grant, M. H., Eds.; Wiley: New York, 1996; Vol. 22, p 465.
(185) Rosen, M. A. *Int. J. Hydrogen Energy* **1995**, *20* (7), 547.
(186) Stoll, R. E.; von Linde, F. *Hydrocarbon Process.* **2000**, 42.
(187) Perret, R.; Weimer, A.; Besenbruch, G.; Diver, R.; Lewis, M.; Chen, Y. DOE Hydrogen Program, 2006 Annual Progress Report, U.S. Department of Energy, II.I.1 Development of Solar-Powered Thermochemical Production of Hydrogen from Water; pp 210; available at http://www.hydrogen.energy.gov/.

CR050188A